2

(NASA-CR-135794) A REUSABLE LUNAR SHUTTLECRAFT (RLS): A SYSTEMS STUDY (Cornell Univ.) ~~185~~ 187 p HC $11.25 CSCL 22B

N73-33809

Unclas

G3/31 19862

Reproduced by
NATIONAL TECHNICAL
INFORMATION SERVICE
US Department of Commerce
Springfield, VA. 22151

NOV 1973

COLLEGE OF ENGINEERING
Cornell University
Ithaca, New York 14850

187

A REUSABLE LUNAR SHUTTLECRAFT (RLS)

A SYSTEMS STUDY

Prepared Under
Contract No. NGR 33-010-071
NATIONAL AERONAUTICS AND SPACE ADMINISTRATION

by

NASA-Cornell Doctoral Design Trainee Group
(1968-1971)

August 1973

College of Engineering
Cornell University
Ithaca, New York

I

Table of Contents

Page

Preface i

Chapter I: Introduction I-1
Author: J. J. Miller

Chapter II: Objective, Feasibility and Cost of the RLS Mission
Author: J. J. Miller

Objective. II-1
Feasibility. II-4
Cost II-7
References II-8

Chapter III: Trajectory Analysis
Author: J. J. Miller

The Permanent Orbiting Station III-1
Descent to the Lunar Surface III-4
Lunar Ascent III-6
Minimum-Time Rendezvous. III-7
References III-39
Figures. III-41

Chapter IV: Guidance and Navigation
Author: A. M. Blake

Introduction IV-1
Laser Radar Ranging System IV-1
G and N Requirements IV-2
Bibliography IV-5
Figure IV-6

Chapter V: Communication System: Analysis and Design
Author: A. M. Blake

Introduction V-1
Mission Requirements V-1
System Configurations. V-3
Modulation Techniques. V-5
Coding V-9
Calculation of Transmitter Power V-12
Coptran. V-13
Acquisition and Tracking V-17
Nomenclature V-21
References/Bibliography. V-23
Figures. V-24

Table of Contents, cont.

Page

Chapter VI: Propulsion Systems
Author: J. J. Markowsky

Main Propulsion System VI-1
Reaction Control System. VI-4
General. VI-6
Previous Work. VI-6
Analysis VI-8
Results and Discussion VI-16
Conclusions. VI-25
References VI-27
Nomenclature VI-28
Figures. VI-31

Chapter VII: Electrical Power System
Author: J. J. Markowsky

Introduction VII-1
Power System Requirements. VII-2
Candidate Power Systems. VII-4
Power System Comparison. VII-6
Design Data Requirements VII-7
References VII-9

Chapter VIII: Landing Gear Design
Author: P. J. Rojeski

Introduction VIII-1
Problem Definition VIII-2
Landing Gear Design: An Optimal Solution. VIII-5
Study Objectives and Design Assumptions. VIII-7
Analysis Techniques. VIII-14
Results and Conclusions. VIII-20
Nomenclature VIII-23
References VIII-24
Figures. VIII-26

Preface

This report is the second resulting from an educational project supported by the NASA Office of University Affairs. The project was intended to stimulate interest and activity in the area of systems engineering. In addition to the one at Cornell similar projects were instituted at Purdue, Georgia Tech, Kansas State and Stanford.

As might be expected, the approach taken by each school has been different. At Cornell the pattern of operation has been for the student group to select a project which was in the mandate area of NASA. Decision on, and definition of, the problem was essentially a student function. For the several groups involved problem definition frequently required visits to NASA installations and/or contractors. Periods of up to a year were sometimes needed before all participants, i.e., students, advisors, project director, were reasonably content.

Subsequent to problem definition the work pattern was essentially the usual student/advisor one, but with frequent group meetings. In the majority of cases the thesis work emanated from the aspect of the project with which the student was charged. By this is meant that the deep, thorough study characteristic of thesis work was done but it usually arose in a need-to-know context. Several of the theses could be characterized as analytic design methodologies. This was almost inevitable since contact with the problem suggested need for better analytical design tools. The reader will no doubt be able to identify the chapters of the report which are thesis-like in character.

One student in the present group has not completed his studies for personal reasons. Since his task concerned the structure of the vehicle, the report presents guidance systems, propulsion plants, etc., but no structure on which to hang them. While this is unfortunate, the material presented is sufficiently general so that it is applicable to other craft. There is no assurance that further delay would result in a more complete report.

A listing of the personnel involved in the project follows:

John L. Aho - Aerospace Engineering

Faculty Advisor: Professor R. Gallagher
Thesis: Incomplete
Doctoral Degree: Not granted
Presently with Rose-Hulman Institute, Terre Haute, Indiana

Arthur M. Blake - Electrical Engineering

Faculty Advisor: Professor G. Szentirmai
Thesis: "The Analysis and Design of Multiple Feedback Filters"
Doctoral Degree: Received May 1973
Presently with Bell Telephone Laboratories, Inc., Murray Hill, New Jersey

James J. Markowsky - Mechanical Engineering

Faculty Advisor: Professor H. N. McManus, Jr.
Thesis: "An Analytical Model for Predicting the Pressure and Flow Transients in a Gaseous H_2-O_2 100 lb Thrust Reaction Control System Rocket Engine"
Doctoral Degree: Received February 1972
Presently Staff Engineer with American Electric Power Service Corp., New York, N. Y.

John J. Miller - Theoretical and Applied Mechanics

Faculty Advisor: Professor K. T. Alfriend
Thesis: "Minimum-Time Rendezvous with Constrained Attitude Rate"
Doctoral Degree: Received January 1972
Presently with TRW Corp., Alexandria, Va.

Peter J. Rojeski - Mechanical Engineering

Faculty Advisor: Professor R. L. Wehe
Thesis: "A Systems Analysis Approach to Landing Gear Design"
Doctoral Degree: Received May 1972
Presently with University of Tulsa, Tulsa, Oklahoma

From this writer's point of view, the project has been instructive, interesting, and rewarding. It should be noted that the project was not termed easy since the cooperation of ten people of strong mind is not easily obtained. However, the presentation of this report is the best indication of program success.

HNMcManus Jr

27 July 1973

H. N. McManus, Jr.
Professor of Mechanical Engineering

Program Director

Chapter I: Introduction

This report presents the results of the efforts of a team of Cornell University graduate students who, under the sponsorship of the National Aeronautics and Space Administration (NASA), were given the opportunity to conceive and design an original space vehicle system. The student team was composed of five members selected from diverse fields of study. The purpose of the program was to expose each student to the problems faced by other disciplines and to give him some knowledge of the inter-relationship between these disciplines in designing a complete space vehicle system. Thus each student would emerge from the program with a basic education in the systems approach to solving engineering problems, that is, always keeping the total problem in mind when seeking a solution to any part of it. The students were encouraged to make their work in this program an integral part of their efforts to fulfill the requirements for the Doctor of Philosophy (Ph.D.) degree in their individual areas of interest.

The new space system described in this report was conceived and developed during a period (1968-1971) when the space exploration efforts of the United States had achieved the milestone of manned lunar landing and yet were being subject to criticism on several counts. The most persistent criticism involved the substantial cost associated with each space mission. Particular attention was paid to the lack of reusability in the design of space hardware, with substantial portions of each space vehicle system simply being discarded at a convenient moment during the course of a mission. The space program was also being widely criticized by the scientific community for what it considered to be a failure to fully exploit the scientific potential of some missions, particularly those involving manned lunar landing. The proposed Reusable Lunar Shuttlecraft (RLS) is designed as an answer to these particular criticisms, being an inexpensive vehicle which will assist in providing a large scientific return per dollar invested.

The RLS is designed for service in the 1978-1985 time period. It is thought that in this period the establishment of the first semi-permanent bases on the lunar surface will begin. The RLS is conceived to be an extremely flexible vehicle which will be capable of filling all the logistical requirements generated by the establishment and maintenance of a semi-permanent lunar station.

The complete RLS concept includes a permanent base in orbit about the moon which is capable of extended life support. This station will provide refueling and refitting facilities for the shuttlecraft. Besides its service to the shuttlecraft, it is envisioned that this base would serve as a control point for establishing and maintaining lunar bases. The orbiting base would be supplied by Saturn V/S-IVB vehicles and by shuttlecraft which would be uprated versions of the earth-to-earth-orbit reusable shuttle vehicles currently under development.

Since the concept of a permanent space station is hardly new and is discussed widely in the scientific literature, the effort documented in this report was focused on the design of the RLS. As its name implies, the RLS will shuttle back and forth between its orbiting base and the lunar surface. Barring a catastrophic failure the vehicle will be capable of at least twenty round-trip missions and of landing at any reasonably level point on the lunar surface. In order to minimize costs, the design of the vehicle is based on the existing technology of the Lunar Module (LM) of the Apollo program wherever possible. The most innovative feature of the RLS will be its ability to operate in either a manned or automatic mode. In both modes the prime control of the vehicle will rest with the controller stationed in the orbiting base. In the case of the manned mission, the passengers onboard will have the ability to take control in the case of difficulty.

This volume consists of eight chapters including this Introduction. Each of the chapters presents design information and supporting data which were obtained during the course of this study. In addition, the chapters on trajectory analysis, propulsion, structure, and landing gear contain an in-depth study of a particular design problem pertinent to the RLS. These detailed studies are taken from the doctoral dissertations which were written during the course of this program.

Chapter II: Objective, Feasibility and Cost of the RLS Mission

As soon as Apollo XI, the first lunar landing mission, established that the moon was devoid of life and was surprisingly stark and desolate, public support for further exploration of the moon dwindled dramatically. Attention was turned toward exploration of the mysteries of planet Earth through long-duration orbital missions. The establishment of laboratories which would orbit just above the Earth's atmosphere and be manned for long periods by teams of scientist/astronauts was planned as the next major step in space exploration. These laboratories would eventually be supported by reusable shuttlecraft capable of repeated earth-to-earth orbit round-trip missions.

The withdrawal of priority from immediate intensive lunar exploration appears to have been a wise decision. A lower frequency for missions to the lunar surface will allow for much more thoughtful and cost-effective gathering of information from the moon. But one shortcoming in present plans is very obvious: no lunar landing missions are planned after Apollo XVII. Each lunar landing mission since the first has uncovered new and puzzling facts which, for example, have caused some widely held theories of the origin of the moon to be discarded. It is obvious that the great wealth of scientific information on the moon will scarcely have been touched when the Apollo XVII mission has been completed.

A. Objective

The development of semi-permanent bases on the lunar surface is a next logical step in lunar exploration. In order to maximize scientific return, these bases should be spread over a wide area. The Reusable Lunar Shuttlecraft (RLS) concept has been developed as a means of establishing widely-located scientific laboratories on the lunar surface and supporting these laboratories on a routine basis.

The 1978-1985 time span has been chosen as the operating period for the RLS for a number of reasons. The RLS concept requires the establishment of a permanent station in lunar orbit. This base will be manned for extended periods of time by a single crew. At the time of this writing, little is known about the effect of extended periods of weightlessness on bodily functions, although there are already signs that the effects can cause substantial problems. The manned earth-orbiting laboratory program mentioned above will thoroughly investigate the effect of prolonged weightlessness on humans. By 1978 this program will hopefully have resolved any difficulties by the creation of artificial gravity or by other means.

As is indicated by the name, the RLS will be used repeatedly for various types of missions. At the completion of each mission, the vehicle will have to be refurbished for its next assignment. Again, little is known about the problems of refurbishing a spacecraft since no reusable craft have been flown. The reusable shuttlecraft planned initially for earth-to-earth orbit and return missions should give substantial insight into the problems that are presented by reusability and, in particular, into the difficulties of refurbishing a vehicle while in lunar orbit. Thus it is felt that by 1978 these and several other technical obstacles discussed below will have been faced and overcome. By the year 1985, it is expected that the time will have come for the establishment of permanent bases and perhaps colonies on the lunar surface. These would require payload capabilities exceeding those envisioned for the RLS.

Let us now consider in some detail the concept of lunar exploration using the RLS. A manned vehicle consisting of the permanent orbiting station and the RLS with propellant for one orbit-surface-orbit round-trip will be placed in orbit about the moon. The total vehicle is envisioned to weigh about 150,000 pounds which should be well within the capability of an uprated Saturn V/S-IVB combination. Reference II-1 shows the capability of the current launch vehicle combination to be a total of approximately 100,000 pounds in lunar orbit. The fully-loaded RLS vehicle will weigh just under 20,000 pounds.

The RLS will then be fitted for its first mission, descend to a soft-landing on the lunar surface, unload its payload of approximately 2500 pounds, and return to the orbiting base. The RLS will reach the orbiting station having expended approximately one-half of its original weight, or 10,000 pounds. During its round-trip primary control of the RLS will rest with the manned orbiting laboratory. In the event that astronauts made up all or part of the payload, an override system will be available to allow takeover of control by those on board.

The RLS has been planned to have the capability of performing 20 round-trip missions barring a major system failure. Since the initial earth launch provided resources sufficient for only one round-trip, future payload and propellant must be provided by additional launches from earth. If we use the uprated Saturn V/S-IVB combination with the capability of placing a total of 150,000 pounds in lunar orbit, we can assign 50,000 pounds to structural and other non-payload weight as well as to supplies required by the orbiting station. The remaining 100,000 pounds would provide payload and propellant for 10 round-trip missions. Therefore, after the first, only two earth launches would be required to satisfy the requirements of the RLS on its quota of twenty missions.

At the end of twenty missions it would be time for a new RLS and orbiting station crew. This could be done in a number of ways, possibly by using an uprated earth-to-earth orbit shuttlecraft to bring a new crew and RLS and return the initial team to Earth.

The mention of an uprated shuttlecraft raises the question as to its use as the supply vehicle without requiring additional Saturn V launches. The problem lies in the fact that, as shown in Reference II-2, the payload-into-earth-orbit capability of projected shuttlecraft is ten to twenty percent that of the Saturn V. This fact will probably preclude, for reasons of cost, resupply by an earth-based shuttlecraft during the 1975-85 time period.

It may, however, be possible to place all support supplies for twenty RLS missions in earth orbit with one Saturn V launch. A shuttlecraft could then ferry these supplies from earth-to-lunar orbit and return. Again this method faces drawbacks in terms of cost and because a very substantial increase in Saturn V payload capability will be required. However, a significant increase in the flexibility of the overall project would be obtained.

B. Feasibility

The approach taken in this study was to establish a concept based on thoroughly established capabilities and requiring a minimum number of advances in the state of the art. Where innovations were specified they often were based on ideas that were already under development in the space program. In summary, the philosophy was to optimize the scientific gain while minimizing the development cost.

The descent of the RLS to the lunar surface and its subsequent ascent to rendezvous while under the control of the permanent orbiting station presents what is felt to be the most difficult development problem in the RLS concept. The ability to provide the astronaut who is remotely controlling the RLS with sufficient visual information about the characteristics of the proposed landing site presents a major problem. However, although it is not part of present plans, this capability could be developed and thoroughly tested from an earth-orbiting laboratory, perhaps as a vehicle which retrieves worn out satellites and returns them to the laboratory for repair. The remote control flight problems are discussed in greater detail in the chapters on trajectory analysis (Chapter III), guidance and navigation (Chapter IV), and communications (Chapter V).

The development of a shuttlecraft which will be capable initially of round-trip missions to earth orbit is another Unites States space program which is well along in the planning stages, with first launch tentatively set for 1975. This program should provide the information on the problems of vehicle refurbishment necessary to make possible twenty RLS round-trip missions.

Chapter VIII extensively examines the development of a landing gear/liftoff platform which is a permanent integral part of the RLS vehicle. This is an advance from the Apollo program in which the landing gear was detached from the Lunar Module, serving as a launch platform which remained on the lunar surface. The permanent landing gear/liftoff platform part of the RLS vehicle is considered to be easily attainable by 1978.

The RLS concept requires the development of the following capabilities:

(1) A life-support system which will enable an astronaut to remain in lunar orbit for periods extending up to six months.

(2) An RLS vehicle weighing approximately 20,000 pounds which will

deliver a payload of about 2,500 pounds to the lunar surface and return to orbit.

(3) A computer and surface scanning system aboard the RLS vehicle which transmits sufficient information about the position and velocity of the vehicle and the condition of the lunar surface below it so as to make possible piloting of the spacecraft from the permanent orbiting base.

(4) An RLS vehicle which will be refurbishable in lunar orbit and have an expected life of twenty round trip missions.

(5) RLS landing gear which will repeatedly absorb landing shocks and provide a platform for up to twenty liftoffs.

Each of these developments will be considered briefly in the following paragraphs.

As mentioned in Section A of this chapter, a series of long-duration Earth-orbital missions is planned as the next major step in the United States manned space exploration program. It is reasonable to expect that the long-duration life support needed for the permanent orbiting base will be developed in this program.

An RLS vehicle with the payload capability described in the second item above will require some development effort as described in the chapter on propulsion (Chapter VI). Much of the needed development work has already been done, particularly in the propulsion area. No major problems are envisioned in the attainment of these vehicle capabilities by 1978.

In summary, the feasibility of the RLS concept rests on two points: extended vehicle life through continued refurbishment in space and remote piloting of the vehicle. It is felt that only on the second point will significant development effort be required that is not part of current programs. Should such a development effort be conducted the resulting capability would have applications far broader than that proposed for the RLS.

C. Cost

Any attempt to specify the actual dollar costs associated with the execution of the RLS concept would produce data that would be meaningless because of the long lead times involved. Rather let us consider the major components of the RLS from the standpoint of what costs will be attributable to the RLS mission.

	Item	Comment
1.	3 Saturn V/S-IVB launch vehicles with lunar orbit payload of 150,000 pounds	Normal state-of-the-art development will uprate Saturn to this level. RLS bears hardware and small development costs
2.	Lunar orbiting base	Modification of Earth orbiting bases previously developed. RLS bears hardware plus small development cost
3.	RLS vehicle structure	Scale-down of Apollo Lunar Module. RLS bears all costs.
4.	RLS remote control guidance and navigation system	System based on that of Lunar Module. RLS bears all costs which will be substantiated.
5.	RLS landing/liftoff system	New system. RLS bears all costs.
6.	RLS Propulsion	Off-the-shelf system. RLS bears hardware costs only.
7.	Additional RLS Subsystems	All additional subsystems will be off the shelf items. RLS bears hardware costs only.
8.	Shuttlecraft	Minor uprating of off-the-shelf vehicle. RLS bears these development plus hardware costs.

It can be seen from the above that the RLS concept has been developed so as to use existing technical capability and hardware as much as possible. The resulting costs are considered to be quite reasonable, particularly since development costs will yield systems with wide applicability in other space ventures.

D. References

II-1. Moore, R. P., "Detailed Computer Printout of Nominal Lunar Module Descent to the Lunar Surface," Private Communication, March 1970.

II-2. Watts, A. F., and Dreyfuss, D. J., "The High Cost of Reusable Orbital Transports," Journal of Astronautics and Aeronautics, January 1968.

Chapter III: Trajectory Analysis

The techniques for soft-landing on the lunar surface a payload launched from earth fall into two categories: direct and indirect. Both methods inject the vehicle on a translunar trajectory. Upon nearing the moon, the direct approach calls upon the vehicle to brake and land immediately on the lunar surface. The indirect approach requires the vehicle to first insert itself into lunar orbit. Either the entire vehicle or a separate lander vehicle can then proceed from orbit to the surface of the moon.

Obviously, the direct approach could be used to establish and support lunar bases. However, an establishment or supply mission to any point on the lunar surface requires a trip from earth of approximately three days duration, and only one point is serviced. This lack of flexibility in supporting lunar exploration efforts makes the indirect approach using the RLS concept appear far superior.

The indirect approach has been used on the Apollo missions because it allows greater flexibility in landing site selection, provides a longer period of time for final orbit determination, and often permits the use of free-return trajectories. A free-return trajectory uses the gravitational attraction of the earth and moon to return the spacecraft to the earth should the braking rockets fail when it comes time to place the vehicle in lunar orbit. Because of proposed inclination of the lunar orbit of the permanent base, it will generally not be possible to employ free-return trajectories to establish or support the RLS. Thus, this advantage is negated while the others remain.

A. The Permanent Orbiting Station

The specification of the state of a spacecraft at any instant requires the definition of six parameters, three to specify position and three to specify velocity. Using orbital elements the state of a vehicle is given by the orbital eccentricity, the semi-major axis, the inclination, the longitude of the ascending node, the argument of the perifocus, and the mean anomaly. The first three elements fix the shape of the orbit, and these are our prime concern in designing an orbit for the permanent station.

The RLS has been conceived to assist in the intensive exploration of the entire lunar surface without limitation on latitude or longitude. The RLS has, therefore, been designed to land on any reasonably flat site on the lunar surface. The primary control of the RLS will rest with the orbiting station. Thus, it is necessary that the orbiting station be in a position to monitor the RLS during thrusting periods. This requires that line-of-sight communication between the RLS and the orbiting station be maintained during periods of thrust. Although an orbiting vehicle has a range of visibility over the lunar surface depending on its altitude, the highly irregular lunar surface, including mountains rising up to 20,000 feet in height, could easily obstruct the orbiting station-RLS line-of-sight during the final critical stages of descent. In order to assure that any point on the lunar surface can be reached without discrimination, the orbiting station will be placed in an orbit having zero eccentricity and with an inclination of ninety degrees, that is, a polar circular orbit. The altitude of the orbiting station was established at eighty nautical miles. This allows the orbiting station to monitor the separation and descent-orbit-injection burns of the RLS and, assuming that the RLS employs a minimum-fuel Hohmann descent to reach an altitude of 50,000 feet above the landing sight, permits the station to be passing directly overhead during the final descent of the RLS to the landing site.

Using information from Chapter VII of Reference III-15 it is found that the surface track of a polar circular orbit of eighty nautical mile altitude will experience a westward longitude drift of 1.12 degrees/revolution. Since the orbiting base will make approximately 11.8 revolutions of the moon daily, the ground track will drift 13.2 degrees each day. It will take about twenty-seven days for the ground track to complete a circuit of the moon, so the orbiting base will pass within about one degree of longitude of every point on the lunar surface every 13.5 days.

The placing of the permanent orbiting station in polar orbit about the moon presents some drawbacks which are thought to be acceptable. The supply vehicle traveling to the station from earth may suffer a payload handicap because of the additional ΔV requirement necessary to maneuver into polar orbit. Data from Chapter IX of Reference III-15 indicates this ΔV penalty to be of the order of 2%. A polar orbit also has the disadvantage of requiring a costly (in terms of propellant) inclination change by the RLS to reach on an emergency basis a point on the lunar equator ninety degrees away from an orbital node of the station. But this same drawback would exist for a vehicle in equatorial orbit trying to reach a base at the lunar pole. In addition, it is thought to be a small penalty to pay for the negligible inclination changes required to reach any point on the lunar surface on a routine semi-monthly basis.

B. Descent to the Lunar Surface

Using information obtained from Reference III-14, a time history of the altitude and mass of the Lunar Module of an Apollo spacecraft is given in Table I for a nominal descent to the lunar surface. The profile of this descent trajectory is shown in Figures 1 and 2. This trajectory will serve as a starting point in the design of a descent trajectory for the RLS.

As shown in Figure 1 the angle between the local vertical and the line-of-sight to the orbiting vehicle at touchdown is about 21 degrees. This exceeds the maximum line-of-sight angle of 15 degrees which was established for the RLS mission. In order to achieve this line-of-sight condition the circular-orbit altitude was raised from the 60 nautical miles of the Apollo mission to 80 nautical miles. Using data from Reference III-1, the period of an orbiting vehicle in an 80 nautical mile circular orbit was calculated as 7440 seconds. The period of a Hohmann ellipse having an apofocal altitude of 80 nautical miles and a perifocal altitude of 50,000 feet is 7000 seconds. If the final phase of the RLS descent to the lunar surface is initiated at 50,000 feet and extends for a nominal duration of 450 seconds, the maximum angle between the local vertical and the line-of-sight from the orbiting station to the RLS will be about 12 degrees. This is well within our admittedly very conservative design criterion. Obviously the payload capability of the RLS could be expanded if this line-of-sight angle limit could be increased and the altitude of the orbiting station lowered. You will note that the nominal time of 450 seconds for the terminal phase of RLS descent is considerably less than the 691 seconds shown in Table III.1. This reduction is due to the

TABLE III.1

Lunar Module Altitude and Mass during Nominal Descent from Orbit

PHASE	TIME (SEC)	ALTITUDE (FT/N. MILES)	MASS(LBS)
Hohmann Transfer Burn	0.0	354653./58.5	33681.
	27.6	354697./58.5	33438.
Descent Hohmann Coast	0.0	354697./58.5	33438.
	900.0	305534./44.9	33438.
	1800.0	187465./30.7	33438.
	2700.0	73914./12.1	33438.
	3330.0	40310./6.6	33438.
Lunar Module Realignment	0.0	40310./6.6	33438.
	25.0	40071./6.6	33438.
Lunar Module Ullage Burn	0.0	40071./6.6	33438.
	7.5	40016./6.6	33372.
Descent Trim	0.0	40016./6.6	33372.
	26.0	39862./6.5	33261.
Braking, Visibility And Final Descent	0	39862./6.5	33261.
	96	37906./6.2	30155.
	200	32272./5.3	26770.
	296	22690./3.7	23629.
	400	9022./1.5	20755.
	496	-5184./-.9	18863.
	600	-9839./-1.6	17441.
	691	-10077./-1.7	16553.

fact that the RLS will weigh about one-half the amount of the Lunar Module and will have a considerably greater thrust capability.

Figure 3 depicts the three phases of powered terminal descent to the lunar surface. Since it will be more difficult for a controller in the orbiting station to evaluate the quality of a landing sight using a television camera or other viewing device than an onboard astronaut using the naked eye, emphasis will be placed on assuring adequate controller visibility and decision time during the transition phase of descent. Reference III-2 parametrically considered various landing trajectories from an altitude of 50,000 feet. In this study the problem of visibility was considered from the viewpoint of an onboard pilot. It was pointed out that the use of a scanning device of some type alleviates considerably one constraint on a pilot looking through a window, since the scanning device can be fixed externally and can be gimballed to include a wide field of view. In order to assure adequate decision time for the controller and at the same time make the institution of abort maneuvers less dangerous, it is desirable to limit the vertical descent rate and to increase the time for descent from 5,000 feet. As might be expected both these conditions require an increase in fuel over the demands of the fuel optimal trajectory. However, it was demonstrated by Bennett and Price in Reference III-2 that a trajectory having a descent rate of 100 ft/sec at 5,000 feet and a duration of about 60 seconds from the 5,000 foot altitude can be traversed with a fuel penalty on the order of 5 per cent. In addition this trajectory has satisfactory visibility conditions for an onboard pilot, thus giving a passenger on the RLS adequate information on which to base a judgment involving his overriding the command of the station controller and flying the RLS himself.

C. Lunar Ascent

As the RLS sits on the lunar surface the moon is rotating the landing site out of the plane of the orbiting station. This rotation amounts to approximately 11.8 degrees per day. The longer the RLS sits on the lunar surface, the greater the fuel penalty that will have to be paid during the ascent phase. In keeping with the support role of the RLS it is not expected that a stay-time exceeding that required for off-loading would be required.

The termination of the ascent maneuver will be a rendezvous with the orbiting station. The RLS must thus be launched with the objective of intercepting the orbiting base which is orbiting with a period of about two hours. The ascent can accomplish the interception objective by direct or indirect rendezvous. Using indirect rendezvous the interceptor would be launched into an intermediate parking orbit without considering the position of the target in its orbit at launch time. The interceptor and target would be in coplanar orbits but would have different altitudes and different periods. When the required relative angular position was achieved, the interceptor would be injected on a trajectory which would place it in the close vicinity of the target. The direct rendezvous technique requires that the interceptor not be launched from the lunar surface until the proper phasing is obtained for direct ascent to a point close enough to the target vehicle for electronic or optical acquisition.

The requirement that the initial liftoff phase of the RLS trajectory be within the line-of-sight of the orbiting base dictates an ascent trajectory that is very similar to that of descent. The ascent sequence will be initiated by the orbiting controller when the line-of-sight angle to the landing site becomes less than 15 degrees. After a vertical liftoff to an altitude of approximately 500 feet, the RLS will be injected into a Hohmann transfer ellipse having a pericynthion altitude of 50,000 feet and an apocynthion of approximately 79 miles. This initial thrust maneuver will require about 400 seconds. Upon reaching apocynthion the RLS will be again well within the field of view of the orbiting station and slightly behind it. The ensuing rendezvous will be direct. Since the RLS will be in a lower altitude orbit, it will start to decrease the phase angle between it and the orbiting station. At the discretion of the orbiting controller, the RLS-orbiting station rendezvous maneuver can be performed. The RLS ascent sequence is depicted in Figure 4.

D. Minimum-Time Rendezvous Trajectories

Up to this point in the consideration of trajectories all optimization was directed toward the minimization of fuel. It is easy to envision in the operation of the RLS that emergency situations would arise which would necessitate the return of the RLS to the orbiting base in the minimum time. This section contains an in-depth study of minimum-time rendezvous trajectories, with emphasis on the generation of trajectories that are compatible with reasonable physical constraints.

1. Introduction

An investigation of minimum-time rendezvous procedures was published by Kelley and Dunn in 1963 (Reference III-10), but no optimal control solutions were synthesized. Paiewonsky and Woodrow investigated time-optimal rendezvous when the target vehicle is in a circular orbit and in 1965 published their results including optimal trajectories (Reference III-16). In 1966 Kaminski (Reference III-8) published the results of his study of minimum-time rendezvous when the target and the interceptor are initially in the same circular orbit. Kashiwagi and Alfriend developed minimum-time trajectories for a target in an elliptical orbit and published these results in 1968 (Reference III-9).

In each of these studies the attitude of the intercepting vehicle was left free to vary at the terminals. The intercepting vehicle in the studies by Paiewonsky and Woodrow, Kelley and Dunn, and Kaminski was one with a single main thruster whose thrust direction with respect to the vehicle was fixed. Since the magnitude of the thrust was in some way limited in each case, the minimum-time rendezvous maneuver in these singular-thruster studies could be specified by finding the attitude of the thrust vector with respect to some reference as a function of time. The propulsion system of the interceptor, rather than having a single fixed-direction thruster, may be one which can apply thrust independently in the longitudinal and two transverse directions. Both the Gemini and Apollo command modules used this type of engine, while the Lunar Module used a single fixed-direction thruster. Kashiwagi and Alfriend presented results for both the single and multiple thruster cases. In all the studies the interceptor was considered to have low-magnitude thrusters, independent of the main engine, which controlled the attitude of the interceptor.

The analyses mentioned in the two preceding paragraphs found the optimal control scheme subject only to constraints on the magnitude(s) of the propulsive thrust. The results for the single-thruster case, which is the situation for the RLS, showed that during the minimum-time rendezvous maneuver the attitude of the interceptor (that is, the direction of the thrust vector) often undergoes a rapid change. It will be shown that it is possible for this rate to approach infinity. Thus, because of autopilot considerations, structural constraints, or physiological limits in the case of manned flight, it may be necessary to constrain the attitude rate of the interceptor. Such an investigation of time-optimal control with a bounded attitude rate was performed by Winfield and Johnson (Reference III-7), but no results of their proposed solution were published.

The purpose of this study is to find the control procedure, subject to both thrust magnitude and attitude rate constraints, which provides the minimum-time rendezvous of a single-thruster interceptor with a target vehicle. The optimal control problem is thus to specify the thrust magnitude and direction histories for the mission to be performed in minimum time.

The equations of motion of the interceptor are written with respect to a moving coordinate system. The origin of this system is located at the target vehicle, and the coordinate frame rotates with the angular velocity of the radius vector from the center of the gravitational field to the target. The true anomaly of the target vehicle is used as the independent variable instead of time. The relative position coordinates, normalized with respect to the initial length of the vector from the interceptor to the target, are used as the dependent variables. The equations of the vehicle are found and linearized, the linearization being valid only if the initial distance between the two vehicles is small compared to the length of the radius vector from the center of attraction to the target vehicle. Finally a system of linear differential equations representing the motion of the interceptor relative to the target are found.

It is shown that the necessary conditions for optimization, Pontryagin's maximum principle, (Reference III-17) leads to a multiple-dimensional two-point boundary value problem in the equations resulting from the satisfaction of the necessary condition. The initial values of the adjoint variables, introduced in the optimization process, and the terminal true anomaly are the missing conditions to be found in the boundary value problem.

For the particular problem of minimum-time rendezvous with bounded attitude rate, it is shown that singular controls may arise. Singularity is seen to imply that the Hamiltonian in the Pontryagin maximum principle ceases to be an explicit function of the control. Because singular arcs correspond to minimum-time transfers without attitude-rate constraint, it is hypothesized that the minimum-time constrained rate problem can be solved by employing a non-singular (regular) arc during periods of unacceptably high rate and then returning to the singular arc as soon as possible. The control problem is thus evolved as a composite of optimal arcs, the regular arcs corresponding to transfer with the attitude rate at the maximum allowable and the singular arcs corresponding to transfer at less than the maximum attitude rate.

Solution of the resultant two-point boundary-value problem having a multi-dimensional system of non-linear equations is obtained by repeated solution of a set of simultaneous linear equations. These linear equations are obtained by first generating the partial derivatives of the components of the terminal state vector with respect to the iteration variables. These partials are then used to find the change in the iteration parameters which will drive each terminal state vector component to zero. The iteration variables may include adjoint components or be all physical variables, which in turn dictate the initial adjoint vector. The term "physical variable" denotes a parameter which has explicit physical significance, such as an angle, an angular rate, the length of a subarc of a trajectory, or the total length of a trajectory. The components of the adjoint vector are replaced as iteration parameters when the use of physical variable simplifies the satisfaction of regular-singular arc junction conditions. When the initial guess at the solution is not sufficiently accurate to allow convergence by repeated solution of simultaneous linear equations, a search procedure is used to improve the initial guess.

2. Equations for the Terminal Phase of Orbital Rendezvous

The development of the terminal phase rendezvous equations used in this study are presented in detail in Reference III-9 and will only be outlined here. The original development was by Clohessy and Wiltshire in Reference III-4. The following assumptions are employed which are standard in rendezvous studies of a preliminary design nature:

(1) The target and the interceptor operate in the gravitational field of a central body with spherically symmetric mass distribution.

(2) Both vehicles are considered to be point masses.

(3) The distance between the vehicles is small relative to the distance of the target from the center of

gravitational attraction.

(4) The attitude of the interceptor, and hence the direction of thrust, is controlled by a low-thrust device which operates independently of the main engine and has no translational effect on the vehicle.

The two coordinate systems used in this development are depicted in Figure 5. The XYZ frame is inertial with its origin fixed at the center of gravitational attraction. The xyz system is centered at the target and rotates with the orbital angular velocity of this vehicle. The x-axis is directed outward along the radius vector from the origin of the XYZ system to the target; the y-axis is perpendicular to the x-axis, lies in the orbit plane of the target, and is pointed in the direction of motion of the target; the z-axis is normal to the orbit plane of the target and completes a right-handed coordinate frame. In Figure 5 the inertial positions of the target and the interceptor are denoted by the vectors $\underline{r}_t$ and $\underline{r}_i$ respectively. The $\underline{\rho}$ vector denotes the position of the interceptor with respect to the target.

Assuming that the initial magnitude of $\underline{\rho}$ is much less than the initial magnitude of $\underline{r}_t$, the scalar equations of motion of the interceptor with respect to the target are

$$\ddot{x} - 2\dot{\theta}\dot{y} - \ddot{\theta}y - \left(\dot{\theta}^2 + \frac{2\mu}{r_t^3}\right)x = \frac{T_x}{m} \qquad \text{(III-1a)}$$

$$\ddot{y} + 2\dot{\theta}\dot{x} + \ddot{\theta}x - \left(\dot{\theta}^2 - \frac{\mu}{r_t^3}\right)y = \frac{T_y}{m} \qquad \text{(III-1b)}$$

$$\ddot{z} + \frac{\mu z}{r_t^3} = \frac{T_z}{m} \qquad \text{(III-1c)}$$

where θ is the true anomaly, $\underline{T}$ is the thrust vector, μ is the gravitational constant, and m is the mass of the interceptor.

Equations (III-1) are a set of linear differential equations with periodic coefficients, since r_t, $\dot\theta$ and $\ddot\theta$ are periodic with a period equal to the orbital period of the target vehicle. A much simpler form of these equations is obtained if the true anomaly is substituted for time as the independent variable, and if the transformation

$$\xi \equiv \frac{x}{r_t}, \ \eta \equiv \frac{y}{r_t}, \ \zeta \equiv \frac{z}{r_t} \tag{III-2}$$

is made. By using several basic equations of orbital mechanics and differentiating, the following identities are obtained:

$$\dot\theta r_t \xi' = \dot x - \frac{e\dot\theta \sin\theta}{1+e\cos\theta}\, x \tag{III-3}$$

$$\dot\theta^2 r_t \xi'' = \ddot x + \left(\frac{\mu}{r_t^3} - \dot\theta^2\right)x \tag{III-4}$$

$$\ddot\theta = -2\dot\theta^2 e \sin\theta/(1+e\cos\theta) \tag{III-5}$$

where ( )' denotes differentiation with respect to the true anomaly θ and e is the eccentricity of the orbit of the target vehicle. Employing similar identities for η and ζ, the scalar equations of motion become

$$\xi'' - \frac{3\xi}{1+e\cos\theta} - 2\eta' = \frac{T_x}{m r_t \dot\theta^2} \tag{III-6a}$$

$$\eta'' + 2\xi' = \frac{T_y}{m r_t \dot\theta^2} \tag{III-6b}$$

$$\zeta'' + \zeta = \frac{T_z}{m r_t \dot\theta^2} \tag{III-6c}$$

For computational purposes it is advantageous to make the following additional transformations:

$$x_1 = \frac{R_p}{L}\xi\,, \quad x_2 = \frac{R_p}{L}\xi'$$

$$x_3 = \frac{R_p}{L}\eta, \quad x_4 = \frac{R_p}{L}\eta' \qquad \text{(III-7)}$$

$$x_5 = \frac{R_p}{L}\zeta, \quad x_6 = \frac{R_p}{L}\zeta'$$

and

$$\frac{T_x}{m} = \frac{U}{\beta(\theta)}u_x$$

$$\frac{T_y}{m} = \frac{U}{\beta(\theta)}u_y \qquad \text{(III-8)}$$

$$\frac{T_z}{m} = \frac{U}{\beta(\theta)}u_z\,.$$

The perifocal distance of the target vehicle orbit is denoted R_p and L is an arbitrary length whose magnitude is chosen so that $x_i = o(1)$, $i = 1, 2, \ldots 6$. A reasonable value of L is

$$L = x^2(\theta_o) + y^2(\theta_o) + z^2(\theta_o). \qquad \text{(III-9)}$$

U is the thrust per unit mass being generated by the interceptor, and $\beta(\theta)$ is the ratio of the mass of the interceptor to its initial mass. The control functions, u_x, u_y, u_z are restricted by the equation

$$1 - \underline{u}^T\underline{u} = 0 \qquad \text{(III-10)}$$

which limits the control vector to the unit hypersphere.

Using matrix notation the equation of motion becomes

$$\underline{x}'(\theta) = A(\theta)\underline{x}(\theta) + B(\theta)\underline{u}(\theta) \tag{III-11}$$

where $\underline{x}(\theta)$ is the state vector defined by

$$\underline{x} = \begin{vmatrix} x_1 \\ x_2 \\ x_3 \\ x_4 \\ x_5 \\ x_6 \end{vmatrix} \tag{III-12}$$

and $\underline{u}(\theta)$ is the control function defined by

$$\underline{u} = \begin{vmatrix} u_x \\ u_y \\ u_z \end{vmatrix} \tag{III-13}$$

The matrices $A(\theta)$ and $B(\theta)$ are

$$A = \begin{bmatrix} 0 & 1 & 0 & 0 & 0 & 0 \\ \frac{3}{1+e\cos\theta} & 0 & 0 & 2 & 0 & 0 \\ 0 & 0 & 0 & 1 & 0 & 0 \\ 0 & -2 & 0 & 0 & 0 & 0 \\ 0 & 0 & 0 & 0 & 0 & 1 \\ 0 & 0 & 0 & 0 & -1 & 0 \end{bmatrix} \tag{III-14}$$

$$B = \frac{UR_p^3(1+e)^2}{\mu L(1+e\cos\theta)^3}\begin{bmatrix} 0 & 0 & 0 \\ 1 & 0 & 0 \\ 0 & 0 & 0 \\ 0 & 1 & 0 \\ 0 & 0 & 0 \\ 0 & 0 & 1 \end{bmatrix} \qquad \text{(III-15)}$$

where the relation

$$\frac{1}{r_t\dot{\theta}^2} = \frac{R_p^2(1+e)^2}{\mu(1+e\cos\theta)^3} \qquad \text{(III-16)}$$

was used in defining B. Note that for simplicity $\beta(\theta)$ has been fixed as 1.0, thus assuming that the mass of the interceptor remains fixed during rendezvous.

From (III-1) or (III-6) it is apparent that the equations governing motion in the orbit plane of the target vehicle are decoupled from the equations governing motion normal to the orbit plane. Thus the one problem can be considered as two completely independent problems.

As noted above, several investigator's have discovered that periods of very rapid change in the interceptor's attitude often occur when seeking a solution to the in-plane minimum-time rendezvous problem and using an interceptor with a single body-fixed thruster. Since we are seeking to limit the interceptor's attitude rate in solving the in-plane problem, the equations of motion in this study are limited to (III-6a) and (III-6b). In this investigation it has been assumed that the interceptor has only a single main thruster available which has no gimbal capability.

It was also assumed that the target vehicle is moving in a circular orbit. This assumption was made to simplify the equations of motion and has no significant bearing on the results of this investigation. Using this last assumption the in-plane equations of motion can be written in matrix form as

$$\underline{x}'(\theta) = C(\theta)\underline{x}(\theta) + D(\theta)\underline{u}(\theta) \tag{III-17}$$

where

$$\underline{x} = \begin{pmatrix} x_1 \\ x_2 \\ x_3 \\ x_4 \end{pmatrix} \tag{III-18}$$

$$\underline{u} = \begin{pmatrix} u_x \\ u_y \end{pmatrix} \tag{III-19}$$

$$C = \begin{bmatrix} 0 & 1 & 0 & 0 \\ 3 & 0 & 0 & 2 \\ 0 & 0 & 0 & 1 \\ 0 & -2 & 0 & 0 \end{bmatrix} \tag{III-20}$$

$$D = \frac{UR_p^3}{\mu L} \begin{bmatrix} 0 & 0 \\ 1 & 0 \\ 0 & 0 \\ 0 & 1 \end{bmatrix} = \frac{\gamma}{\varepsilon} \begin{bmatrix} 0 & 0 \\ 1 & 0 \\ 0 & 0 \\ 0 & 1 \end{bmatrix} \tag{III-21}$$

In (III-21) $\varepsilon = \frac{L}{R_p}$ and $\gamma = \frac{U}{g_o}$ where $g_o = \frac{\mu}{R_p^2}$ is the gravitational acceleration at perifocus in the orbit of the target vehicle.

3. Formulation of the Minimum-time Rendezvous Problem with Constrained Attitude Rate

By applying the Pontryagin maximum principle to the general time-optimal control problem, we obtain the following equation for the Hamiltonian.

$$H = p_1x_2 + p_2(3x_1 + 2x_4 + n\cos\alpha) + p_3x_4 + p_4(-2x_2 + n\sin\alpha) - 1. \qquad \text{(III-22)}$$

The p_i represent the components of an auxiliary vector introduced by the maximum principle and are called the adjoint or costate variables. The variable $n = \frac{U_{max}R_p^3}{\mu} = \frac{\gamma}{\varepsilon}$ and α is the angle measured counterclockwise between the thrust direction vector and the x-axis of the rotating coordinate system so that $u_x = \cos\alpha$, $u_y = \sin\alpha$. The complete derivation of (III-22) and the following equations which govern the adjoint vector and the state vector can be found in Reference III-9.

$$\underline{p}' = E\underline{p} \qquad \text{(III-23)}$$

$$\underline{x} = C\underline{x}(\theta) + d\underline{u}(\theta) \qquad \text{(III-24)}$$

where

$$E = \begin{bmatrix} 0 & -3 & 0 & 0 \\ -1 & 0 & 0 & 2 \\ 0 & 0 & 0 & 0 \\ 0 & -2 & 0 & 1 \end{bmatrix} = -C^T, \qquad \text{(III-25)}$$

C is defined as in (III-20), and

$$D = n \begin{bmatrix} 0 & 0 \\ 1 & 0 \\ 0 & 0 \\ 0 & 1 \end{bmatrix} \qquad \text{(III-26)}$$

We find that in order to maximize H, $\underline{u}$ and $\underline{s} = \begin{pmatrix} p_2 \\ p_4 \end{pmatrix}$ must be collinear. Their cross product is zero so that

$$p_2 \sin\alpha - p_4 \cos\alpha = 0 \ , \tag{III-27}$$

and the attitude angle α can be defined in terms of the adjoints as

$$\tan\alpha = p_4/p_2 \ . \tag{III-28}$$

Note that it is quite possible for p_2 and p_4 in (III-28) to switch sign simultaneously. This would give a 180 degree jump in the value of α and imply that the angular rate α' was infinite. This point will be discussed further in the following section.

After considering the above equations it becomes clear that solving the minimum-time in-plane rendezvous problem without constraining the attitude rate is a two-point boundary value problem with unknown parameters at both boundaries. An initial adjoint vector must be selected such that by using (III-23) and (III-28) an attitude-angle time history is generated which, when used in (III-24), will produce a state vector trajectory passing through the origin. At the terminal boundary the time at which the state vector reaches the origin must be chosen.

In adjusting the optimization equations, i.e., (III-23), (III-24), and (III-28), to include a constraint on the attitude rate, a suggestion of Johnson and Winfield in Reference III-7 is followed. The state vector is expanded to include the control variable α which is now denoted x_5. The attitude rate (α') is then designated as the control variable and is denoted as σ. The Hamiltonian then becomes

$$H = p_1x_2 + p_2(3x_1 + 2x_4 + n \cos x_5) + p_3x_4 + p_4(-2x_2 + n \sin x_5) + p_5\sigma - 1. \tag{III-29}$$

The optimal control is that which maximizes H and is therefore

$$\sigma = \Omega \text{ sign}(p_5) \tag{III-30}$$

where Ω is the magnitude of the maximum allowable attitude rate. The governing equations for the state and adjoint vectors can then be written out as

$$x_1' = x_2 \tag{III-31a}$$

$$x_2' = 3x_1 + 2x_4 + n \cos x_5 \tag{III-31b}$$

$$x_3' = x_4 \tag{III-31c}$$

$$x_4' = - 2x_2 + n \sin x_5 \tag{III-31d}$$

$$x_5' = \sigma \tag{III-31e}$$

and

$$p_1' = - 3p_2 \tag{III-32a}$$

$$p_2' = - p_1 + 2p_4 \tag{III-32b}$$

$$p_3' = 0 \tag{III-32c}$$

$$p_4' = - 2p_2 - p_3 \tag{III-32d}$$

$$p_5' = n(p_2 \sin x_5 - p_4 \cos x_5). \tag{III-32e}$$

There are numerous meaning attached to the word "singular" when used in a mathematical context. Dunn in Reference III-5 discusses at length the classification of singular and nonsingular extremals in the Pontryagin maximum principle. In the present investigation a "singularity" is said to occur when the Hamiltonian in the maximum principle ceases to be an explicit function of the control variable.

A singular arc is generated when this singularity exists over a finite length of time. A nonsingular or regular arc is generated while the Hamiltonian remains a function of the control variable. In the context of this study, a regular arc is further described to be one on which the attitude rate has its maximum allowable magnitude.

From (III-29) it is obvious that a singularity occurs when $p_5 = 0$. If this condition lasts only for an instant, then the attitude rate has simply changed sign (bang-bang control). If the conditions $p_5 = 0$ and $p_5' = 0$ are reached simultaneously, then the singularity will extend over finite period, and a singular arc will be generated.

It should be pointed out that should $p_5 = 0$ in (3.29), then the Hamiltonian would become identical to that which was obtained when considering the control problem without an attitude rate constraint. However, this is not sufficient to guarantee that the singular arc occuring as a subarc of the total extremal in the constrained attitude rate problem satisfies the necessary condition that H be maximized. The generalized Legendre-Clebsch condition presented by Robbins in Reference III-19 and Kelley, Kopp, and Moyer in Reference III-10 must be met. This condition states that

$$(-1)^q \frac{\partial}{\partial u}\left(\frac{d^{2q}}{dt^{2q}}\left(\frac{\partial H}{\partial \underline{u}}\right)\right) \leq 0 \qquad \text{(III-33)}$$

where q is the least positive integer such that

$$\frac{d^{2q}}{dt^{2q}}\left(\frac{\partial H}{\partial \underline{u}}\right) \equiv \underline{0}^T \qquad \text{(III-34)}$$

is explicitly dependent on $\underline{u}$. Performing the operations defined in (III-33) we find that $q = 1$ and

$$-(p_2 \cos x_5 + p_4 \sin x_5) \leq 0 \qquad \text{(III-35)}$$

From (III-28)

$$\tan x_5 = p_4/p_2 \qquad \text{(III-36)}$$

which yields

$$\sin x_5 = \frac{\pm p_4}{(p_4^2+p_2^2)^{1/2}}, \quad \cos x_5 = \frac{\pm p_2}{(p_4^2+p_2^2)^{1/2}} . \qquad \text{(III-37)}$$

Substituting (III-37) in (III-35) and choosing the positive sign for the square root gives

$$-(p_2^2+p_4^2)^{1/2} \leq 0 , \qquad \text{(III-38)}$$

and the Legendre-Clebsch condition is obviously satisfied.

4. A Solution of the Minimum-time Rendezvous Problem with Constrained Attitude Rate

a. Solution of the Unconstrained Minimum-time Rendezvous Problem

Kashiwagi and Alfriend applied a dependable iteration procedure for solving the two-point boundary-value problem which results when seeking a solution to the unconstrained minimum-time in-plane rendezvous problem. The technique involved the utilization of the Fletcher-Powell search procedure (Reference III-6) with gradient directions determined by using Neustadt's method. Their solution allowed the attitude of the interceptor to vary at the terminals. Details of the technique are contained in Reference III-9.

The attitude and attitude rate time histories for two typical trajectories generated using the procedure employed by Kashiwagi and Alfriend are shown in Figures 2-5. These two cases both contain regions of high attitude rate. In Case I the high-rate region occurs near a terminus, in this case at the start of the trajectory. The high rate region in Case II appears in the middle of the trajectory. The unconstrained minimum-time trajectories considered in this investigatio will be distinguished by whether the high rate region occurs near a terminus (Type I trajectory) or in the middle of the trajectory (Type II trajectory).

b. Constructing Minimum-time Trajectories with Free Terminal Attitude Angles Using Singular and Regular Arcs

When presented with the task of developing a minimum-time rendezvous for a given target and interceptor position, it is assumed that one would first generate a solution with no attitude rate constraint. If a trajectory with no unacceptable attitude rate regions resulted, the problem would be solved. If an unacceptable region did occur, the following method of solution appears to be a very satisfactory means of obtaining constrained optimal trajectories.

In place of the high rate segment of the unconstrained trajectory, generate an arc using the maximum allowable attitude rate. As described in Section 3, this portion of the trajectory will be termed a "regular" arc. If the high rate region occurred near a terminus of the trajectory, the regular arc would be followed or preceded by an unconstrained or "singular" arc on which the maximum attitude rate is never achieved. The two arcs in combination would satisfy the state vector conditions at both terminals.

Since the initial and final state vectors of a trajectory can be chosen arbitrarily (It is always possible to start at the origin and travel to any other point.), only cases where the high rate region occurs near the beginning of the trajectory have been considered in this study. The constrained minimum-time solutions for these cases will be termed "regular-singular" trajectories. If the unacceptable region occurs in the middle of the trajectory, the regular arc would be preceded and followed by singular arcs. These constrained trajectories will be denoted "singular-regular-singular" trajectories.

c. Degrees of Freedom in Solving the Constrained Minimum-time Problem

It has been pointed out above that the development of minimum-time rendezvous trajectories without rate constraint requires the solution of a two-point boundary-value problem with unknown parameters at both terminals. The solution of the constrained problem likewise requires the determination of unknown parameters at both ends of the trajectory. Since the state vector equations of motion are non-linear in both the constrained and unconstrained problems, it is necessary to integrate these equations numerically. The adjoint time history may be generated by using a state transition matrix which will be discussed below. State and adjoint vector time histories must be generated repeatedly, adjusting the free variables until the state vector conditions (and in some cases adjoint vector conditions) are satisfied at both terminals. The degrees of freedom in the problem are the actual number of variable quantities or parameters in the iteration procedure.

d. Junction and Terminal Conditions

The first problem that must be surmounted in generating multiple-arc minimum-time trajectories is the determination of the required adjoint conditions at junction and terminal points and the development of means to satisfy these conditions. Consider first junction points. Both the state vector $\underline{x}$ and the adjoint vector must be continuous across the junction. Thus, since $p_5 = p_5' = 0$ on a singular arc, both p_5 and p_5' must reach zero simultaneously at the point on the regular arc that is to be a junction point with a singular arc.

At terminal points the first four components of the expanded state vector (two components of position and two components of velocity) are specified. The fifth component, the angle specifying the direction of thrust, is left free to vary. If a component of the state vector is left free to vary, by the transversality condition (see Reference III-3) the corresponding component of the adjoint vector must be zero. Therefore, p_5 must be zero at the terminals. Obviously this requirement is already satisfied if a terminus is reached while on a singular arc. Regular arcs must be adjusted so that this condition is met.

Before proceeding with the development of the equations that must be satisfied in order to ensure that the adjoint junction and terminal conditions are satisfied, it is necessary to consider the state transition matrix governing the adjoint vector. Recalling that the true anomaly has been substituted for time as the independent variable, the state transition matrix is

$$\Phi = \begin{bmatrix} 4-3\cos\theta & -3\sin\theta & 6\theta-6\sin\theta & 6\cos\theta-6 \\ -\sin\theta & \cos\theta & 2\cos\theta-2 & 2\sin\theta \\ 0 & 0 & 1 & 0 \\ 2-2\cos\theta & -2\sin\theta & 3\theta-4\sin\theta & 4\cos\theta-3 \end{bmatrix} . \qquad \text{(III-39)}$$

Then

$$\begin{vmatrix} p_1(\theta) \\ p_2(\theta) \\ p_3(\theta) \\ p_4(\theta) \end{vmatrix} = \Phi \begin{vmatrix} p_1(0) \\ p_2(0) \\ p_3(0) \\ p_4(0) \end{vmatrix} \qquad \text{(III-40)}$$

e. Regular-Singular Trajectories

As stated previously regular-singular trajectories will be substituted for unconstrained trajectories having an unacceptably high attitude rate near the start of the trajectory. Recall that at the start of the regular arc, i.e., at the initial point of the trajectory, p_5 is zero since s_5 is free. At the end of the regular arc, when jumping to a singular arc, both p_5 and p_5' must be zero.

The true anomaly will be defined to be zero at the initial point of the trajectory. At this point we can say in general that

$$p_4(0) = k\,p_2(0) \tag{III-41}$$

$$p_2(0) = k\ell\,p_1(0) - \ell\,p_3(0) \tag{III-42}$$

where k and ℓ are arbitrary constants. The motivation for the choice of these equations will be made clear later in this section. On a regular arc the attitude angle varies at a constant rate so that

$$x_5(\theta) = x_5(0) + \sigma\theta \quad . \tag{III-43}$$

From (III-32e)

$$p_5' = n(p_2 \sin x_5 - p_4 \cos x_5) \quad . \tag{III-44}$$

Setting the constant n to unity and using (III-43), (III-44) becomes

$$p_5' = p_2 \sin(x_5(0)+\sigma\theta) - p_4 \cos(x_5(0)+\sigma\theta) \quad . \tag{III-45}$$

The use of the components of the adjoint vector in optimization problems has always suffered from the fact that the values of these parameters generally have no physical significance. For this reason obtaining a reasonable first guess to start the iteration procedure is usually very difficult. Without a first guess that is close to that which gives convergence, many iteration procedures fail to converge to the desired solution. In making a first guess to solve the constrained minimum-time problem, the components of the adjoint vector and the total flight time that gave convergence in the unconstrained problem serve to provide reasonable values. However it was noticed that by iterating on variables having physical significance an even better first guess can be made, and the iteration procedure required to specify the initial attitude angle and the length of the regular arc can be avoided.

In the new procedure the following variables are chosen as the iteration parameters; the length of the regular arc, θ_r; the attitude angle at the junction of the regular and singular arcs, $x_5(\theta_r)$; the attitude rate at this junction $x_5'(\theta_r)$; and the total length of the flight. Using these parameters the choice of a first guess was initially made as follows. Take the initial attitude angle from the unconstrained solution and increase the length of the regular arc until the attitude angle on the regular arc will correspond to that at the corresponding time on the unconstrained trajectory. Choose this value as the length of the regular arc, the angle where agreement occurs as $x_5(\theta_r)$, and the angular rate on the unconstrained trajectory at this point as $x_5'(\theta_r)$. Use the minimum time from the unconstrained trajectory as the first guess for the minimum time.

Having chosen the values of these parameters, it becomes necessary to generate the adjoint vector at the beginning of the regular arc which will give these values at the end. Recalling p_5' must be zero at the end of the regular arc we have

$$p_5' = 0 = p_2 \sin x_5 - p_4 \cos x_5 \qquad \text{(III-46)}$$

and

$$\tan x_5 = p_4/p_2 \quad . \tag{III-47}$$

Differentiating with respect to θ in (III-47) gives

$$x_5' \sec^2 x_5 = (p_4' p_2 - p_4 p_2')/p_2^2 \quad . \tag{III-48}$$

Substituting the adjoint differential equations for p_2' and p_4' yields

$$x_5' \sec^2 x_5 = \frac{(-2p_2-p_3)p_2-(2p_4-p_1)p_4}{p_2^2} \tag{III-49}$$

Solving for $\sec^2 x_5$ using (III-47) gives

$$x_5' = \frac{-[(2p_2+p_3)p_2+p_4(2p_4-p_1)]}{(p^2+p_4^2)} \quad . \tag{III-50}$$

Since $x_5(\theta_r)$ has been chosen, k in the following equation has been fixed.

$$p_4 = k\ p_2 \quad . \tag{III-51}$$

Employing the relationship of (III-42), namely,

$$p_2(\theta_r) = k\ell\ p_1(\theta_r) - \ell\ p_3\ (\theta_r) \tag{III-52}$$

and substituting both (III-51) and (III-52) in (III-50), we can solve for ℓ

$$\ell = \frac{1}{(x_5'(\theta_r)+2)(1+k^2)} \tag{III-53}$$

Since $x_5'(\theta_r)$ is chosen ℓ is fixed. Because the solution does not depend on the magnitude of the adjoint vector, p_3 is chosen arbitrarily. At the start of the regular arc $p_5 = 0$. If we assume for the moment that $\theta = 0$ at the end of the regular arc, we can use $\theta = -\theta_r$ and obtain p_1 at the regular-singular junction. Then (III-51) and

(III-52) are used to give p_2 and p_4. The state transition matrix for the adjoint vector is then used to find the adjoint vector at the start of the regular arc. Details of the procedure can be found in Reference III-13.

There is no constraint present which prevents p_2 and p_4 from simultaneously having a small magnitude. Examination of (III-50) shows that should p_2 and p_4 approach zero simultaneously, the magnitude of the attitude rate would become very large. In the event that p_2 and p_4 should pass through zero simultaneously, it is clear from (III-47) that x_5 would rotate 180 degrees instantaneously. As previously mentioned this implies an infinite magnitude for x_5'.

By using (III-51) in (III-50) and solving for p_2, the following equation is obtained

$$p_2 = (p_1 k - p_3)/(x_5' + k^2 x_5' + 2k^2 + 2) = k\ell \, p_1 - \ell \, p_3$$

The motivation for equations (III-41) and (III-42) should now be obvious.

f. Singular-Regular-Singular Trajectories

The solution of the singular-regular-singular minimum-time problem clearly also requires an iteration procedure to solve the two-point boundary-value problem. Again four degrees of freedom are available for iteration. It is possible to directly select values of the adjoint vector at the start of the regular arc and to iterate on these values. However, the procedure required to satisfy the regular arc terminal conditions is so complicated as to be impractical in an iteration scheme. The parameters which have been chosen as iteration variables have the advantage of physical significance as well as simplicity. These parameters are: the length of the initial singular arc, θ_s; the attitude angle at the first singular-regular arc junction, $x_5(\theta_s)$; the length of the regular arc, θ_r; and the total duration of the trajectory.

The basic equations used in developing the procedure to satisfy the regular arc terminal conditions and generate the initial adjoint vector are nearly the same as those presented for the regular-singular trajectory in the previous section. Therefore they will not be presented here, but the exact details are given in Reference III-13.

g. Some Comments about Multiple-arc Optimal Trajectories

Before discussing the numerical technique used to generate multiple-arc optimal trajectories, a number of important points must be made. First of all, although the necessary condition for optimality has been satisfied, there is no sufficiency condition available to guarantee the uniqueness of these trajectories. The comment by Kelley, Kopp, and Moyer in Reference III-11 that very little work has been done toward the development of sufficiency conditions is still correct.

Reference III-11 also contains an excellent discussion of the jump conditions that must be met at regular-singular arc junctions. As mentioned previously a necessary condition for the singular arcs in a regular-singular arc sequence to be maximizing is that

$$(-1)^q \frac{\partial}{\partial u}\left[\frac{d^{2q}}{dt^{2q}}\left(\frac{\partial H}{\partial u}\right)\right] \leq 0 \quad . \qquad \text{(III-55)}$$

along the entire arc. Along the regular arc $(\frac{\partial H}{\partial u})\Delta u<0$, where Δu is any variation from the control on the regular arc. If, as shown in Figure 10, the regular arc corresponds to the upper limit of u, then Δu must be negative and $\frac{\partial H}{\partial u}>0$. However, $\frac{\partial H}{\partial u}$ can also be evaluated in the neighborhood of the junction point on the regular arc by a Taylor series expansion, leading to the conclusion that at the junction point

$$\frac{\partial}{\partial u}\left[\frac{d^{2q}}{dt^{2q}}\left(\frac{\partial H}{\partial u}\right)\right] > 0 \quad . \tag{III-56}$$

In order to satisfy the inequalities in both (III-55) and (III-56), q must be odd. A similar consideration of a jump discontinuity in the control u to the lower bound produces the same conclusion. Therefore, if a maximizing singular arc is joined to a regular arc wtih a jump discontinuity in the control u, q must be odd.

Figure 11 depicts an example in which the singular arc joins the regular arc when the control has become saturated and there is no jump in u. In this case evaluating $\frac{\partial H}{\partial u}$ on the regular arc gives

$$\frac{\partial}{\partial u}\left[\frac{d^{2q}}{dt^{2q}}\left(\frac{\partial H}{\partial u}\right)\right] < 0 \quad . \tag{III-57}$$

To satisfy (III-55) and (III-57) q must be even.

Figure 12 shows the case in which the control has become saturated, but a jump to the lower control limit is desired. In this case q must be odd.

We have previously shown that q = 1 in the minimum-time in-plane rendezvous problem. A jump in the control must therefore occur at the regular-singular arc junctions. This has two significant effects in the present study. First, in the case where we are substituting regular arcs corresponding to a particular control limit for segments of the trajectory with unacceptably high attitude rate, we must be able to jump to a particular control boundary. Thus the control must either not saturate or saturate to the opposite control boundary. Since saturation to the opposite control boundary is highly unlikely physically, we can say in general that the jump to the regular arc must occur prior to the onset of saturation. The second effect results from the fact that a discontinuity in the control must occur at junctions. This discontinuity is undesirable, but is much more physically acceptable than high attitude rates.

It should finally be noted that in the solution there is no explicit control of the attitude rate on the singular arc during the iteration procedure. Thus it is possible for the attitude rate to exceed the limits set for the regular arcs. This problem will be discussed further in the following section.

5. Numerical Technique

A major goal of this study was the development of a dependable iteration procedure which would solve multiple-arc two-point boundary value problems. As mentioned in the previous chapter, the Newton-Raphson or quasilinearization procedure was recommended by Winfield and Johnson in Reference III-7. This method presented a number of difficulties in performing the iteration and had had little previous success in solving problems with free terminal time. Therefore this method was rejected at the outset.

It was initially decided to use the gradient technique to minimize the error norm. The error norm was defined as the square root of the sum of the squares of the position and velocity components at the final point of the trajectory, that is,

$$\text{ERNORM} = [x_1^2(\theta_f)+x_2^2(\theta_f)+x_3^2(\theta_f)+x_4^2(\theta_f)]^{1/2} \quad . \qquad \text{(III-58)}$$

The interceptor was considered to have achieved rendezvous when the error norm became less than .001. This accuracy placed the vehicles within approximately one hundred feet of each other. Numerical integration was performed using a fourth-order Runge-Kutta scheme over the entire trajectory. The first four components of the adjoint vector were updated using the state transition matrix.

The particular gradient technique employed was that suggested by Fletcher and Powell in Reference III-6. This method has the property of second-order convergence, that is, the procedure converges in n iterations when the function is a quadratic of n variables. Although this method is recommended for use only in cases where the gradient can be computed analytically, it was hoped that by using sufficiently small perturbations in generating the numerical partials $\frac{\partial(\text{ERNORM})}{\partial(\text{PARAMETER})}$ satisfactory accuracy could be obtained. It should be noted that this method has no means of distinguishing relative minima from the absolute minimum. In the initial runs made with this method, it appeared it was either converging fairly rapidly to a relative minimum or falling into long narrow valleys that could not be escaped with the accuracy inherent in the use of numerical partials. Subsequent investigations strongly indicated that relative minima were being obtained.

The choice now seemed to be between changing initial guesses until a path to an error norm which satisfied our convergence criterion was found or altering the calculation of the error norm slightly so that the iteration would jump off the flat place at which it had been stopped and toward the convergence limit. The first choice was dismissed as unsatisfactory. The second choice was briefly attempted by placing a multiplicative factor in front of the largest component of the error norm. This had the effect of forcing this component to zero at the expense of the others. At some point the multiplicative factor was removed, and the iteration proceeded in normal fashion. This attempt was completely unsuccessful.

At this stage it was noticed that, although the error norm could not be improved at those points which appeared to be relative minima, the behavior of the components of the error norm was reasonably linear in their neighborhood. Therefore, when the Powell search procedure (Reference III-18) ceased to give improvement in the error norm, the following equations were employed:

$$
\begin{aligned}
x_1 + \frac{\partial x_1}{\partial x_5'} \Delta x_5' + \frac{\partial x_1}{\partial x_5} \Delta x_5 + \frac{\partial x_1}{\partial \theta_r} \Delta\theta_r + \frac{\partial x_1}{\partial \theta_f} \Delta\theta_f &= 0 \\
x_2 + \frac{\partial x_2}{\partial x_5'} \Delta x_5' + \frac{\partial x_2}{\partial x_5} \Delta x_5 + \frac{\partial x_2}{\partial \theta_r} \Delta\theta_r + \frac{\partial x_2}{\partial \theta_f} \Delta\theta_f &= 0 \\
x_3 + \frac{\partial x_3}{\partial x_5'} \Delta x_5' + \frac{\partial x_3}{\partial x_5} \Delta x_5 + \frac{\partial x_3}{\partial \theta_r} \Delta\theta_r + \frac{\partial x_3}{\partial \theta_f} \Delta\theta_f &= 0 \\
x_4 + \frac{\partial x_4}{\partial x_5'} \Delta x_5' + \frac{\partial x_4}{\partial x_5} \Delta x_5 + \frac{\partial x_4}{\partial \theta_r} \Delta\theta_r + \frac{\partial x_4}{\partial \theta_f} \Delta\theta_f &= 0 \quad .
\end{aligned}
\tag{III-59}
$$

Solving for the unknown changes in the parameters which will drive each component of the error norm to zero we have in matrix form

$$
\begin{bmatrix}
\partial x_1/\partial x_5' & \partial x_1/\partial x_5 & \partial x_1/\partial \theta_r & \partial x_1/\partial \theta_f \\
\partial x_2/\partial x_5' & \partial x_2/\partial x_5 & \partial x_2/\partial \theta_r & \partial x_2/\partial \theta_f \\
\partial x_3/\partial x_5' & \partial x_3/\partial x_5 & \partial x_3/\partial \theta_r & \partial x_3/\partial \theta_f \\
\partial x_4/\partial x_5' & \partial x_4/\partial x_5 & \partial x_4/\partial \theta_r & \partial x_4/\partial \theta_f
\end{bmatrix}^{-1}
\begin{pmatrix} -x_1 \\ -x_2 \\ -x_3 \\ -x_4 \end{pmatrix}
=
\begin{pmatrix} \Delta x_5' \\ \Delta x_5 \\ \Delta\theta_r \\ \Delta\theta_f \end{pmatrix}
\tag{III-60}
$$

where $[\ \ ]^{-1}$ denotes the inverse of a matrix. Equation (III-60) was easily solved using a linear simultaneous equation subroutine package available on the IBM 360. Using the results of (III-60) repeatedly, convergence was generally obtained within two or three steps. It was noteworthy that the changes in the iteration parameters required to give convergence were often quite large when compared with the perturbations used in developing the matrix of partials and that the error norm often increased during the process before converging.

The natural question at this point was whether the procedure would converge starting from an initial guess rather than waiting until the Powell method had stopped giving improvement. All types of cases were run using only the simultaneous equation method. Unconstrained cases were included. The results showed that the answer to the question is generally affirmative, with the results depending on the quality of the initial guess and on the sensitivity of the partials in the particular trajectory involved. In those cases which do not converge after several parameter adjustments, the Powell search procedure can be used to improve the best guess found up to that point. The simultaneous equation and Powell search technique are then employed alternatively until convergence is obtained.

6. Presentation and Discussion of Numerical Results

a. Numerical Results for Four Sample Cases

A total of four cases have been selected to demonstrate the use of trajectories with multiple optimal arcs in obtaining minimum-time in-plane rendezvous with constrained attitude rate. Two Type 1 (high initial rate) cases and two Type 2 (high intermediate rate) cases have been chosen. Cases I and II are respectively trajectories of Types 1 and 2. They are typical of the trajectories with high attitude rate which would be encountered most frequently in developing minimum-time rendezvous trajectories. Cases III and IV are also of Types 1 and 2 respectively, but in these cases the unconstrained trajectories contain attitude rates exceeding 1.0×10^5.

The unconstrained minimum-time rendezvous trajectories for Cases I-IV are depicted in Figure 13. Each of these trajectories was generated using n = 3 and an integration step size of .04 radians. It should be noted that the occurrence of high attitude rate is independent of the starting position and the path of the time-optimal trajectory. Only the unconstrained trajectories have been depicted since little change in the shape of the trajectory was found when the attitude rate was constrained.

Figures 14 and 15 present the attitude and attitude rate histories for Case I. It should be noted immediately in Figure 15 that when the attitude rate was constrained to $\alpha' = -3$, the attitude rate on the singular arc at the regular-singular arc junction exceeds the maximum allowable magnitude. As pointed out previously, this is one of the pitfalls that cannot be avoided when using a singular arc as part of the total optimal trajectory. It appears that a second regular arc segment having $\alpha' = +3$ would be required in order to generate a constrained minimum-time trajectory which includes a singular arc and still remains within the attitude rate limit. Rather than attempting to generate such a trajectory, it was felt that it would be more enlightening to generate a bang-bang trajectory with $|\alpha'|_{max} = 3$. The attitude history for this trajectory is shown in Figure 14 and the time required to rendezvous is given in Table III.2.

The trajectories shown in Figures 14 and 15 converged very rapidly using the results of the solution of (III-60). In no instance was a search required and less than fifty trajectory evaluations were required in the worst case. However, when the maximum value of α' was reduced to -2, no convergence could be obtained. Examination of the increasing length of the regular arc as the maximum allowable $|\alpha'|$ is decreased seems to indicate that it is simply not possible to reach the origin using a regular arc having $\alpha'_{max} = -2$.

Table III.2

Comparison of Minimum Rendezvous Times for Four Sample Cases

Case I

Trajectory	Final Time
Unconstrained	.893519
$\alpha'_{max} = 10$	.893529
$\alpha'_{max} = 5$	.893925
$\alpha'_{max} = 3$	.897605
$\alpha'_{max} = 3$ (bang-bang)	.900543

Case III

Trajectory	Final Time
Unconstrained	.999996
$\alpha'_{max} = 15$	1.000196
$\alpha'_{max} = 10$	1.000295
$\alpha'_{max} = 5$	1.000587

Case II

Trajectory	Final Time
Unconstrained	1.586661
$\alpha'_{max} = 10$	1.588008
$\alpha'_{max} = 5$	1.607179

Case IV

Trajectory	Final Time
Unconstrained	.999357
$\alpha'_{max} = 15$	1.009872
$\alpha'_{max} = 10$	1.030205

Figures 16 and 17 provide attitude and attitude rate histories for Case II. The trajectories shown converged very rapidly, but convergence difficulties again appeared when α'_{max} was reduced to 3. From Figure 12 it appears that the optimal trajectory with $\alpha'_{max} = 3$ will be singular-regular. The convergence difficulty in this case may be due to the fact that it is difficult to iterate to a terminal singular arc of zero length.

Case III is presented in Figures 18 and 19. Because the unconstrained trajectory is extremely sensitive, several searches were necessary to improve the guess before convergence was obtained. The constrained trajectories were developed without convergence difficulty, but it is obvious in Figure 9 that the maximum allowable attitude rate is again exceeded at the regular-singular arc junction when $\alpha'_{max} = 10$ and 5. As stated with regard to Case I, this problem can be surmounted by using bang-bang or regular-regular-singular trajectories.

In Case IV it was again found that convergence of the unconstrained trajectory required several searches before convergence was obtained. The trajectories shown in Figures 20 and 21 converged rapidly, but convergence was not obtained when $|\alpha|_{max}$ was reduced to 5. It is apparent in Figure 20 that the angle traversed on the regular arc when $\alpha'_{max} = 10$ is approximately 270 degrees. Since this angle is increasing as $|\alpha'|_{max}$ is reduced and since $\alpha' = -5\frac{rad}{rad} = -286\frac{deg}{rad}$, it appears that this convergence failure is again indicating that it is not physically possible to reach the origin when restricted to this attitude rate level.

A comparison of the times obtained is generating the trajectories shown on Figures 13-21 is shown in Table III.2. It is obvious that there is little loss in time in using multiple optimal arcs to generate the optimal trajectory.

b. Conclusions

The results obtained in the course of this study gave rise to the following conclusions:

(1) Using multiple optimal arcs to generated minimum-time trajectories when the allowable attitude rate limit is exceeded on the unconstrained trajectory is very feasible.

(2) Using the iteration scheme described in Section 5, convergence to the origin occurs very rapidly in all but the most sensitive cases.

(3) Convergence seemed to be obtainable from any reasonable guess. If convergence is not obtained after two or three simultaneous equation - search sequences, a new guess may be tried. If negative arc times are generated during the iteration, a physical difficulty is the probable cause.

(4) As the allowable maximum attitude rate is decreased convergence difficulties will often occur, generally indicating that the rendezvous cannot be obtained using that attitude rate level. In some cases convergence difficulties at the lower attitude rates may indicate that the proposed arc sequence is improper. In this case a new arc sequence may be tried.

E. List of References

III-1 Apollo Navigation Working Group, "Apollo Missions and Navigation Systems Characteristics, "Technical Report 65-AW-1.0, February 1965.

III-2 Bennett, F. V., and Price, T. G., "Study of Powered-Descent Trajectories for Manned Lunar Landing", NASA TN D-2426, August 1964.

III-3 Citron, S. J., Elements of Optimal Control, Holt, Rinehart, and Winstron, 1969.

III-4 Clohessy, W. H. and Wiltshire, R. S., "Terminal Guidance System for Satellite Rendezvous", Journal of Aero/Space Sciences, Vol 27, No. 9, September 1960, pp. 653-658.

III-5 Dunn, J. C., "On the Classification of Singular and Nonsingular Extremals for the Pontryagin Maximum Principle", Journal of Mathematical Analysis and Applications, Vol. 17, 1967, pp. 1-36.

III-6 Fletcher, R. and Powell, M. J. D., "A Rapidly Convergent Descent Method for Minimization", The Computer Journal, July 1963, pp. 163-168.

III-7 Johnson, G. W. and Winfield, D. H., "On a Singular Control Problem in Optimal Rocket Guidance", AIAA Paper 67-582, August 1967.

III-8 Kaminski, P. G., Optimal Co-Altitude Rendezvous with Constant Thrust Acceleration, M.S. Thesis, Departments of Aeronautics and Astronautics and Electrical Engineering, Massachusetts Institute of Technology, June 1966.

III-9 Kashiwagi, Y. and Alfriend, K. T., Time-Optimal Rendezvous for Elliptic Orbits, NASA CR-1036, May 1968.

III-10 Kelley, H. J. and Dunn, J. C., "An Optimal Guidance Approximation for Quasi-Circular Orbital Rendezvous", Proc. 2nd Int. Congress on Automatic Control, Basle, September 1963, pp. 274-282.

III-11 Kelley, H. J., Kopp, R. E. and Moyer, H. G., "Singular Extremals", Topics in Optimization, G. Leitmann (Ed.), Academic Press, 1967.

III-12 Lewallen, J. M., "A Modified Quasilinearization Method for Solving Trajectory Optimization Problems", AIAA Journal, Vol.5, No. 5, 1967, pp. 962-965.

III-13 Miller J. J., "Minimum-Time Rendezvous with Constrained Attitude Rate", Ph.D. Thesis, Cornell University, December 1971.

III-14 Moore, R. P., "Detailed Computer Printout of Nominal Lunar Module Descent to the Lunar Surface", Private Communication, March 1970.

III-15 National Aeronautics and Space Administration, *Lunar Flight Handbook*, Part 2 - Lunar Mission Phases, NASA SP-34, 1963.

III-16 Paiwonsky, B. H. and Woodrow, P. J. *A Study of Time-Optimal Rendezvous in Three Dimensions*, AFFDL-TR-65-20, January 1965.

III-17 Pontryagin, L. S., Boltyanskii, V. G., Gamkrelidze, R. V. and Mischenko, E. F., *The Mathematical Theory of Optimal Processes*, Interscience Publishers, 1962.

III-18 Powell, M. J. D., "An Efficient Method for Finding the Minimum of a Function of Several Variables without Calculating Derivatives", *The Computer Journal*, July 1964, pp. 155-162.

III-19 Robbins, H. M., "A Generalized Legendre-Clebsch Condition for the Singular Cases of Optimal Control", *IBM Journal of Research and Development*, July 1967, pp. 361-372.

FIGURE 1 PROFILE OF TYPICAL APOLLO MISSION LUNAR MODULE DESCENT FROM ORBIT

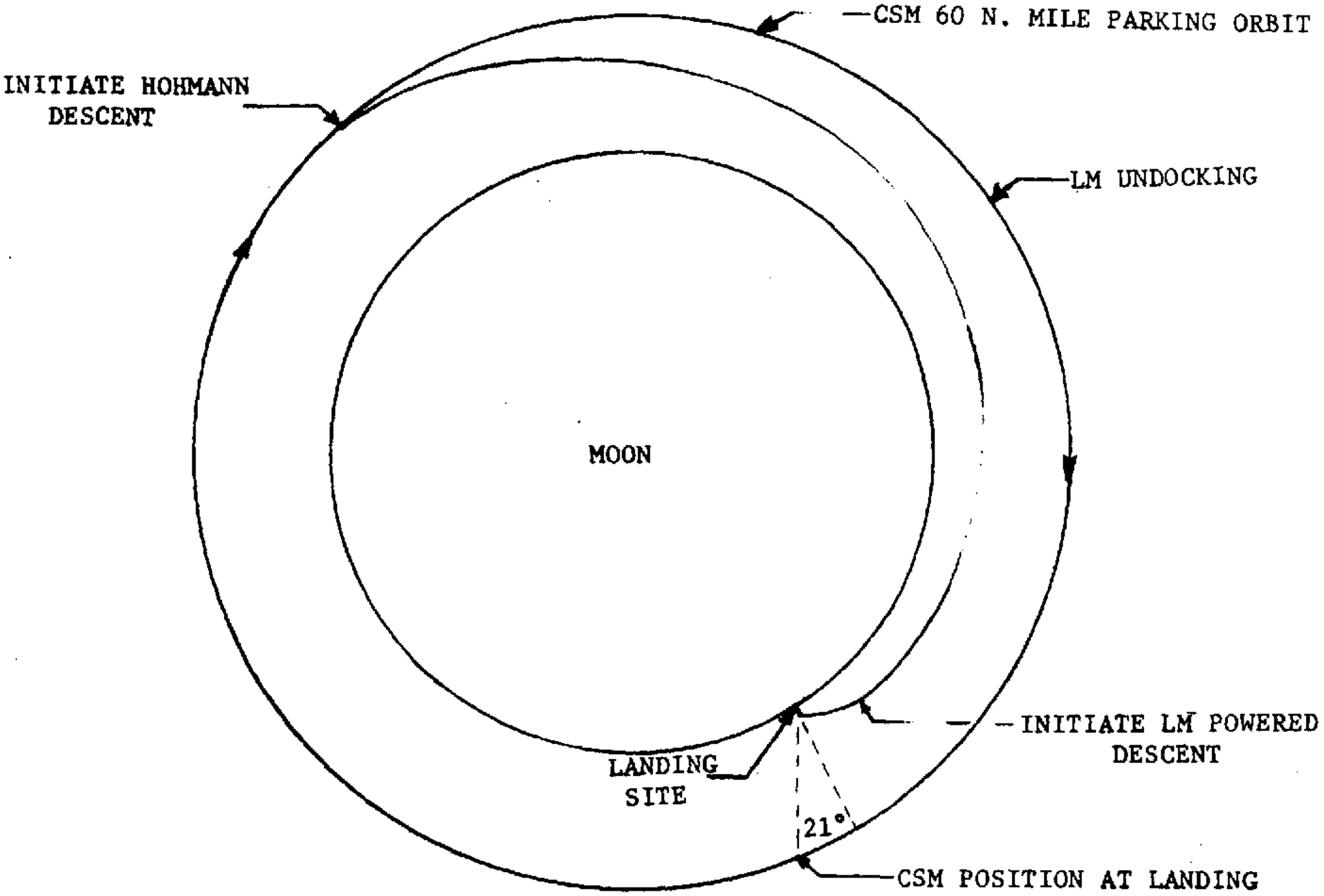
CSM 60 N. MILE PARKING ORBIT
INITIATE HOHMANN DESCENT
LM UNDOCKING
MOON
INITIATE LM POWERED DESCENT
LANDING SITE
21°
CSM POSITION AT LANDING

FIGURE 2 PROFILE OF APOLLO MISSION LUNAR MODULE TERMINAL DESCENT TO A LANDING SITE BELOW THE MEAN LUNAR SURFACE

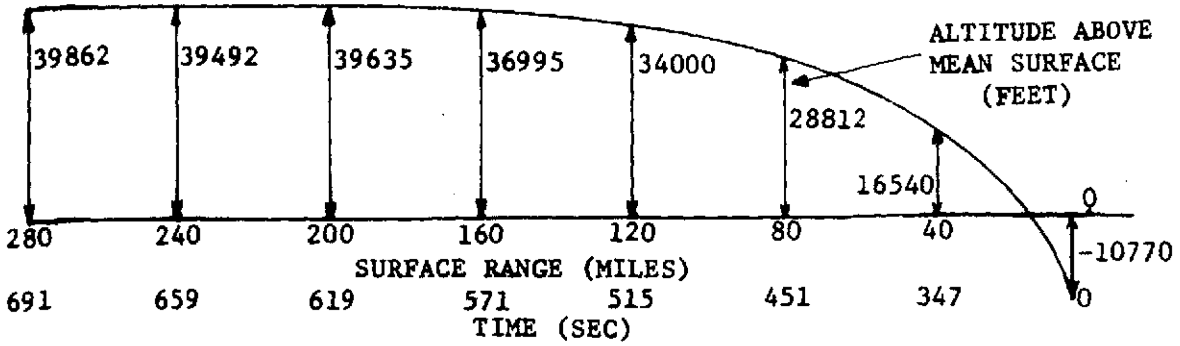

FIGURE 3 THREE PHASES OF TERMINAL POWERED DESCENT

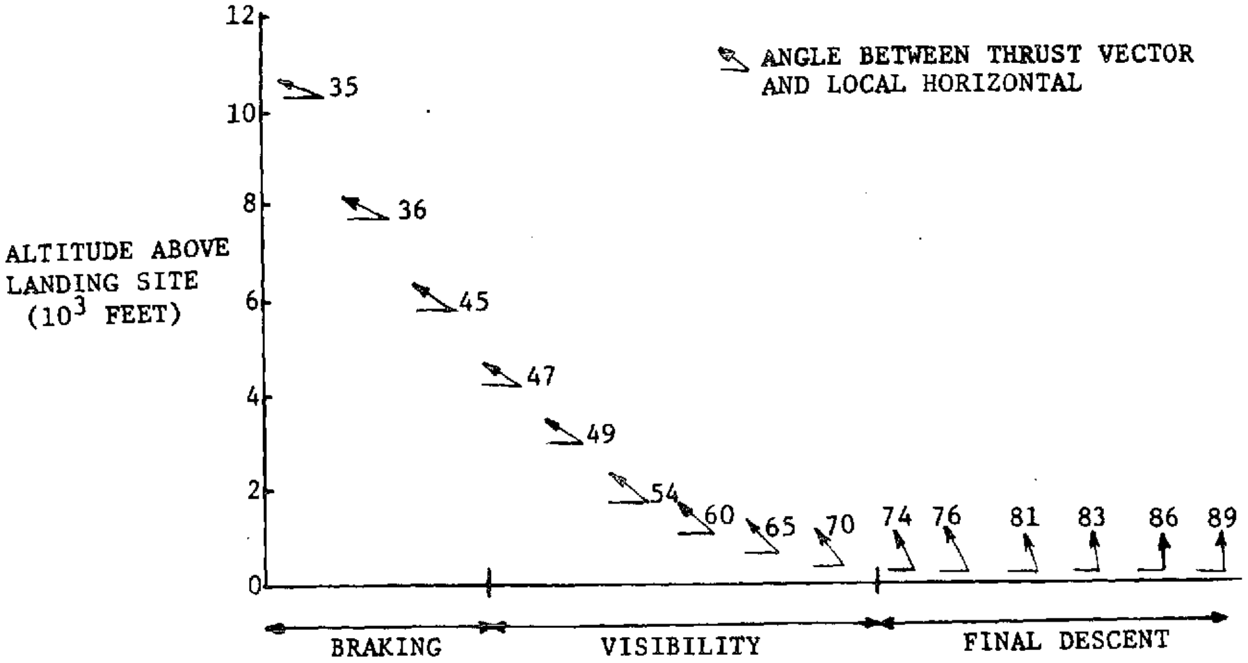

FIGURE 4 RLS ASCENT SEQUENCE

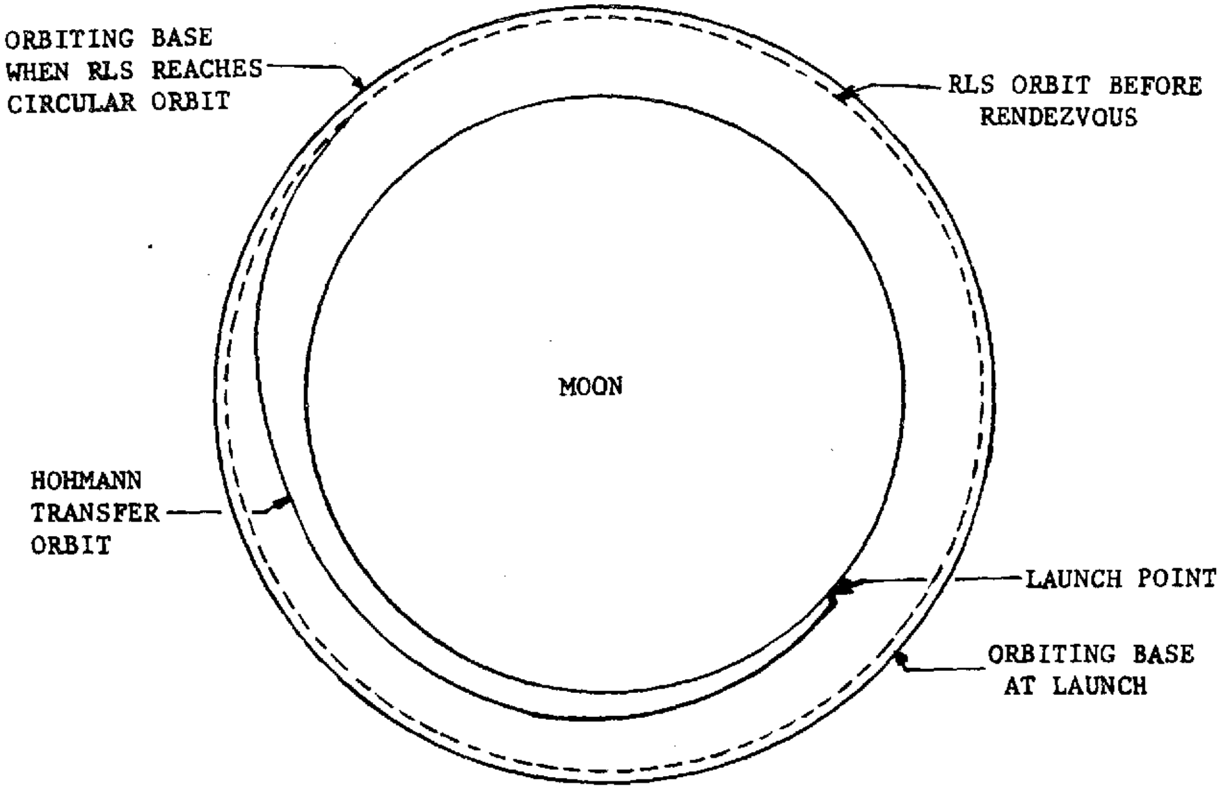

ORBITING BASE WHEN RLS REACHES CIRCULAR ORBIT
RLS ORBIT BEFORE RENDEZVOUS
MOON
HOHMANN TRANSFER ORBIT
LAUNCH POINT
ORBITING BASE AT LAUNCH

Figure 5.

Coordinate Systems

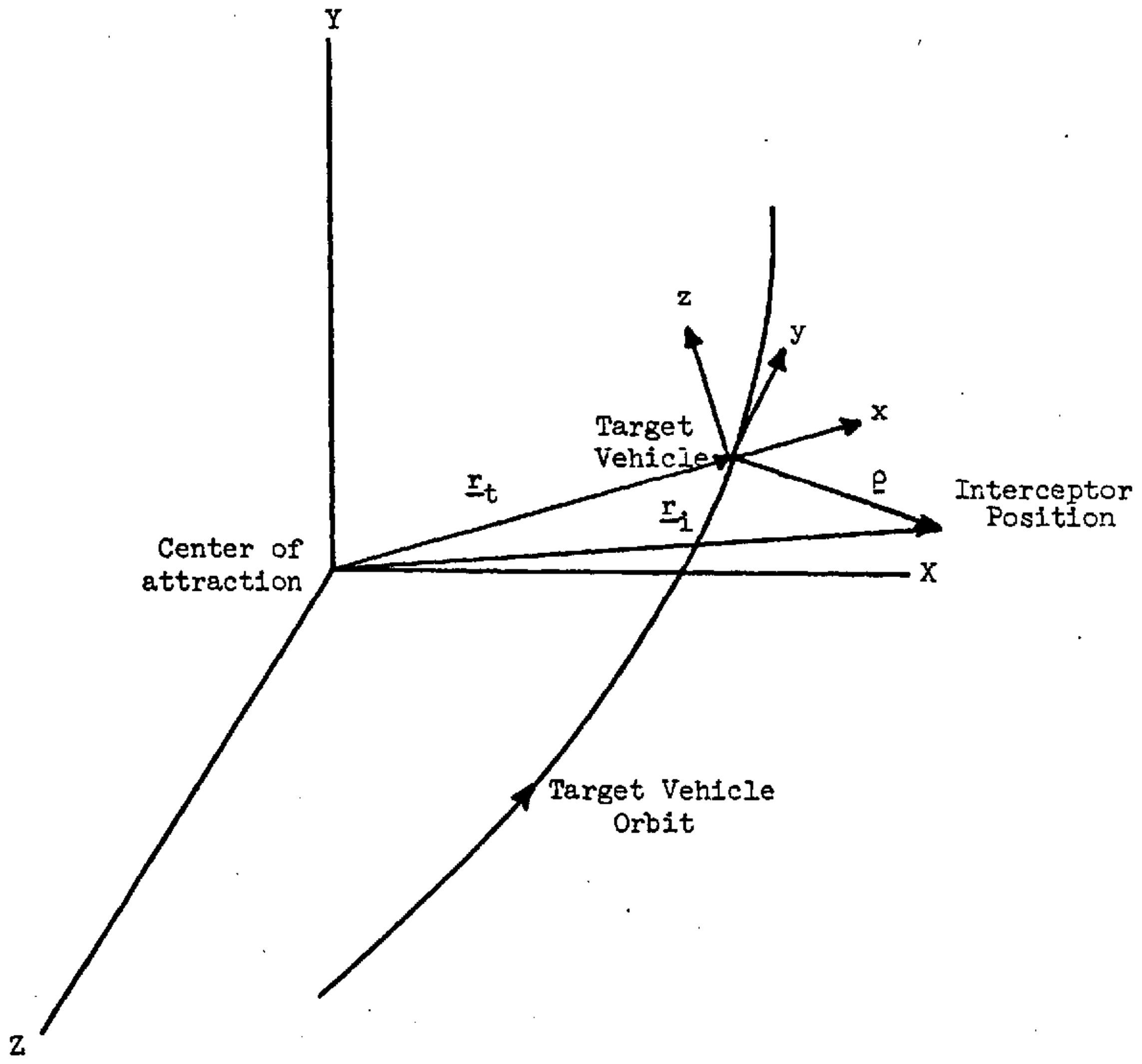
Y
z
y
x
Target
Vehicle
$\underline{r}_t$
$\underline{\rho}$
Interceptor
Position
$\underline{r}_i$
Center of
attraction
X
Target Vehicle
Orbit
Z

Figure 6.

Attitude History (Type I)

$\alpha = \tan^{-1}(u_y/u_x)$

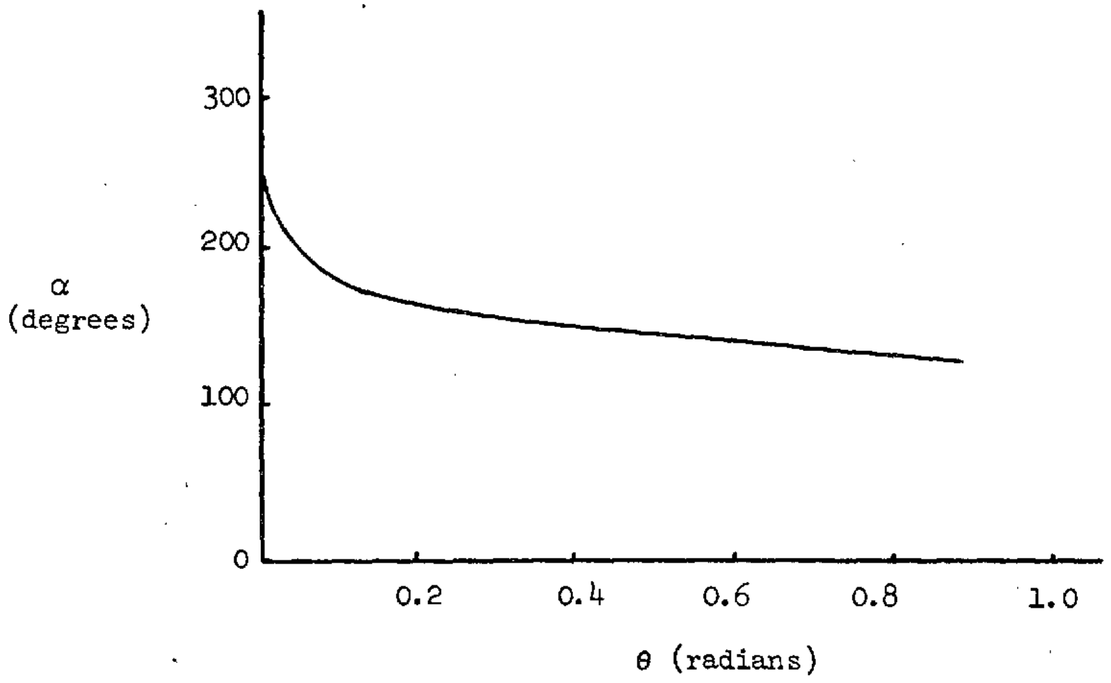

Figure 7.

Attitude Rate History (Type I)

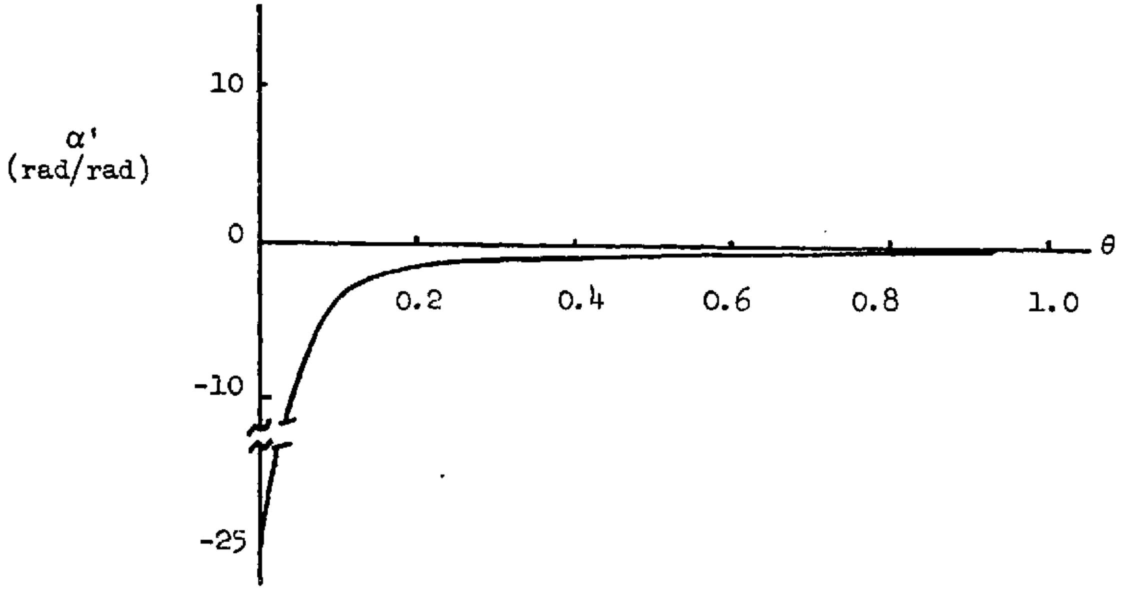

Figure 8.

Attitude History (Type II)

$$\alpha = \tan^{-1} \frac{u_y}{u_x}$$

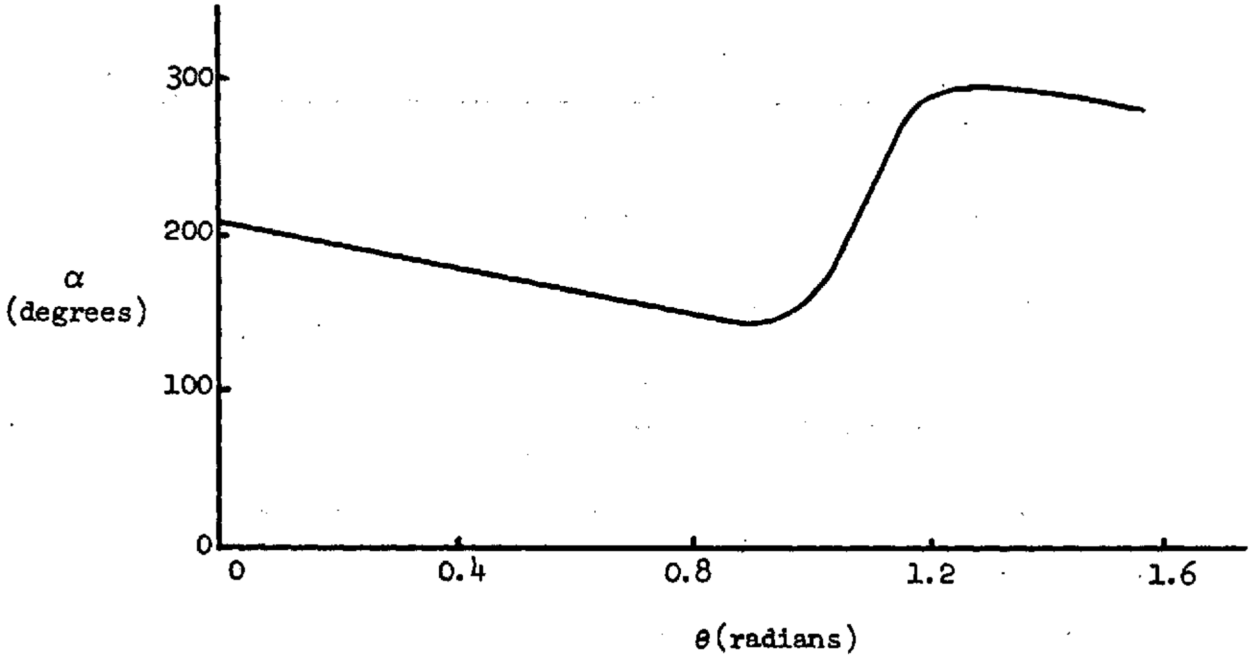

Figure 9.

Attitude Rate History (Type II)

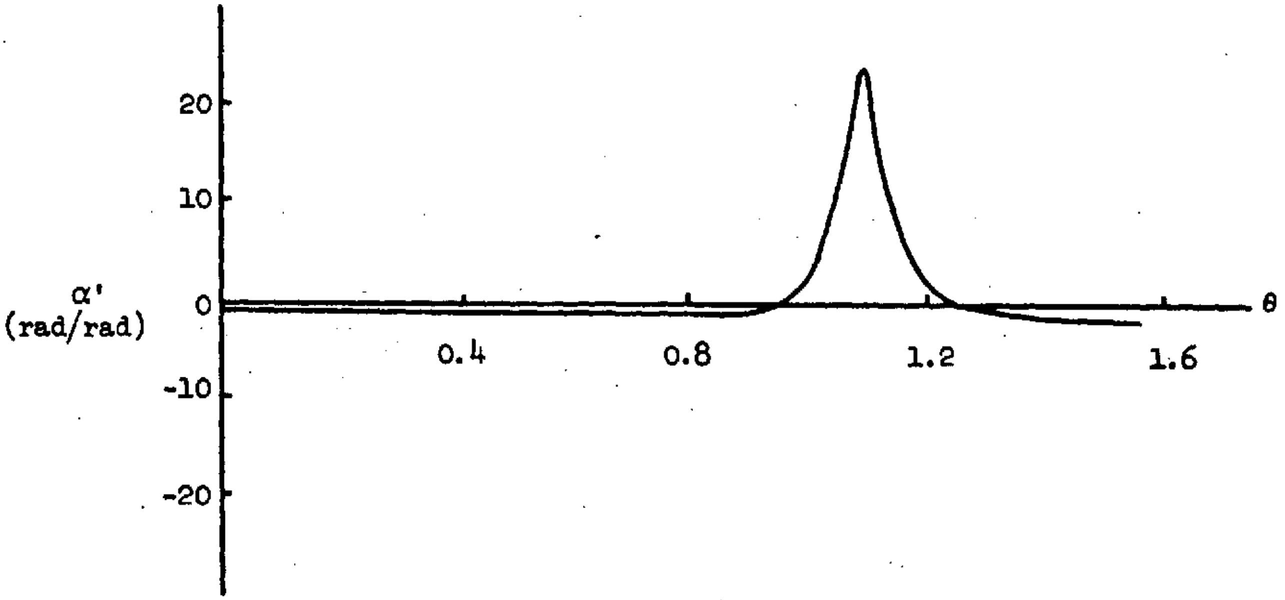

Figure 10*

Jump to the Upper Bound

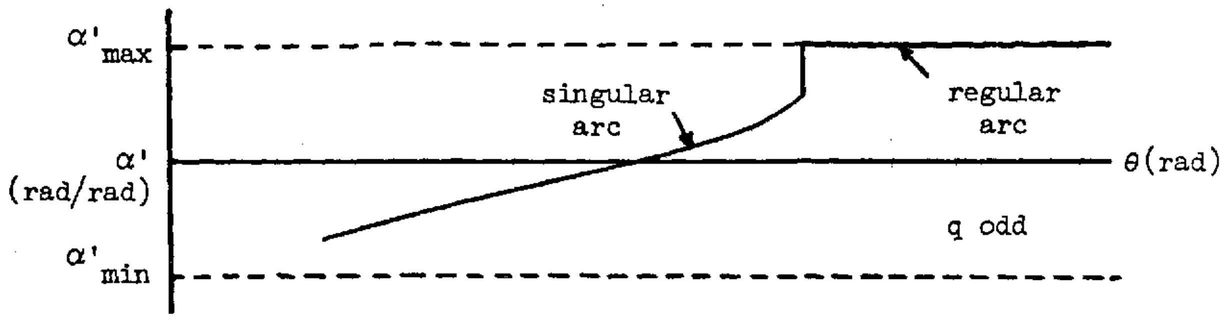

α'_{max}
singular arc
regular arc
α' (rad/rad)
θ(rad)
q odd
α'_{min}

Figure 11.

Saturation to the Upper Bound

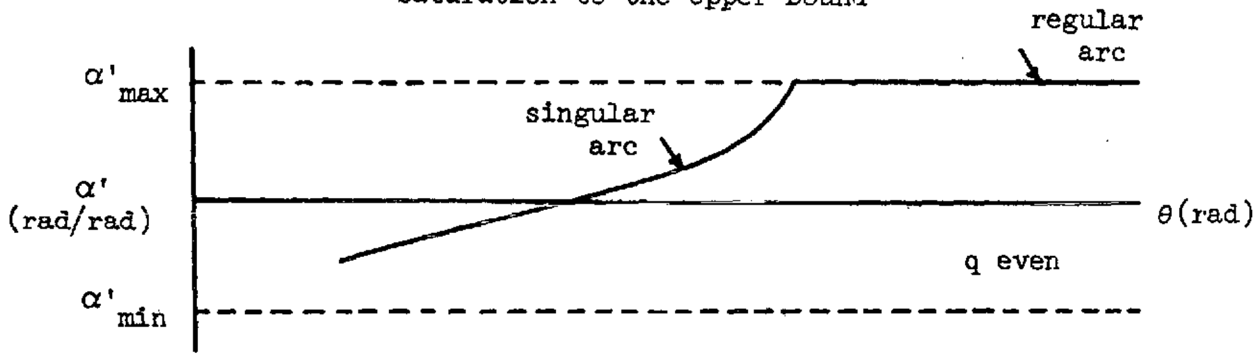

regular arc
α'_{max}
singular arc
α' (rad/rad)
θ(rad)
q even
α'_{min}

Figure 12.

Saturation to the Upper Bound with Jump

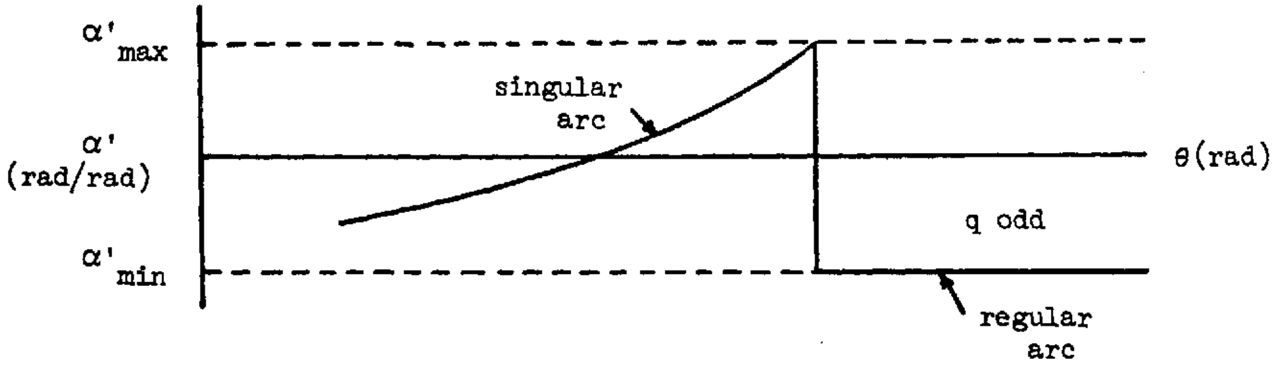

α'_{max}
singular arc
α' (rad/rad)
θ(rad)
q odd
α'_{min}
regular arc

---

[*] These figures have been adapted from similar ones in Reference III-9.

Figure 13.

Unconstrained Minimum-time Rendezvous Trajectories for Cases I-IV

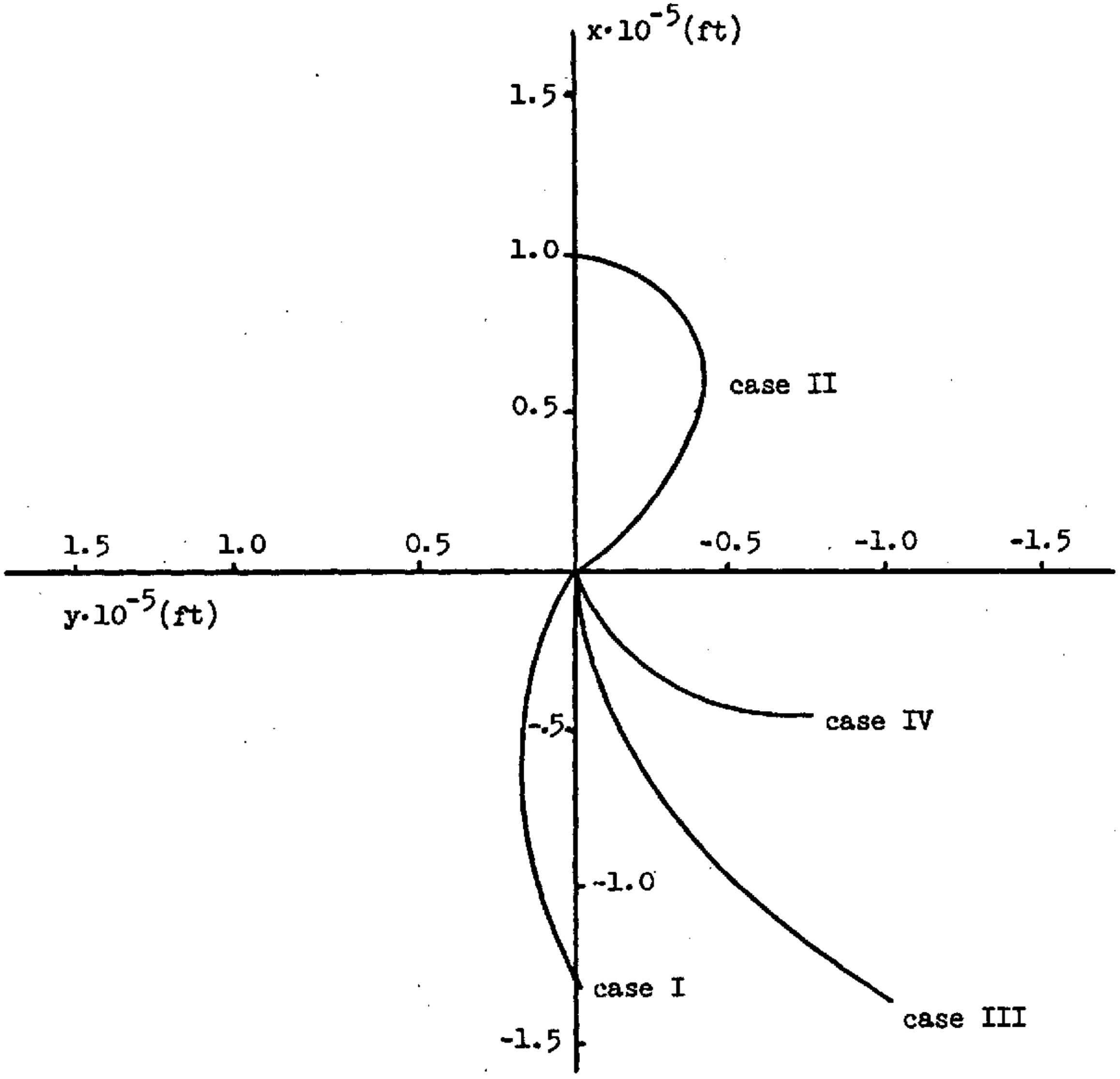

Figure 14.

Attitude Histories for Case I

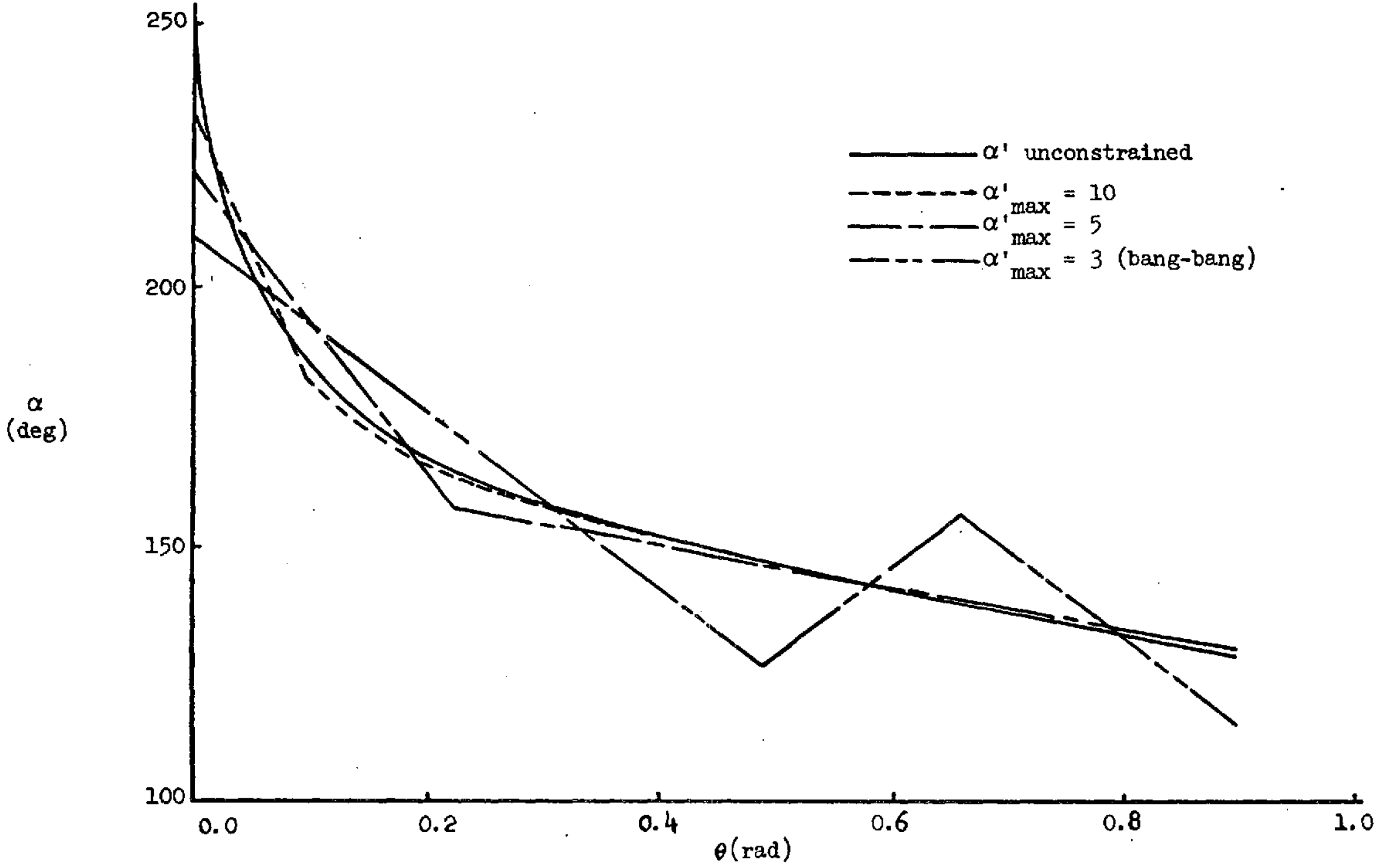

Figure 15.

Attitude Rate Histories for Case I

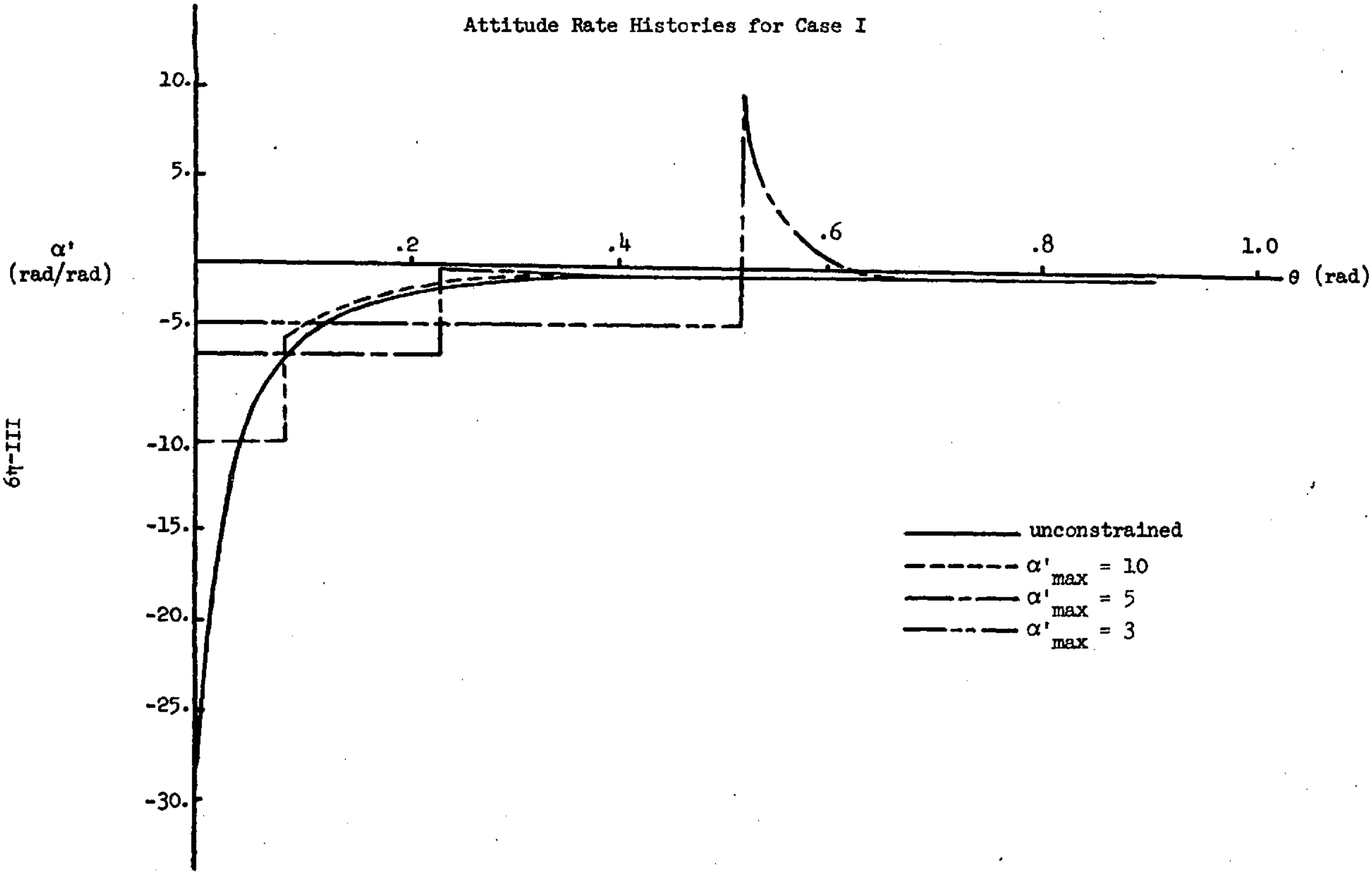

Figure 16.

Attitude Histories for Case II

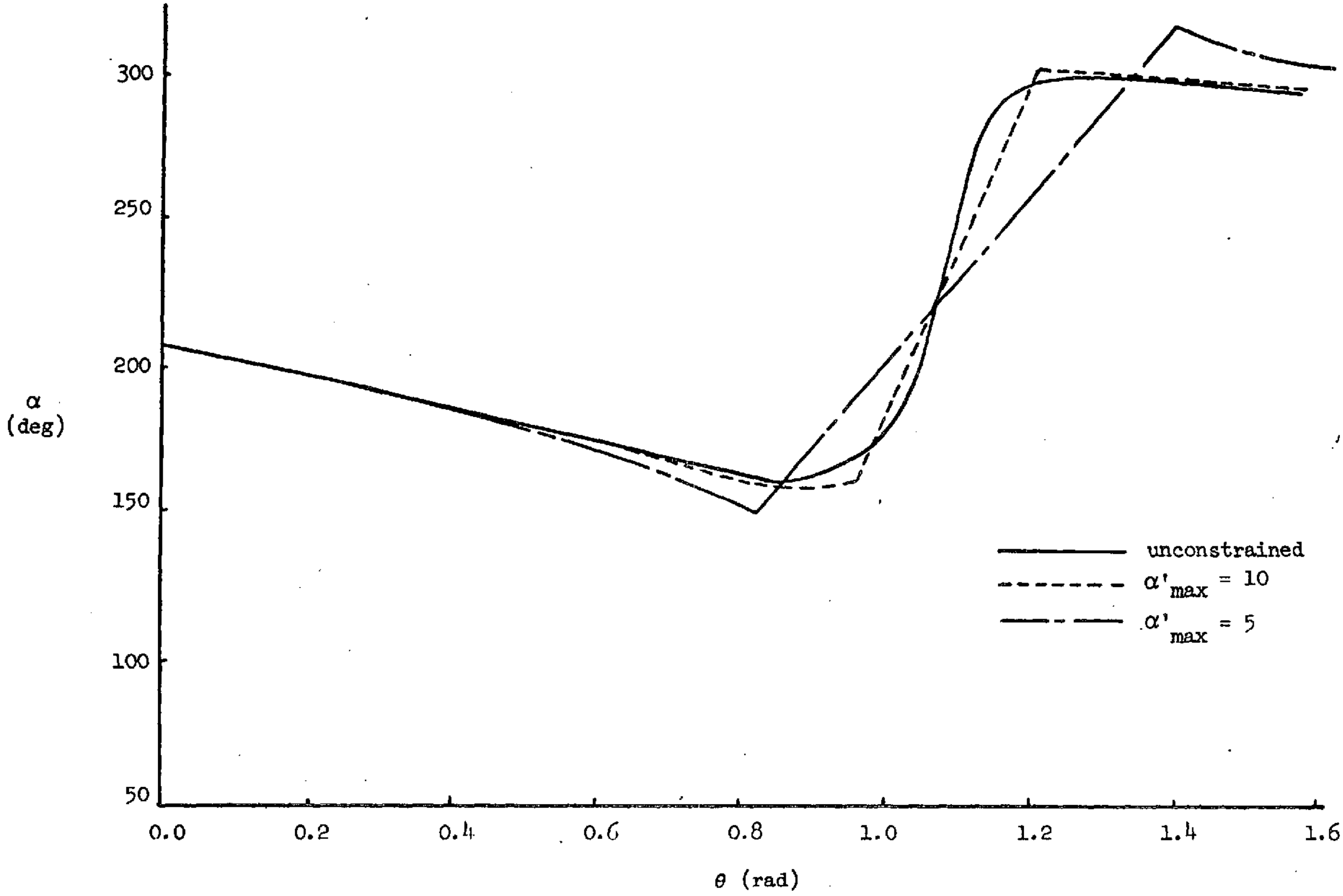

Figure 17.

Attitude Rate Histories for Case II

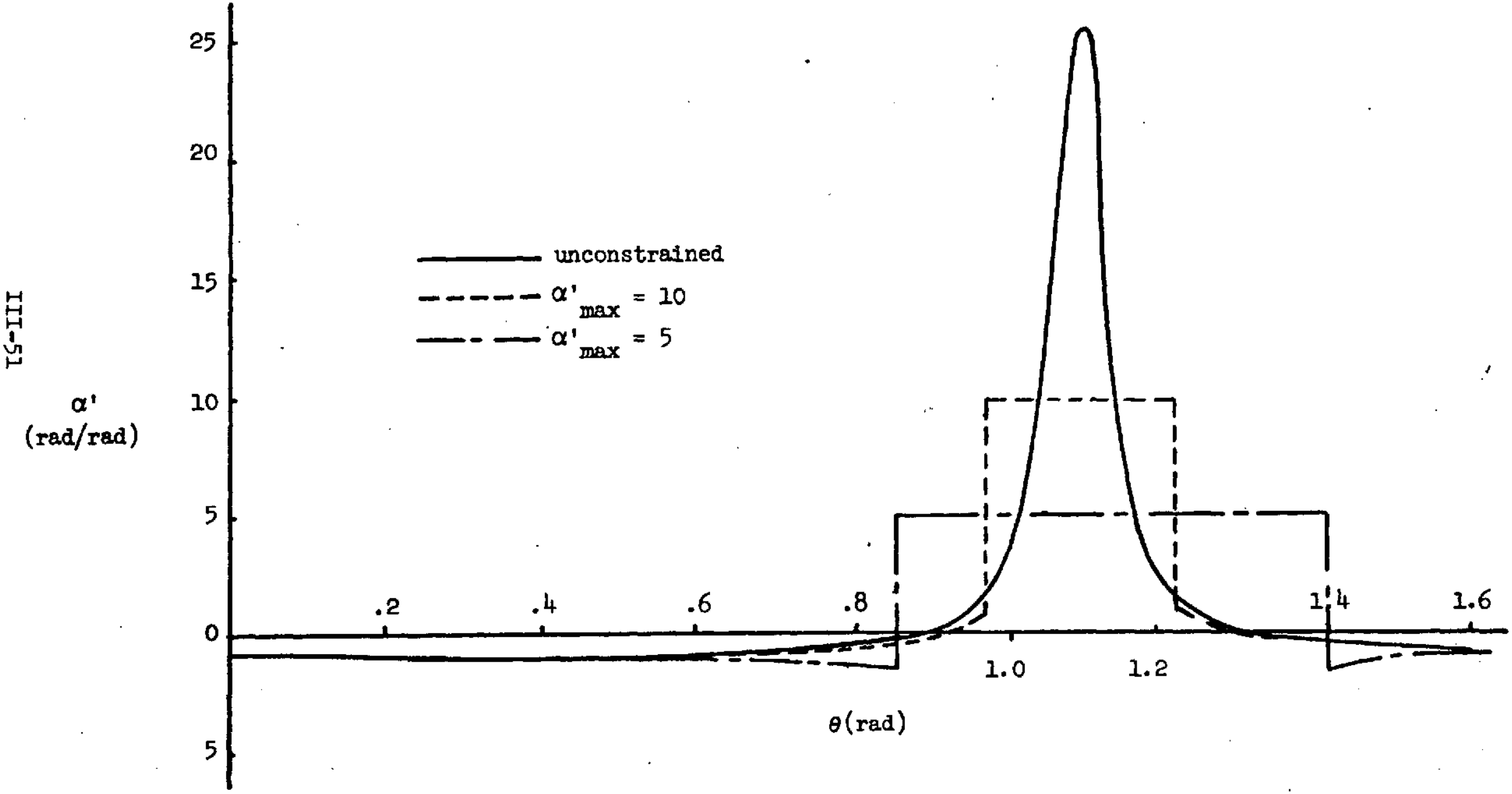

Figure 18.

Attitude Histories for Case III

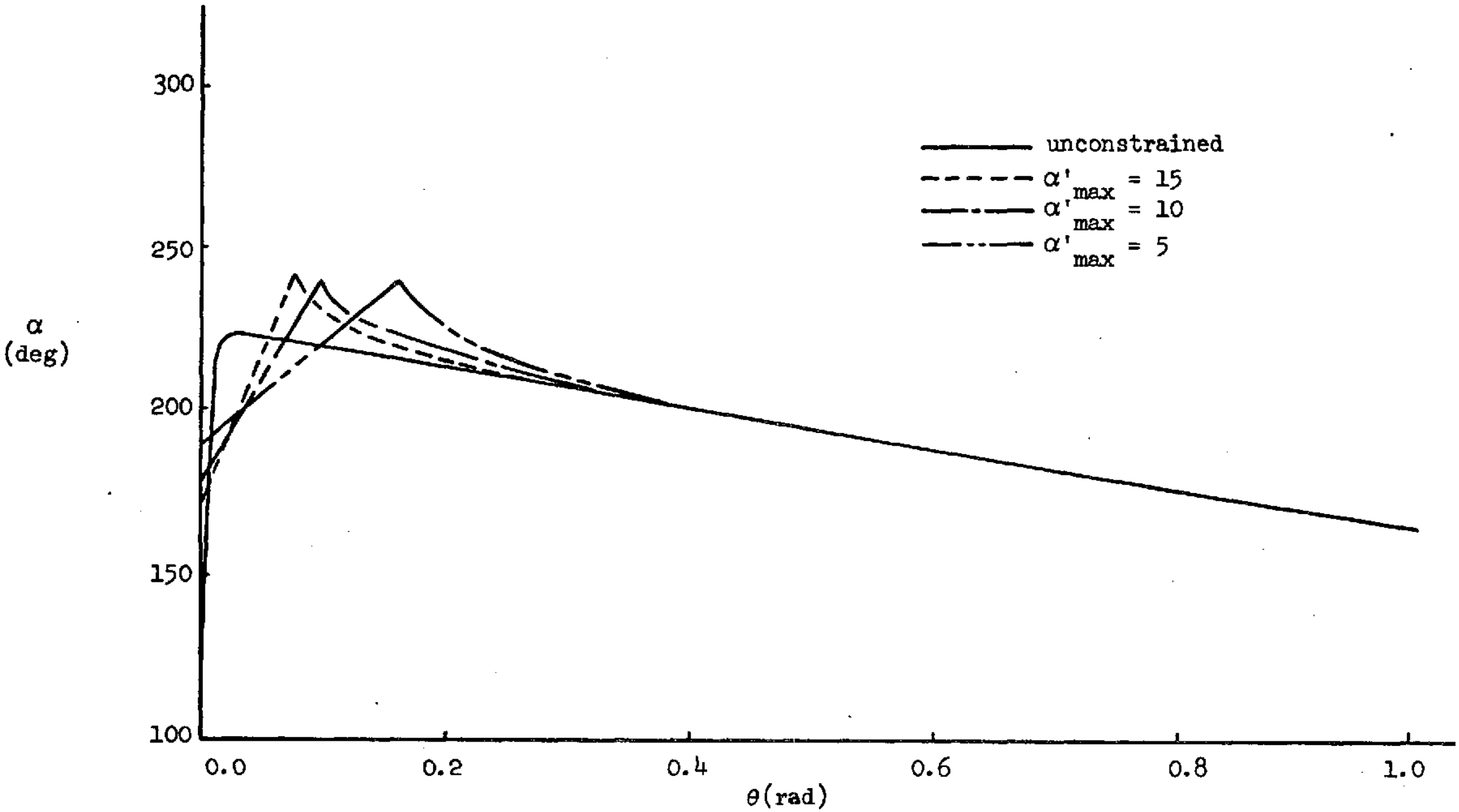

Figure 19.

Attitude Rate Histories for Case III

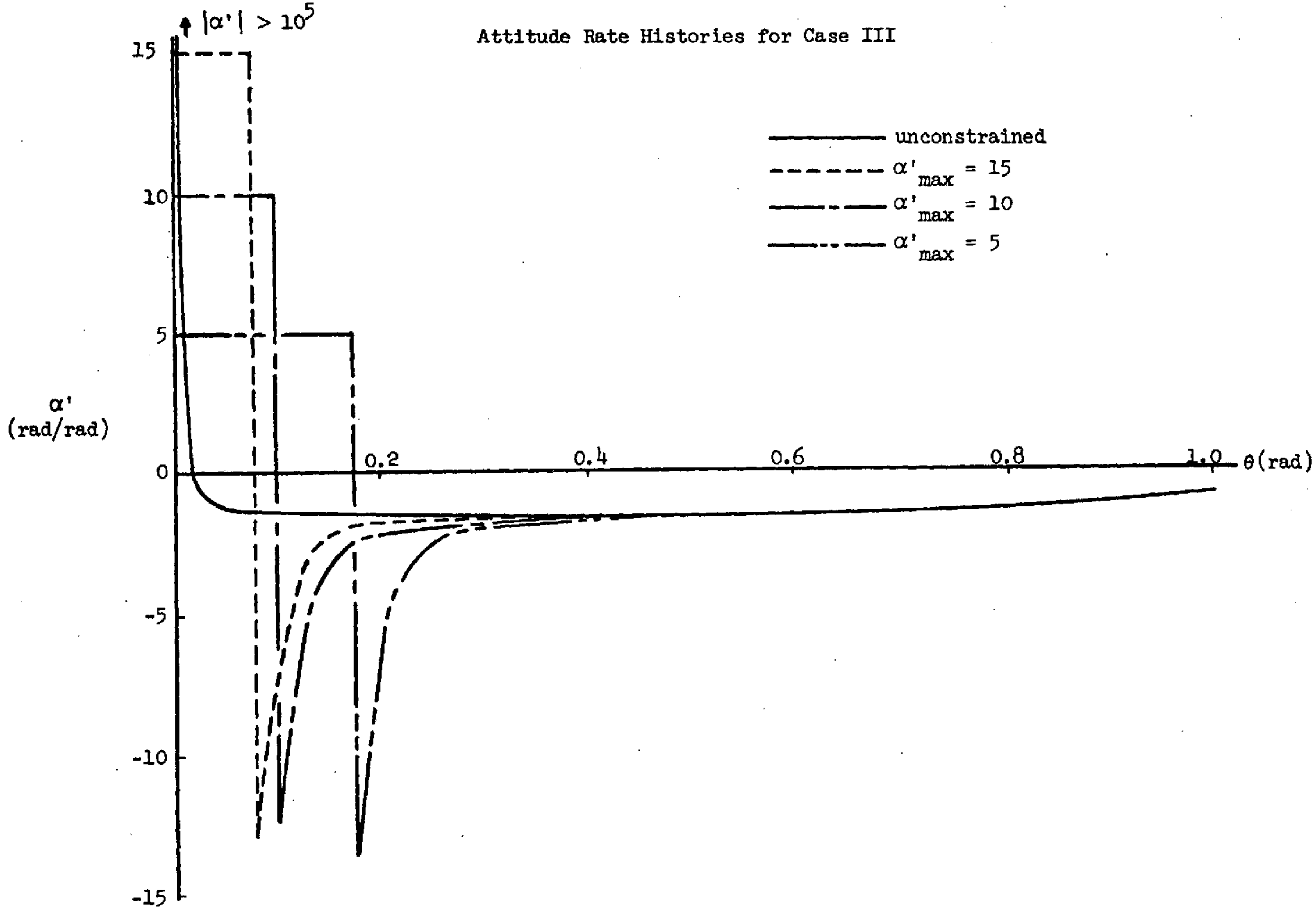

Figure 20.

Attitude Histories for Case IV

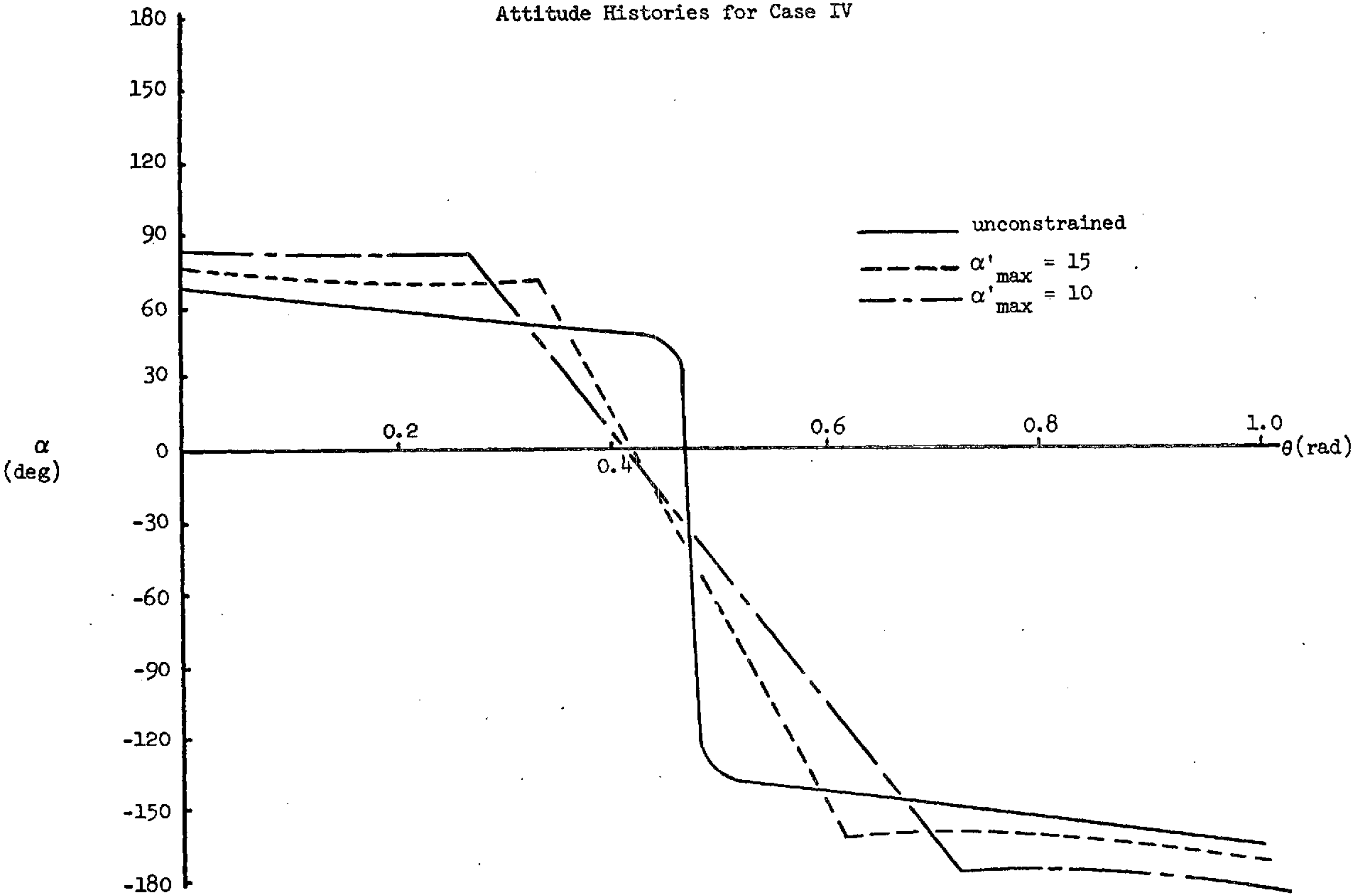

Figure 21.

Attitude Rate Histories for Case IV

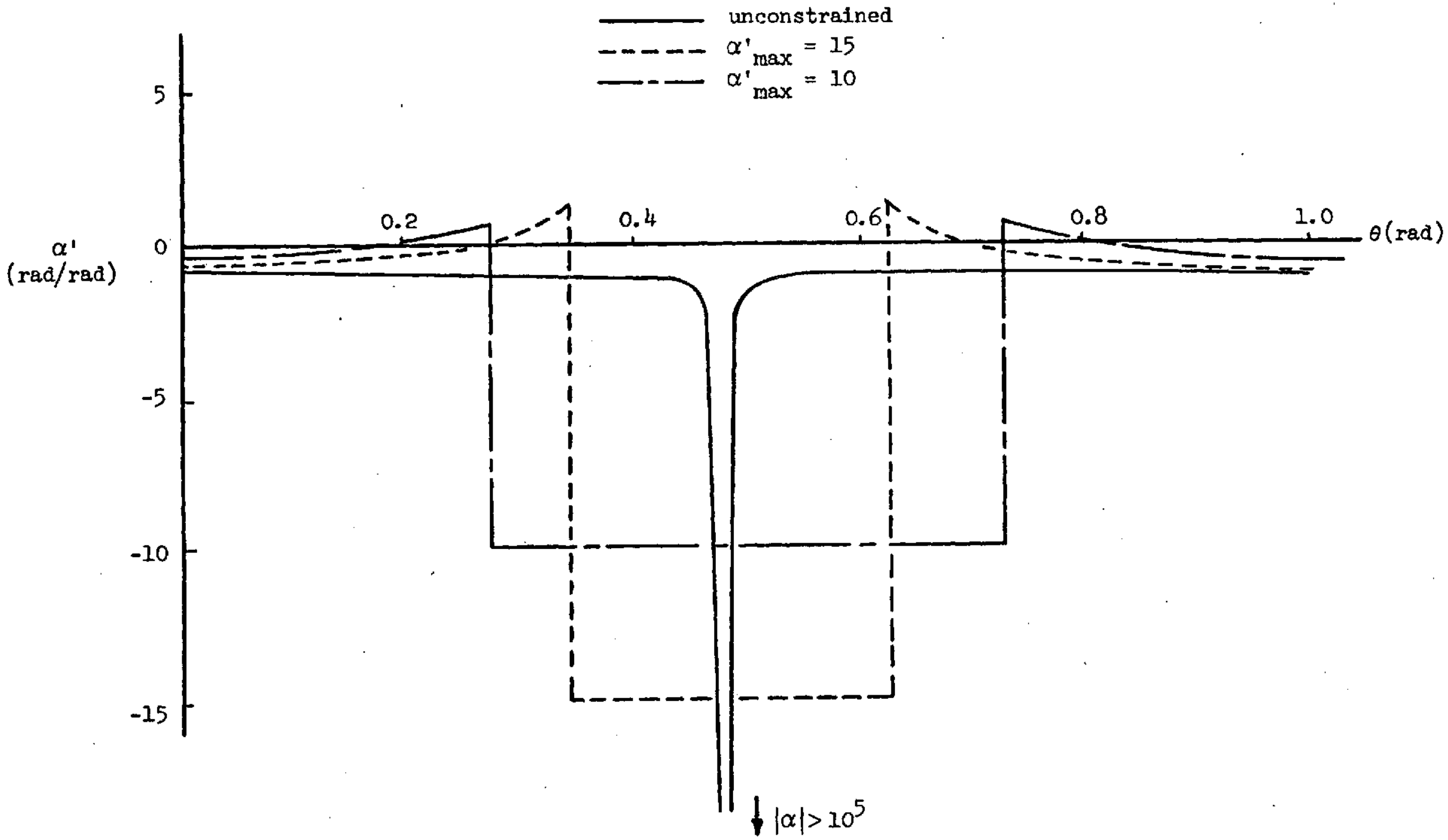

Chapter IV: Guidance and Navigation

1. Introduction

Based upon the mission profile discussed in Chapter II, the Guidance and Navigation (G&N) requirements for the mission can be separated into five distinct phases:

1) descent to hover
2) terminal descent and landing
3) ascent and acquisition
4) rendezvous and docking
5) abort

Since the state-of-the-art in navigation instrumentation is constantly changing, the following discussion will deal solely with the overall systems design of the G&N system. A detailed component design could only be done when the ship is designed in detail.

2. Laser Radar Ranging System

As will be shown in the chapter on communication, one reason why a laser communication system is impractical is that the relative position uncertainty between the LOS and LSV makes it extremely difficult to accurately align the optics necessary for such a system. But, if we use our microwave antenna system to gain position information about the LSV, then we could use this data to "boresight" a set of transmitting receiving optics aboard the LOS. Since modulation of the returning laser beam is not required in a radar system, those problems are eliminated; and by using the microwave system for coarse pointing information, the problems associated with the initial acquisition of the LSV by the LOS are greatly reduced. Thus, a laser-corner reflector system (aboard the LOS) could be used to accomplish the necessary G&N measurements.

Tracking of the LSV would proceed as follows: It is assumed that the laser is located in a fixed position aboard the LOS and that the orbital trajectory of the LOS is accurately known as a function of time. Since the laser optics are mounted aboard the LOS, any movement of the optics relative to some null position can be translated to an angular position relative to the LOS and hence to an absolute angular position in space. Pointing (angular) movements of the laser optics can be thought of as corresponding to changes in the two angular coordinates of a spherical coordinate system mounted aboard the LOS. Range data would be calculated from the elapsed time between the transmission of a laser pulse and the return of its echo from the corner reflector aboard the LSV. Thus, we can accurately pinpoint the location of the LSV in relation to the LOS and by using the known data about the LOS trajectory we can pinpoint the LSV in space. Velocity and acceleration data would be obtained from changes in the angular position and range data. After logging sufficient tracking data, the G&N commands necessary to achieve the desired trajectory would be generated aboard the LOS and transferred via the microwave link the the LSV.

Laser systems to do this job are state-of-the-art and do not require very sophisticated optics nor large amounts of prime power. This subsystem will form a major portion of the system used to fly the LSV. A simplified block diagram of a system to do this job is givin in Figure IV-1.

3. G&N Requirements

3.1 Descent to Hover Phase

Since the LSV will be leaving from the LOS there should not be any problem in setting up either the communications link or the laser ranging system during this phase of the mission. By assumption line of sight contact will be maintained after the LSV separates from the LOS until the post-burn trajectory is established; and reestablished again before the burn-to-hover maneuver. After the LSV is at the hover point, it will use a high resolution T.V. system to gather topographical information on the terrain below. Since line of sight contact (and hence communication) is not required during this portion of the mission, the terrain imaging data will be stored aboard the LSV until conditions are favorable for transmitting it to the LOS.

3.2 Terminal Descent and Landing Phase

After receiving the topographical data from the LSV, the flight crew of the LOS will select the desired landing site. Once a site selection has been made, LOS computers will generate the flight profile necessary for a safe landing. These commands will be transferred to the LSV via the microwave data link. After receiving the command to descend, the LSV will operate independently of the LOS (except if an abort situation arises) until the landing is completed and this phase of the mission terminated. From the above discussion it is apparent that the LOS will need its own landing radar and lunar horizon sensors to operate independently of the LOS during landing; these subsystems will have to be analyzed in detail at a future date.

3.3 Ascent and Acquisition Phase

This phase can be viewed from two different and distinct viewpoints. The first is that the LOS and LSV are in communication prior to and during take-off. If this is the case, the LOS will issue the command to lift-off the lunar surface and then subsequently fly the ship home. Since communication existed prior to and during lift-off, there is no reason to worry about any acquisition problems in this case. The second situation is that the LSV was programmed to lift off the lunar surface at a predetermined time. Assuming that the LSV is programmed to lift-off the lunar surface and then to enter a stable holding orbit, it becomes a matter of reestablishing the communications channel (and hence aligning the laser radar ranging system) before the ship can be flown home. Establishment of the communication channel is covered in Chapter V. Once the communications channel has been reestablished, it becomes a relatively simple matter to boresight the laser optics and go through a simple scanning procedure to lock-in on the corner reflector aboard the LSV.

3.4 Rendezvous and Docking Phase

Many subsystems already exist to handle this phase of the mission with some of the new laser systems being very attractive. As before, this area will require in depth study at a later date.

3.5 Abort

An abort condition will be said to exist if there is a failure of any subsystem aboard either the LOS or LSV which would endanger (or prevent) the LSV from returning to the LOS. Broadly speaking, this could happen for two reasons:

Type-1: component failure

Type-2: communication failure; i.e., communication between the LOS and LSV is lost, interrupted, or not reestablished during any vital (communication dependent) phase of the mission. The general philosophy governing the action(s) to be taken in the event that an abort situation does arise is that of trying to place the LSV in a stable holding orbit (using its own landing radar and horizon sensors) until the situation

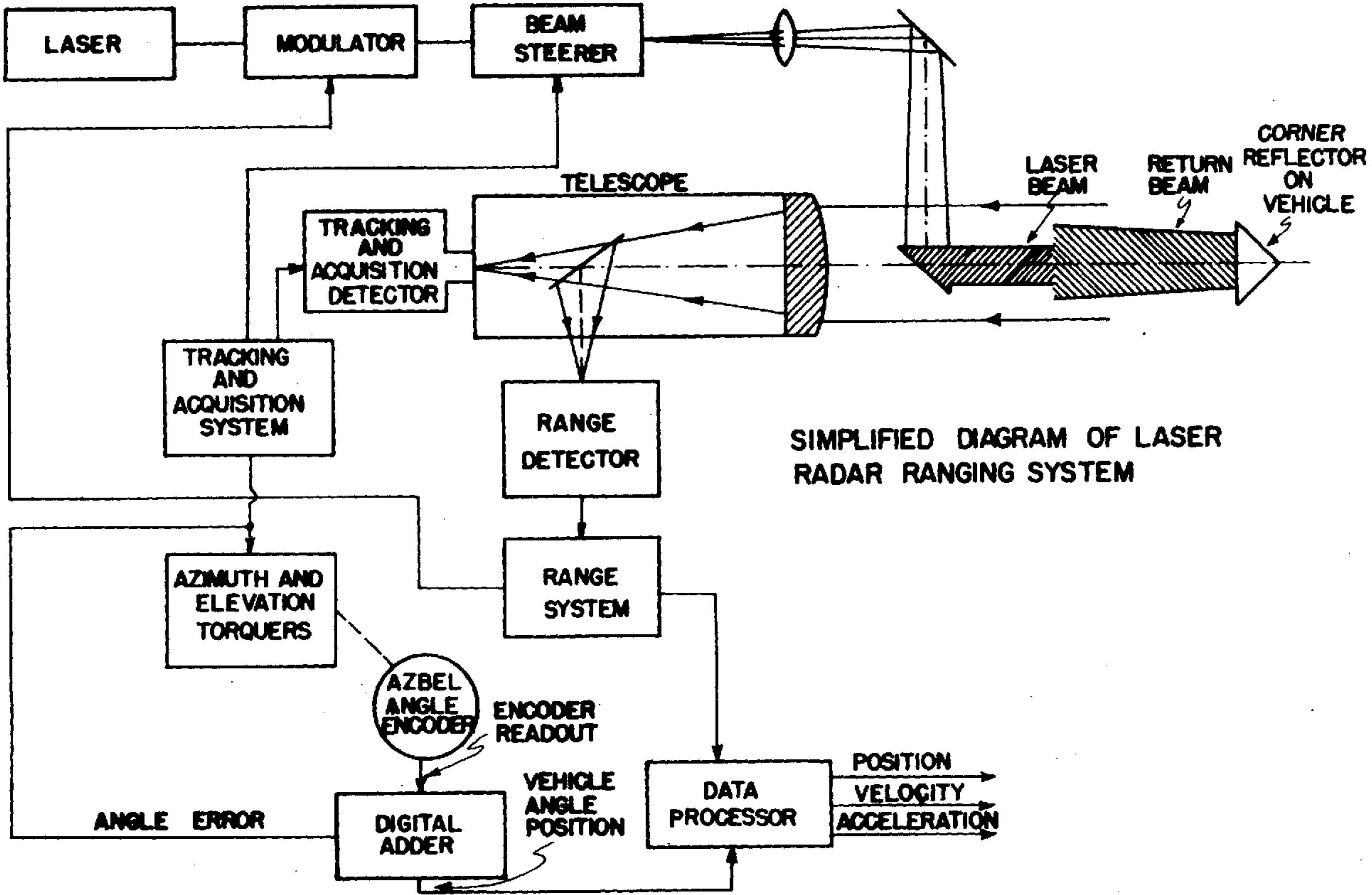
LASER
MODULATOR
BEAM STEERER
TELESCOPE
LASER BEAM
RETURN BEAM
CORNER REFLECTOR ON VEHICLE
TRACKING AND ACQUISITION DETECTOR
TRACKING AND ACQUISITION SYSTEM
RANGE DETECTOR
RANGE SYSTEM
AZIMUTH AND ELEVATION TORQUERS
AZBEL ANGLE ENCODER
ENCODER READOUT
DIGITAL ADDER
ANGLE ERROR
VEHICLE ANGLE POSITION
DATA PROCESSOR
POSITION
VELOCITY
ACCELERATION

SIMPLIFIED DIAGRAM OF LASER RADAR RANGING SYSTEM

Figure IV-1

changes and/or the necessary repairs are completed. The possibilities of a type-1 abort are too numerous to be itemized and can only be minimized by the design of a reliable vehicle. Type-2 aborts might arise from either a component failure or an obstruction in the line of sight link between the LOS and LSV, but the action to be taken in either case is one of achieving (or maintaining) a stable orbit and of initiating the acquisition procedure as described in Chapter V, as is necessary to reestablish the communications channel and terminate the abort situation.

Bibliography

1. Harden, J. W., Jr., "Advanced Spaceborn Detection Tracking and Navigation System Studies", NASA N67-30597.
2. Wyman, C. L., "Laser Systems Research at Marshall Space Flight Center", NASA N67-30561.
3. "Improved Lunar Cargo & Personnel Delivery System", final report, Vol III-A, 28 June 1968, Report No. 7-28-68-4, LMSC, Sunnyvale, California.

Chapter V: Communications System: Analysis and Design

1. Introduction

As with most other space-communications systems, the LSV communications system is predicated on direct line of sight contact between the LOS and LSV. Ideally, this line of sight contact would be maintained throughout the mission, but it will be sufficient to require direct line of sight contact during the following phases of the mission:

1) from the time that the LSV leaves the LOS until the postburn trajectory is established
2) before and during the burn-to-hover maneuver
3) before beginning terminal descent
4) after ascent from the lunar surface
5) during rendezvous and docking.

2. Mission Requirements

2.1 Maximum Communication Range

To calculate the maximum communication range we must make some assumptions as to the orbit of the LOS. Assuming a circular moon of radius 1738 km and that the LOS is in a nominal 100 km circular orbit about the moon we can calculate: R = maximum communication range, using the Pythagorean Theorem:

$$\left(\frac{R}{2}\right) = \sqrt{(1738 + 100)^2 - (1738)^2}$$

$$\therefore R \doteq 1166 \text{ km}$$

For the purpose of the present investigation it will be sufficient to assume that

$$R = 10^3 \text{ km}$$

Table V.1

Typical (PCM) Data Rate Requirements

Type	Source Signal Bandwidth, f_m (i.e.,baseband)	Representation Bits/Sample n	Maximum Bit Rate ($B_{if} \doteq 2nf_m \doteq R_B$)	Tolerable Error Rate
Scientific Data	0 to 1 kHz	9	18 kbps	10^{-2}
Engineering data	0 to 1 kHz	7	14 kbps	10^{-2}
Command data			50 bps	10^{-5}
Teletype			75 bps	10^{-5}
Speech	0 to 4 kHz	5	40 kbps	10^{-3}
Real-time television (500x500 - element picture)	15 Hz to 4 MHz	6	48 Mbps	10^{-3}
Picture transmission (500x500 - element picture in 12.5 sec)	15 Hz to 10 kHz	6	120 kbps	10^{-3}

2.2 Data Requirements

There are many possible signal (message) sources, each with its own spectral requirements. Assuming the use of PCM (pulse code modulation), which will turn out to be the case, Table V.1 can be used to estimate the maximum data rate: R_B, and the acceptable bit error rate (or probability of error, per bit): P_e. It turns out that due to navigational requirements the capability of high resolution television transmission is needed and, hence, a choice of $R_B = 5 \times 10^7$ bps is made. As shown in Section 5, it is possible to select $P_e = 10^{-3}$ and still be able to transmit command data at the rate of 50 bps with $P_e = 10^{-5}$ (for command data). In order to minimize quantitization errors 9 bits/sample is used, in other words at most 9 binary bits is used to quantify any piece of data. This gives a resolution of 1 part in 2^9 (1 part in 512) or approximately 0.5%.

3. System Configurations

Table V.2 summarizes the basic system configurations. The reasons for considering only the S-band and CO_2 laser systems are summarized in Ref. V-2.

Table V.2

Basic System Configurations

Type of System	Wavelength	
	S-Band λ=13 cm	CO_2 laser λ = 10.6
Active	acceptable	acceptable
Passive	not acceptable	acceptable

3.1 "Active" Configuration

This configuration can be realized at both microwave and laser frequencies. It is what one normally thinks of in terms of a communications system. Namely, independent transmitters and receivers are located in both the LOS and LSV; see Fig. V-1.

Both systems are required to track each other independently and sufficient power and transmitting capabilities are aboard the LSV to establish the desired communications channel.

3.2 "Passive" Configuration

This configuration is most easily implemented by optical systems. It consists of a transmitter and receiver in the LOS and only a receiver and modulator/reflector system in the LSV: see Fig. V-2. Thus, no high power transmitting facilities are required on the LSV, but a modulator/reflector system capable of removing and/or inserting information on the laser beam and then reflecting the beam back on itself is needed. There are numerous ways that this can be achieved at optical frequencies with or without a change in frequency of the reflected wave.

3.3 Comparison of Active and Passive Configurations

Besides comments already made about the power requirements of the respective systems it should be noted that as long as line of sight communication is never lost, the passive configuration is more efficient than the active one both from a power and weight standpoint. If however, transmission should be lost, or acquisition of the LOS not achieved after ascent from the lunar surface, the passive system would greatly complicate the reestablishment of the communications channel due to the inherent lack of any "searching" capability by the passive LSV. On the other hand, with the active configuration each system (LOS and LSV) can independently search out the other. Since laser systems employ very narrow beamwidths, the acquisition problem is a critical one. Current state-of-the-art laser modulators and physically realizable single section corner reflectors require very accurate alignment of the incoming beam for proper operation.

3.4 Choice of a System Configuration

The primary factors to be considered in the choice of a communication system configuration are: data rate, acceptable probability of error, power requirements, acquisition and tracking requirements, weight, volume, technical feasibility and maintenance. Taking these factors into account, it was decided to employ an active, microwave (S-band, $\lambda = 13$ cm) configuration. This decision was based upon predicted power and weight requirements as well as the availability of space-qualified hardware (with suitable allowances for projected capabilities).

4. Modulation Techniques

Modulation refers to the way that information is impressed upon a carrier waveform. There are three basic ways to do this:

1) The signal waveform is used to directly (continuously) modulate the carrier; e.g., FM, AM.
2) The signal waveform is time sampled and these samples are used to directly modulate the carrier; e.g., PAM, PPM, PDM.
3) The signal waveform is time sampled, quantized, and then used to "key" a carrier; e.g., PCM/AM, PCM/FM, PCM/PM.

Type-3 modulation systems have become very popular due to the availability of low cost, low power, high speed digital electronics. State-of-the art type-3 systems are characterized by being PCM (pulse-code-modulation) systems; i.e., systems where the signal waveform is time sampled and each sample is coded as a finite length binary number. The envelope of the carrier waveform is then a string of rectangular pulses. The various fundamental PCM systems are:

a) PCM-AM: Amplitude modulation. Data is conveyed by the presence or absence of the carrier.

b) PCM-FM: (FSK) Frequency modulation (frequency shift keying) Data is transmitted by transmitting a pulse of carrier at one or two distinct frequencies.

c) PCM-PM: (PSK or PSK) Phase modulation (phase shift keying or differential phase shift keying). Data is transmitted by the phase of the carrier (0° or 180°) for PSK; or by a change in the phase of the carrier (from 0° to 180° or vice versa) for ΔPSK.

4.1 Modulation Schemes and Bit Error Rates

If reasonable assumptions are made about the message set and communications channel, we can compute the probability of error (≡ bit error rate), P_e, for each of the modulation schemes as a function of the bit signal to noise ratio; E/N_o can be calculated. Assume that the message set consists of {0,1} and that autocorrelation between the two messages is -1 for PSK and 0 for FSK.[*] As far as the channel is concerned, assume that the a priori probability that either a 1 or 0 was sent is identically 1/2, and that our communications channel can be modeled by an additive noise gaussian channel. Table V.3 gives the mathematical expressions for P_e as a function of E/N_o that result from an analysis employing the above assumptions. The detailed derivations can be found in Lawton, Refs. V-3 and V-4.

---

[*] If this is not the case, then everywhere E/N_o appears it should be replaced by $E(1-\gamma)/2N_o$, where γ is the autocorrelation of the two messages in question.

Table V.3

P_e vs. E/N_o for Various Modulation Schemes

Modulation Scheme		P_e: Probability of Error
PCM/PSK:	coherent detection	$P_e = 1/2 \{1 - \text{erf} \sqrt{E/N_o}\}$
PCM/ΔPSK:	differentially coherent detection	$P_e = 1/2 \exp \{-E/N_o\}$
PCM/FSK:	coherent detection	$P_e = 1/2 \{1-\text{erf} \sqrt{E/2N_o}\}$
PCM/FSK:	non-coherent detection	$P_e = 1/2 \exp \{- E/2N_o\}$

These expressions for P_e are plotted in Fig. V-3 as a function of E/N_o. Inspection of Table V.3 shows that:

1) The coherent or non-coherent PSK scheme offers a factor of 2 (± 3db) reduction in the required E/N_o (for the same P_e) when compared to the corresponding FSK scheme.

2) The difference between PSK and ΔPSK approaches 0 as E/N_o gets large. For example:

$P_e = 10^{-3} \Rightarrow (E/N_o)_{PSK} =$ 6.78 db, and $(E/N_o)_{\Delta PSK} =$ 7.93 db

$P_e = 10^{-5} \Rightarrow (E/N_o)_{PSK} =$ 9.58 db, and $(E/N_o)_{\Delta PSK} =$ 10.33 db

Based upon the fact that ΔPSK systems are state-of-the art, and the relatively small difference in the E/N_o required (for a given P_e)

as compared to a straight PSK system it was decided to employ ΔPSK in the communications system.

4.2 Synchronization

Any time division multiplex communications system such as this requires precise synchronization of the receiver and transmitter to insure accurate, message decoding. The degree to which synchronization is established directly effects the performance of the communications system. For a PCM system, perfect synchronization is achieved when the receiver locks in on both the frequency and phase of the transmitted signal. This lock must be maintained even under very adverse noise situations. A PCM synchronizer must have the following properties:

1) It must be able to detect transmitted sync (synchronization) codes even when they are severely corrupted by noise.
2) It must verify that these codes are transmitted periodically.
3) It must compute the frequency of occurrence of the sync codes.
4) It must measure the mean squared error rate to ascertain whether or not the detected code is compatible with the expected code.

To accomplish these four tasks, a PCM synchronizer operates in three successive modes:

1) Search mode — here the synchronizer looks throughout the received data for the sync pattern.
2) Check mode — having found a pattern which is suspected as being a sync code, it tries to verify that this pattern is indeed received periodically, thus increasing the probability that it was in fact the transmitted sync pattern.

3) Lock mode — during which data is received and decoded as long as the mean squared error rate of the sync codes remain small, i.e., as long as synchronization is maintained.

Most realistic time division multiplex PCM communications systems employ many levels of synchronization; e.g., bit, word, subframe, and frame synchronization. A more detailed discussion of this topic can be found in Ref. V.1. It suffices to say that any detailed signal design criteria for the system must include adequate provisions for accurate synchronization.

5. Coding

The question of coding is itself a very complex one. First of all, given that the communications channel is capable of transmitting 5×10^7 bps at an error rate of 10^{-3}, it is trivial to demonstrate the feasibility of sending 50 bps at an error rate of 10^{-5}. Consider the following scheme: for each bit of command data desired to be transmitted, (2n + 1) identical bits of the same type are sent. For a decision rule if #1's > #0's, then a "1" was transmitted and vice versa. It is evident that as $n \to \infty$, the probability of a decision error approaches zero. Thus select (n) such that:

$$\{1 - Q_k^{2n+1}\} \equiv \left[1 - \sum_{k=o}^{n} \begin{matrix}\text{Probability that k errors occur in} \\ \text{(2n+1) independent trials}\end{matrix}\right] \leq 10^{-5}$$

where $p = 10^{-3} \triangleq$ probability of error in one trial.

Basic probability theory says that (n) must be selected such that

$$\left[1 - \sum_{k=o}^{n} \binom{2n+1}{k} (1-p)^{2n+1-k} p^k\right] \leq 10^{-5} .$$

A simple calculation shows that:

$$n = 1 \quad (2n + 1 = 3) \Rightarrow [1 - Q_k^{2n+1}] = 6 \times 10^{-6} < 10^{-5}$$

Thus, for every single bit of command data desired to be transmitted three identical copies should be sent to insure the desired accuracy. Hence, 50 bps at an error rate of 10^{-5} is equivalent (with simple coding) to 150 bps at an error rate of 10^{-3}; well within the channel capabilities.

5.1 Data Compression

If desired, each type of data (e.g., voice, picture, scientific, engineering and command can be coded separately and differently in an effort to reduce the required bit rate. Thus, each individual source coder/decoder can be designed to detect only the salient features of the information it is processing. If this is done, the reduction in the required bit rate could approach a factor of 10. Table V.4 shows typical figures for the type bit rate reductions which can be expected using data conditioning (compression) techniques. Fig. V-4 shows the general configuration of the signal coding elements of a communication system. The source coders are designed to handle specific types of input data, and the channel coder is used to arrange the source messages sequence in a form that will minimize the effects of channel noise during transmission (note: synch coding facilities have been ignored here).

5.2 Cost Effectiveness of Coding

After the final signal specifications are set, it will be necessary to see if a reduction of a factor of 10 in the bit rate would warrant the increase in weight, power, and complexity of the system due to coding.

Table V.4

Communication Coding Source Bit Rate Reduction

Type of Data	Bandwidth	PCM Equivalent	Delta Coding	Stop Scan Edge Detection	Multiple Interlace Encoding	Predictive Coding	Vocoding
Scientific	0 to 1 kHz	Up to 18 kilobits/ second				Up to 6 kilobits/ second	
Engineering	0 to 1 kHz	Up to 18 kilobits/ second				Up to 6 kilobits/ second	
Pictorial information (real-time TV)	4 MHz	48 megabits/ second	24 megabits/ second	12 megabits/ second	12 megabits/ second		
Voice	4 kHz	40 kilobits/ second	20 kilobits/ second				3 to 6 kilobits/ second

This decision can be done only during the final design phases of any communications system. For the rest of the discussion any use of coding will be neglected.

6. Calculation of Transmitter Power

To summarize, the salient features of the communications system are:

1) $R = 10^3$ km
2) $R_B = 5 \times 10^7$ bps at $P_e = 10^{-3}$
3) $\lambda = 13$ cm (S-band microwave system)
4) ΔPSK modulation
5) $E/N_o = 10$ db for $P_e < 10^{-3}$; actually could have $E/N_o \geq 8$ db but we will use the larger figure to be conservative.

A typical block diagram for this communications system is given in Fig. V-5. This system is well characterized by the one-way range equation:

$$\left[\frac{C}{N}\right] B_{IF} = \frac{\pi^2}{16} \left[\frac{P_T d_T^2 d_R^2 \eta_{aT} \eta_{aR}}{\lambda^2 R^2 (KT) L_T L_R}\right]$$

Since PCM is used, employing a matched filter receiver gives:

$\frac{C}{N} \doteq \frac{E}{N_o}$; in practice a 1 db degradation can be expected when non-ideal matched filter receivers are used. (Note: our conservative value for E/N_o will account for this.)

Also, if: τ = bit width (in seconds)

then: $R_B = 1/\tau$ = bit rate in bps

Define: B_{IF} = required I/F bandwidth

then: $B_{IF} \geq \frac{1}{\tau} = R_B$

thus, the one-way range equation becomes

$$\left[\frac{E}{N_o}\right] R_B = \frac{\pi^2}{16} \left[\frac{P_T d_T{}^2 d_R{}^2 \eta_{aT}\, \eta_{aR}}{\lambda^2 R^2\ (KT)\ L_T L_R}\right]$$

Values for the system parameters, T, η_{aT}, η_{aR}, L_T, L_R, must be selected. Based upon Ref. 1:

$\eta_{aT} = 0.60$

$\eta_{aR} = 0.55$

$L_T = 1.5$ db

$L_R = 4.5$ db

$T = 27°$ K

were chosen. Rewriting the range equation in a slightly different form:

$$P_T d_T{}^2 d_R{}^2 = \frac{16}{\pi^2} \left[\frac{\lambda^2 R^2 (KT) L_T L_R}{\eta_{aT}\, \eta_{aR}}\right] \left[\frac{E}{N_o}\right] R_B$$

Using the above information, it is found that:

$$P_T d_T{}^2 d_R{}^2 = 6.16 \times 10^{-2} \text{ watts} - m^4$$

Antenna diameters and transmitted power can be traded-off. However, the final decision can be made during the actual design of the communications system.

7. COPTRAN - Communication OPtimization Program TRANslator

7.1 Introduction

Previous sections of this chapter have dealt with the primary decisions necessary to design a communications system. The approach taken was that of a first order design, and each topic (e.g., coding, modulation techniques, etc.) was handled as a separate entity — without regard as to how a decision in one area might affect the choices available in another. Of course, the reality of life is not so simple. As an example, consider the results of the first order analysis with

$$P_T d_T^2 d_R^2 = \text{constant}$$

Even here the choice of how to trade off LSV transmitting power vs. LSV antenna size vs. LOS antenna size remains. Obviously, it is necessary to develop new decision criteria to guide in this trade-off analysis. The two most pertinent ones (for space applications) are those of designing a minimum cost system or a minimum weight system. As will be explained in section 7.2, weight optimization is the proper choice in the design of the LSV. Hence, to continue the first order design, analytical (or at least functional) relationships between P_T, d_T, d_R, and the weight of the entire LOS/LSV communications system must be developed. This includes such things as: transmitter and receiver weights, antenna weights, acquisition and tracking system weights, power supply weights, etc. It should be quite clear that even the first order analysis no longer remains straightforward and might not be entirely solvable without resorting to digital computers. NASA realized this problem and in 1965 awarded a study contract (NAS 5-9637) to Hughes Aircraft Company, Culver City, California, which in part:

> ... was undertaken to make a comparative analysis of microwave and laser space telecommunication systems. A fundamental objective of the study was to provide the mission planner and designer with reference data (weight, volume, reliability, and costs), supplementary material, and a trade-off methodology for selecting the system (microwave or optical) which best suits his requirements.[Ref. V.1]

In addition to achieving the above stated goals, a FORTRAN IV computer program called COPTRAN was developed which implemented the major results of the study. Now, the systems design of either a weight optimized or cost optimized communication system is reduced to inputing the proper data to the COPTRAN program.

7.2 COPTRAN Methodology

It is necessary to investigate more deeply the ideas governing COPTRAN. First, why the choice of either a weight or cost optimized system, when in the final analysis a system is wanted which meets the desired performance criteria of a minimum cost. The answer lies in the fact that if the communications system is part of a one-shot mission with no severe weight restrictions, then cost optimization should be used. But, if we do have severe weight restrictions (e.g., booster limitations) or if the system is part of a refurbishable vehicle (where ΔV is the dominant costing factor), then weight optimization should be used.

Next comes the problem of implementing the chosen optimization scheme. It can be shown (see Ref. V.1) that only four major system parameters are needed to express the weight or cost of the entire communications system. These major system parameters have the characteristic that all the communications system parameters can be expressed in terms of at least one of them. Of the possible sets of major system parameters, Hughes selected the following to be the basis of their study (and hence, COPTRAN):

1) transmitter power
2) receiver field of view
3) transmitter antenna diameter (or gain)
4) receiver antenna diameter (or gain)

The parametric weight and cost data was gathered for all the various communications system components (with respect to the above major system parameters). Finally, from this data, Hughes developed monotonic, single-valued, piecewise differentiable weight and cost "burden relationships" again in terms of the major system parameters. For example, they found that:

> the weight and fabrication cost of a transmitter antenna system are dependent upon the transmitter antenna diameter... For small transmitter apertures, the weight is proportional to the antenna area, and hence to the square of the aperture diameter...For larger size apertures the weight dependence becomes volumetric. [Ref. V-1]

(Note: The exact functional relationships described above, including all necessary constants are given in Ref. V-1.)

Thus, what remains of the systems design of a communications channel is to:

1) Specify the desired performance criteria (e.g., that it must satisfy the one-way range equation for a certain set of fixed parameters) and then,

2) optimize the remaining major system parameters using the aforementioned "burden relationships" subject to either weight or cost optimization, in such a way that both the desired performance criteria and any design limits (e.g., maximum available transmitter power or maximum available antenna diameter) are met.

Since for any realistic system it would be impossible to do this by hand (especially if a general parametric study was desired), COPTRAN was developed.

7.3 COPTRAN As Applied to the Design of the LSV-LOS Communications Channel.

Through the generous help given us by NASA-GSFC, and in particular Messrs. S. Schneider and R. Wigand, a copy of COPTRAN was provided. Weight optimization was chosen since the LSV is a refurbishable vehicle, and the input data to the program is exactly that used in the first order analysis previously presented. A summary of the major COPTRAN results are given in Table V.5 and Fig. V-6. Examination of these results show that:

For $R_B(E/N_o) = 5 \times 10^8$

which was the nominal design point of the first order analysis,

$$P_T d_T^2 d_R^2 = 2.5 \times 10^{-1} \text{ watts } -m^4$$

which is an excellent agreement (differs by a factor of ≈ 4) with the first order design. Since the COPTRAN results are known to be more accurate, as well as more inclusive, they can be used with confidence to predict the performance of the communications system and also to obtain baseline data necessary for the design of other segments of the LSV (e.g., the on-board power systems and the structural loading scheme).

8. Acquisition and Tracking

8.1 Acquisition

"Acquisition" is the process of aligning the antennas of the LOS and LSV so that data transmission is possible. A simple way of doing this employs a (radio) beacon aboard the LSV. A block diagram of the system is shown in Fig. V-1. The basic operation consists of the LSV transmitting a beacon signal and the LOS searching pre-determined

Table V.5

Summary of COPTRAN Results for the Nominal

Design Point of $R_B \cdot (E/N_o) = 5 \times 10^8$

Parameter	Optimum Value
$d_T = d_R$ (cm)	57.6
P_T (Watts)	2.25
(1) P_A (Watts)	24.2 (*)
(2) P_B (Watts)	15.2 (*)
(3) W_A (#)	24.4 (*)
(4) W_B (#)	19.0 (*)
(5) Projected Cost ($)	5×10^5 (*)

(1) P_A = total (LSV) transmitter input power requirement from all sources (e.g., acquisition and tracking equipment, modulator, etc.)

(2) P_B = total (LOS) receiver input power requirement; from all sources.

(3) W_A = total (LSV) transmitter weight including all subsystems and power supply.

(4) W_B = total (LOS) receiver weight including all subsystems and power supply.

(5) Includes costs for all subsystems and power supply of both the transmitter and receiver.

(*) All values presented in this table are based on current (1970) state-of-the-art burden relationships and might be expected to decrease slightly (10-15%) by the proposed date of the mission.

sectors of space for that signal. To do this, the LOS would employ a sensitive programmable scanning receiver with a steerable, variable field of view antenna. At the start of the acquisition sequence, the LOS would scan with a very broad (large) field of view antenna characteristic till it found the beacon signal. Then, the antenna pattern would be narrowed, and the scan procedure reexecuted. Thus, by alternately scanning and narrowing its antenna characteristic, the LOS would eventually lock-in on the beacon signal being transmitted by the LSV. Next, the LOS would transmit alignment commands to the command receiver aboard the LSV. These commands serve to orient the LSV in the proper attitude for (re-)establishment of the communications channel. After achieving the proper orientation, control would be transferred to the normal communications system, pending confirmation from the LOS that the channel was indeed operating. If for some reason the channel was not established or was inadvertently lost, control of the LSV would revert to the command receiver, and the acquisition sequence would begin again.

8.2 Tracking

"Tracking" is the term used to identify that procedure by which, after acquisition is achieved, the antennas of the LSV and LOS are kept in the proper orientation for communication to occur. The LOS and LSV will have separate tracking subsystems, each consisting of coupled mechanical and electronic servo systems. Coarse mechanical positioning would be done by a mechanical positioner with the fine adjustments being accomplished electronically (through proper antenna phasing).

The ideas governing such a system are as follows: with communication taking place, the effective orientation of the receiving antennas will constantly be perturbed ever so slightly in an effort to locate the direction that would maximize the mean squared received signal power. This information (coupled with any prior knowledge of the trajectory of the signal source) would then be used to electronically steer the transmitting antennas. This form of "electronic steering" works well, but only for small deviations from the true mechanical orientation of the antenna. Hence, once the difference between the true position of the transmitting antenna and its "electronic position" exceeds some prescribed limit, the mechanical positioner would be called upon to reorientate the antenna in such a way as to null out that difference. Following this, control would revert to "electronic steering" beginning the tracking sequence all over again.

SYSTEM NOMENCLATURE

Symbol	Description
B_{IF}	equivalent noise bandwidth of the IF stage. The maximum $R_B = B_{IF}$.
$\left[\frac{C}{N}\right]_{IF}$ or $\left[\frac{S}{N}\right]_{IF}$	total receiver signal-to-noise power within B_{IF}. With a matched filter receiver $S/N_{IF} = (E/N_o)$.
$\frac{E}{N_o}$	predetection signal energy in each bit/noise power spectral density
d_T	transmitter antenna diameter
d_R	receiver antenna diameter
K	Boltzman's constant, 1.38047×10^{-23} Joules/degree Kelvin
$1/L_T$	transmitter line losses
$1/L_R$	receiver line losses
N	thermal noise power in the IF bandwidth, $N = N_o B_{IF}$
N_o	equals KT
N_R	resultant noise in the analog output signal of a PCM System caused by both quantization and bit error noises
P_e	probability of a bit detection error
P_T	transmitter power output at the transmitter output terminals
R	communication range
R_B	downlink bit rate
S	signal energy
T	total effective system noise temperature referred to the preamplifier input
η_{aT}	transmitter aperture efficiency

η_{aR}	receiver aperture efficiency
τ	transmitted bit width = $1/R_B$
λ	transmitter carrier wavelength

MODULATION NOMENCLATURE

Analog Systems

AM	amplitude modulation
FM	frequency modulation

Uncoded Pulse Systems

PAM	pulse amplitude modulation
PPM	pulse position modulation
PDM	pulse duration modulation

Coded (Digital) Pulse Systems

PCM	pulse code modulation

REFERENCES

V-1. "Parametric Analysis of Microwave & Laser Systems for Communication and Tracking", Hughes Aircraft Company, Culver City, California, work done under NASA Contract No. NAS 5-9637:

Volume I ; October 1970; NASA CR-1686
Volume II ; February 1971; NASA CR-1687
Volume III; February 1971; NASA CR-1688
Volume IV ; February 1971; NASA CR-1689

V-2. Blake, A. M., "Lunar Shuttle Vehicle Communications Systems, August 1970 (Internal Interim Report).

V-3. Lawton, J., "A Comparison of Binary Data Transmission Systems", Proceedings of the 2nd Annual Conference on Military Electronics, IRE, 1958.

V-4. Becker, H. and Lawton, J., "Theoretical Comparison of Binary Data Transmission Systems", Cornell Aeronautical Laboratory, Report CA-1172-5-1, May 1958.

BIBLIOGRAPHY

1. Kalil, F., "Optical and Microwave Communications — A Comparison", NASA TN-D-3984, May 1968.

2. Anon., "Parametric Analysis of Microwave & Laser Systems for Communication and Tracking — A Summary", NASA TR-R-309, April 1969.

3. Wyman, C. L., "Laser Systems Research at Marshall Space Flight Center", NASA N-67-30561.

4. McElroy, J. H., "Carbon Dioxide Laser Systems for Space Communications", presented at ICC 1970, San Francisco, California.

5. Lawton, J., "Investigation of Digital Data Communication Systems", Cornell Aeronautical Laboratory, January 1961, UA-1420-S-1; Phase-1 Report.

6. Lawton, J., "Investigation of Analog and Digital Communications Systems", Cornell Aeronautical Laboratory, May 1963, UA-1420-S-3; Phase-3, final report.

7. Harden, J. W.,Jr., "Advanced Spaceborn Detection, Tracking and Navigation System Studies", NASA N-67-30597.

8. Stokes, L. S., Brinkman, K. L., Pratt, W. K., Weber, J. W., "User's Manual for COPTRAN II; A Method of Optimum Communications System Design", NASA Electronic Research Center, Cambridge, Mass., Report No. P68-267. Work done under contract # NAS-12-566.

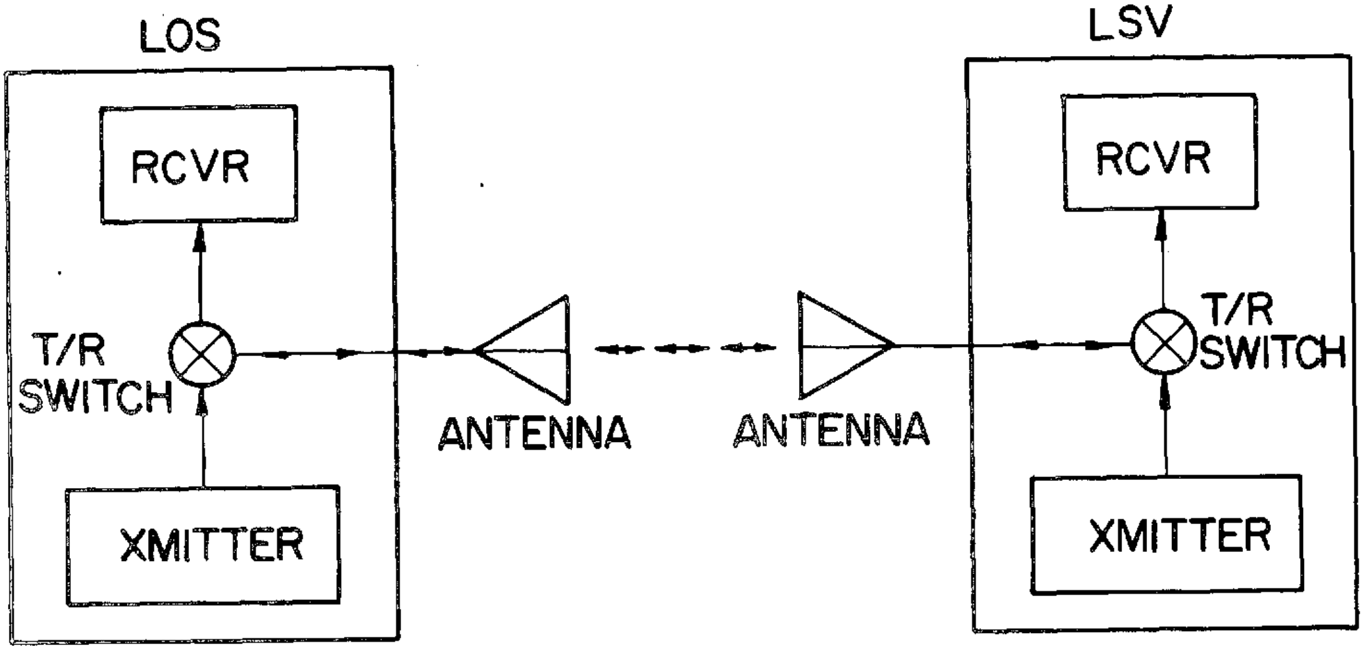
LOS
RCVR
T/R SWITCH
XMITTER
ANTENNA
ANTENNA
LSV
RCVR
T/R SWITCH
XMITTER

"ACTIVE" CONFIGURATION

Figure V-1

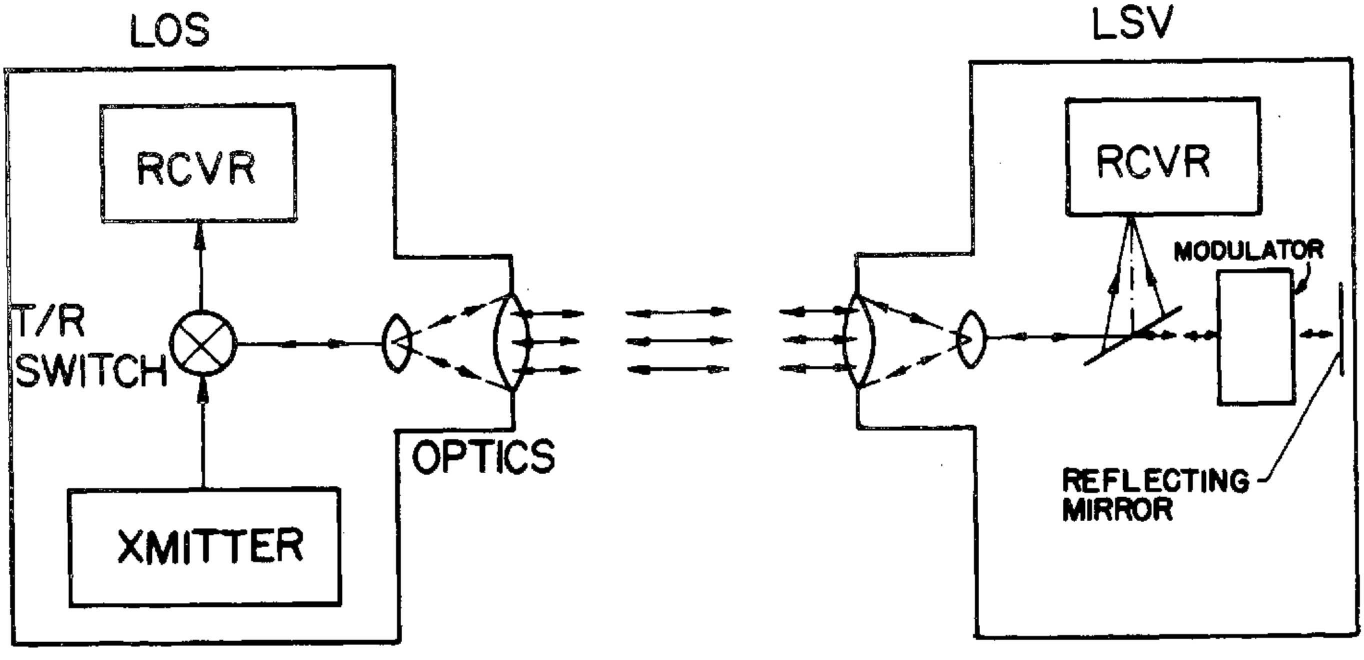
LOS
RCVR
T/R SWITCH
XMITTER
OPTICS
LSV
RCVR
MODULATOR
REFLECTING MIRROR

"PASSIVE" CONFIGURATION

Figure V-2

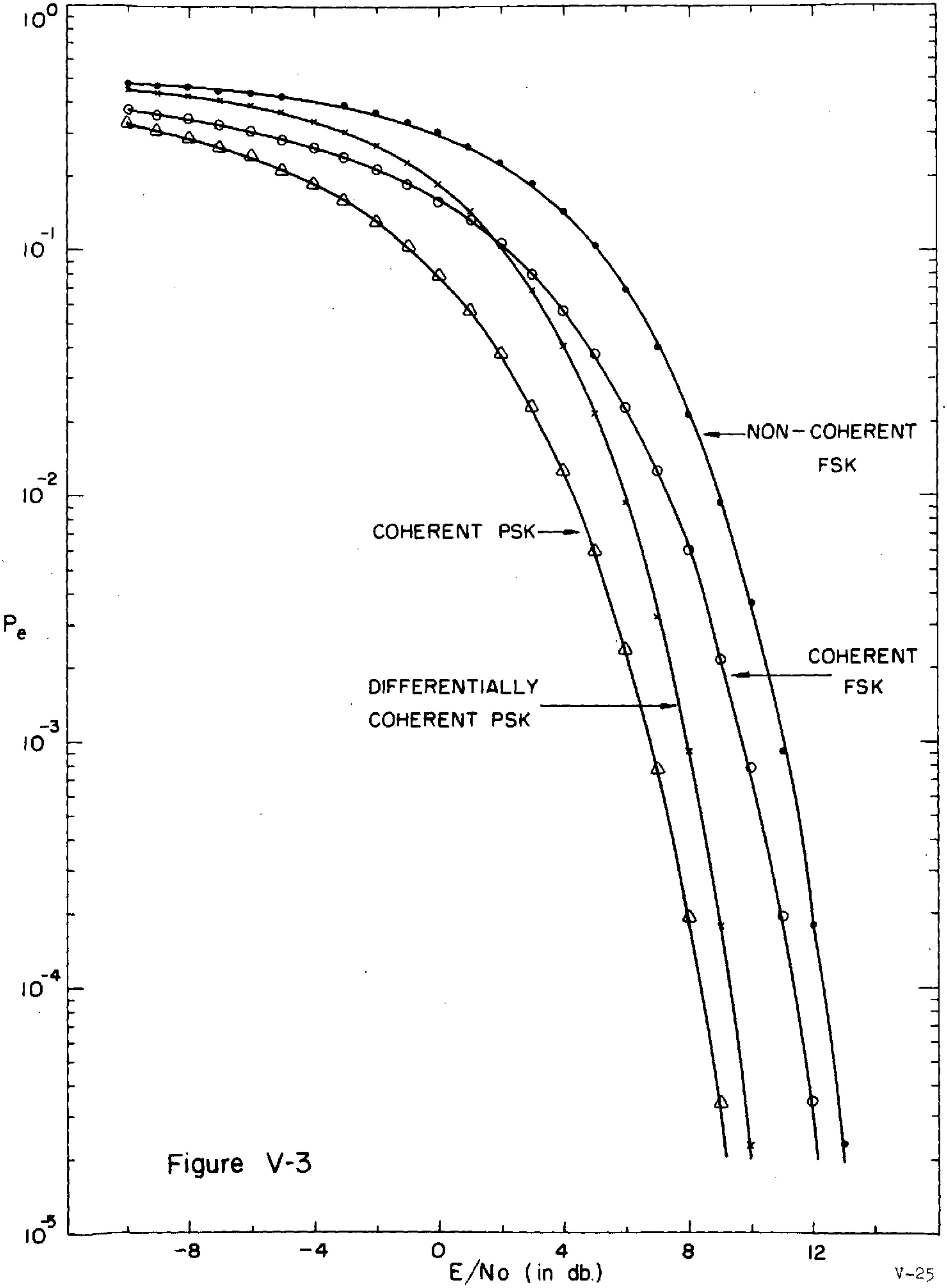

10^0
10^{-1}
10^{-2}
10^{-3}
10^{-4}
10^{-5}
P_e
NON-COHERENT FSK
COHERENT PSK
COHERENT FSK
DIFFERENTIALLY COHERENT PSK
-8
-4
0
4
8
12
E/No (in db.)

Figure V-3

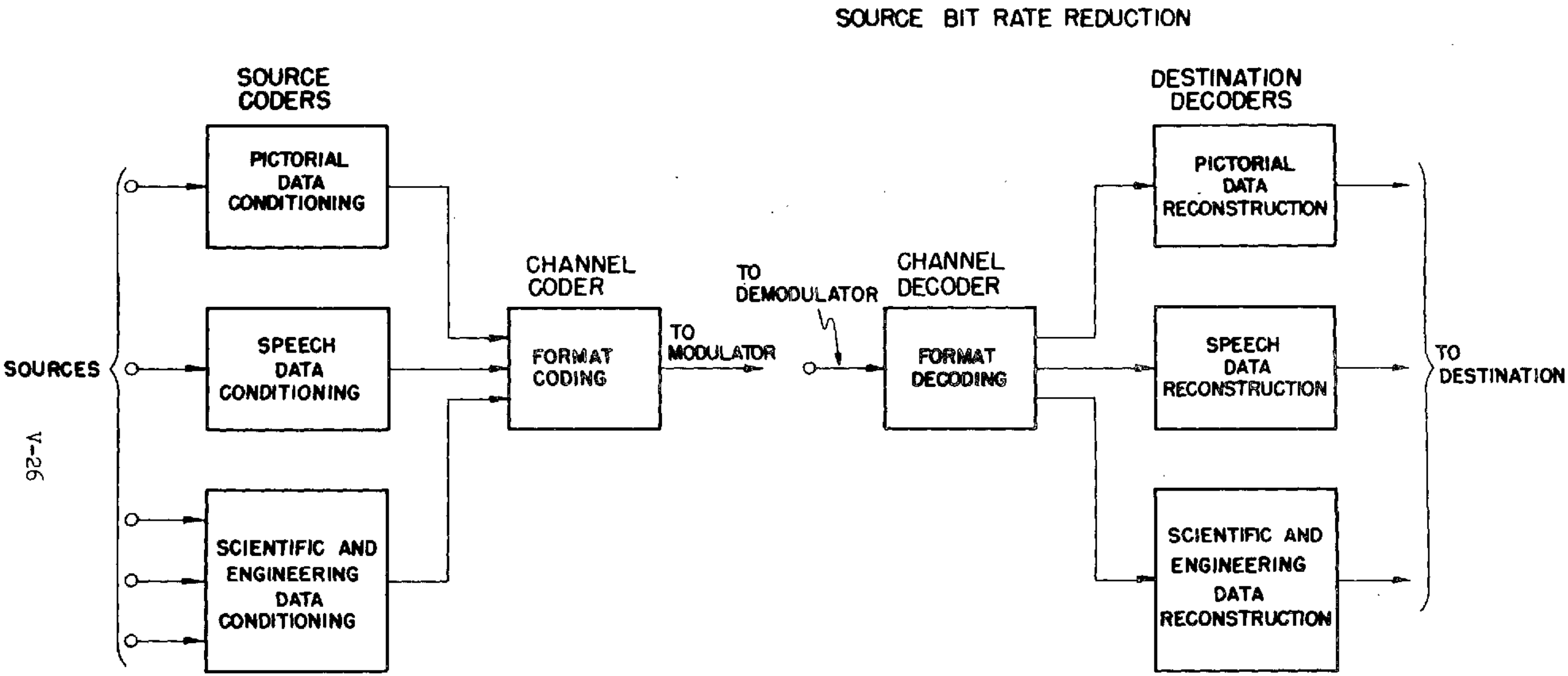
SOURCE BIT RATE REDUCTION
SOURCE CODERS
SOURCES
PICTORIAL DATA CONDITIONING
SPEECH DATA CONDITIONING
SCIENTIFIC AND ENGINEERING DATA CONDITIONING
CHANNEL CODER
FORMAT CODING
TO MODULATOR
TO DEMODULATOR
CHANNEL DECODER
FORMAT DECODING
DESTINATION DECODERS
PICTORIAL DATA RECONSTRUCTION
SPEECH DATA RECONSTRUCTION
SCIENTIFIC AND ENGINEERING DATA RECONSTRUCTION
TO DESTINATION

a. TRANSMITTING SYSTEM

b. RECEIVING SYSTEM

Figure V-4

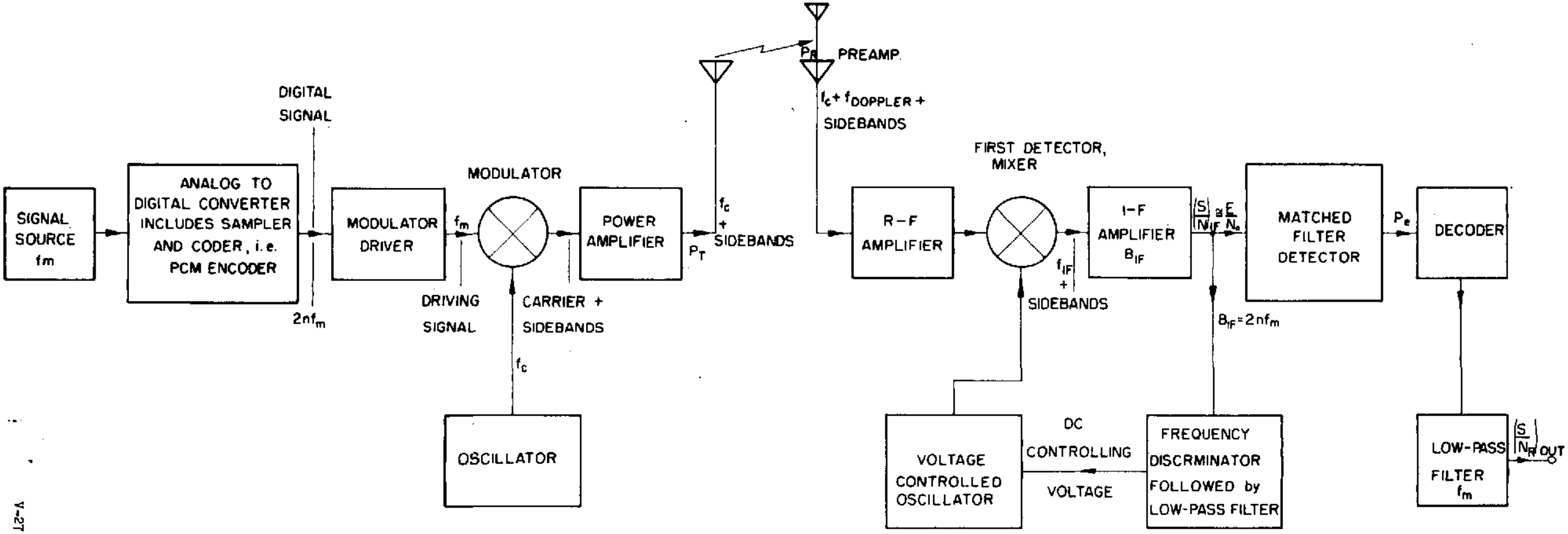
FUNDAMENTAL DIGITAL COMMUNICATIONS SYSTEM BLOCK DIAGRAM

SIGNAL SOURCE fm
ANALOG TO DIGITAL CONVERTER INCLUDES SAMPLER AND CODER, i.e. PCM ENCODER
DIGITAL SIGNAL
2nf$_m$
MODULATOR DRIVER
f$_m$
DRIVING SIGNAL
MODULATOR
CARRIER + SIDEBANDS
f$_c$
OSCILLATOR
POWER AMPLIFIER
P$_T$
f$_c$ + SIDEBANDS
P$_R$
PREAMP.
f$_c$ + f$_{DOPPLER}$ + SIDEBANDS
R-F AMPLIFIER
FIRST DETECTOR, MIXER
f$_{IF}$ + SIDEBANDS
I-F AMPLIFIER B$_{IF}$
$\left(\frac{S}{N}\right)_{IF} \cong \frac{E}{N_o}$
B$_{IF}$=2nf$_m$
MATCHED FILTER DETECTOR
P$_e$
DECODER
VOLTAGE CONTROLLED OSCILLATOR
DC CONTROLLING VOLTAGE
FREQUENCY DISCRMINATOR FOLLOWED by LOW-PASS FILTER
LOW-PASS FILTER f$_m$
$\left(\frac{S}{N}\right)_R$ OUT

Figure V·5

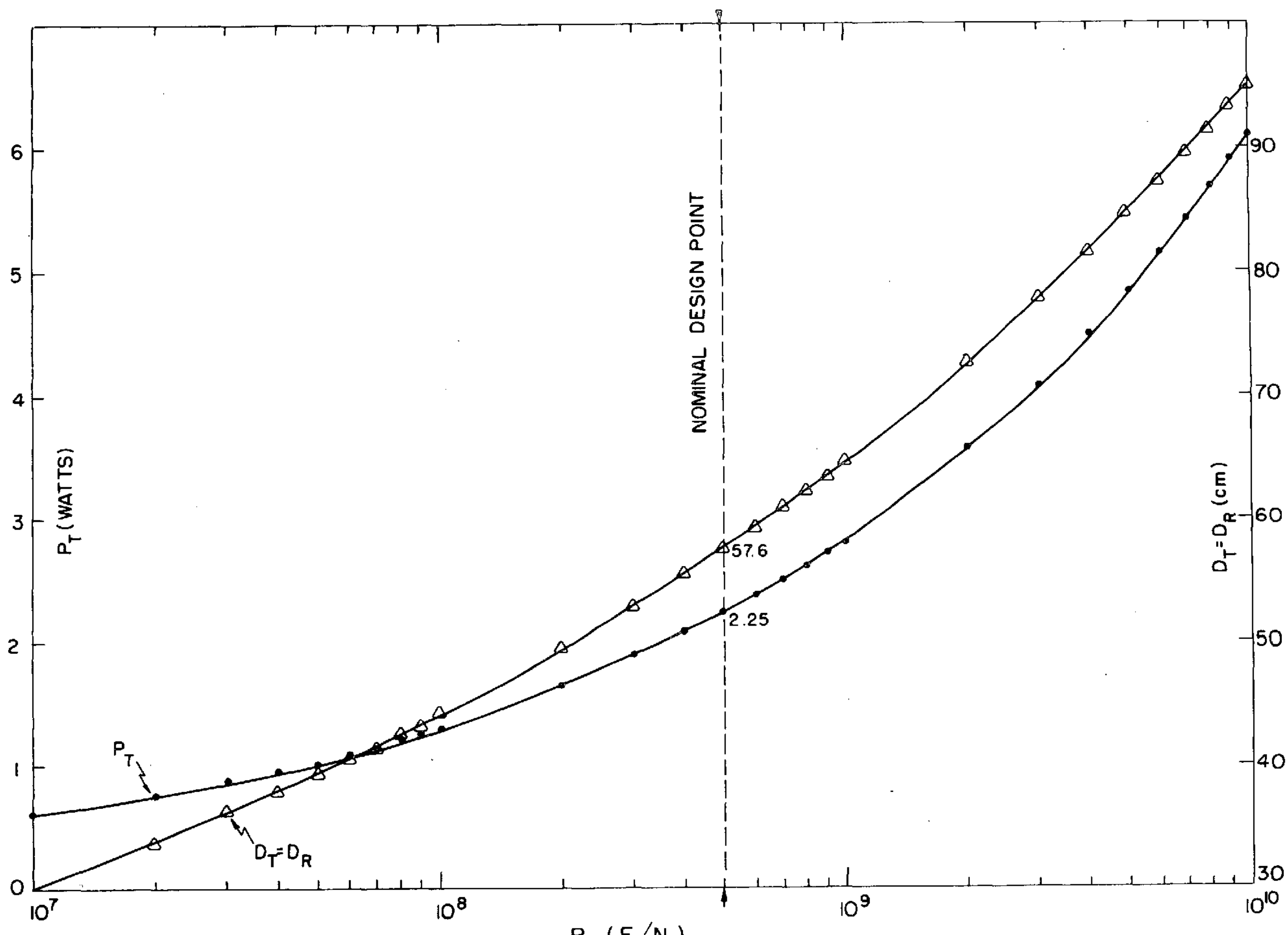

0
1
2
3
4
5
6
P_T (WATTS)
30
40
50
60
70
80
90
$D_T = D_R$ (cm)
NOMINAL DESIGN POINT
57.6
2.25
P_T
$D_T = D_R$
10^7
10^8
10^9
10^{10}
R_B (E/N_0)

Figure V-6

Chapter VI: Propulsion Systems

This chapter summarizes the reasons for the selection of a liquid oxygen - liquid hydrogen (LO_2/LH_2), pump-fed Bell rocket engine for the lunar shuttle vehicle (LSV). The chapter also develops an analytical model which can be used to predict pressure and flow transients in a gaseous oxygen-hydrogen (GO_2/GH_2) reaction control rocket engine feed system.

1. Main Propulsion System

The candidate propellants can be grouped as cryogens, i.e., LO_2/LH_2 or LF_2/LH_2, or space storables, i.e., $FLOX/CH_4$. The cryogens using liquid hydrogen as fuel, are characterized by low bulk density, high specific impulse, and non-overlapping liquidus range. $FLOX/CH_4$ exhibits a moderate high specific impulse and high bulk density.

Earth storables were not considered because of the low specific impulse and storage problem associated with maintaining earth ambient temperatures in order to keep the propellant from freezing.

Table VI.1 lists the propellant combinations considered and the propellant weight penalties (+) or savings (-) incurred, when compared to LO_2/LH_2 with a specific impulse (Isp) of 451 seconds. The calculations for the propellant weight penalty assumed LEM (Lunar Excursion Module) ascent and descent velocity data with a vehicle (w/o propellant) and payload weight of 6,011 pounds and propellant weight of 14,238 pounds.

The weight summary indicates that LF_2/LH_2 yields a slightly lower propellant weight. LF_2/LH_2 was ruled out because of the highly toxic and reactive character of florine and it was felt that the slight weight saving over LO_2/LH_2, did not warrant development of a reliable and space proven

Table VI.1

Propellant Combination	Isp (seconds)	Mixture Ratio O/F	% Difference From Baseline
FLOX/CH_4	400	5.25	+ 20.3
FLOX/CH_4	410	5.75	+ 15.7
LO_2/LH_2	440	6	+ 3.8
LO_2/LH_2	451	6	—
LF_2/LH_2	468	13	- 5.35

engine using LF_2/LH_2. Successful launches of the Centaur and Saturn vehicles have demonstrated the reliability of pump-fed rocket engine systems with LO_2/LH_2 as the propellants. The choice of LO_2/LH_2 over FLOX/CH_4 was based on weight saving.

Table VI.2 indicates the propellant combinations along with the various rocket engines which were considered in the selection of the main propulsion system. The LO_2/LH_2 pump-fed Bell engine was selected for the LSV. A pump-fed system was selected over a pressure-fed system due to the weight savings in propellant storage equipment and improved performance for the Bell engine.

The tank pressurization which is required to provide net positive suction head for full thrust pump-fed engine operation can be obtained by bleeding warmed propellant from the regenerately cooled engine during an idle phase. The engine pump can operate on the propellant head available from the propellant setting without external pressurization of the tanks at idle. Thus, the requirement for leakproof storage and control of a high pressure tank pressurization gas such as helium is eliminated.

Table VI.2

Engine Data*

Propellant Combination	Feed	Mixture Ratio O/F	Chamber Pressure (psia)	Isp Delivered (seconds)	Expansion Ratio (ε)	Engine dia/length in/in	Engine Weight lbs.	Thrust Rated	Throttle
LO/$_2$LH$_2$	Pump	6	900	451	100	25/53	152	8,000	8:1
	Pressure	6	100	445	100				
1. LF$_2$/LH$_2$	Pump	13	900	468	100	25/54	152	8,000	8:1
	Pressure	13	100	442	100				
FLOX/CH$_4$	Pump	5.75	600	410	100	31/61	152	8,000	8:1
	Pressure	5.75	100	387	100				
2. O$_2$/H$_2$	Pump	5		440(nom) 439(min)	57:1	39.67/70.23	290	15,000	No
3. O$_2$/H$_2$	Pump	5		444(nom) 439(min)	60:1	39.67/70.23	315	15,000	10:1
4. FLOX/CH$_4$	Pump	5.25	500	399	60:1	41/21	89	5,000	10:1
	Pump	5.25	800	399					

*All engines are regeneratively cooled.

1. Bell Engines
2. RL10A-3-3
3. RL10A-3-7
4. Rocketdyne

The gaseous propellant boiloff can be used for the bi-propellant reaction control system (RCS) supplemented with an auxiliary means to transform the liquid propellant to the gaseous phase.

The Bell engine uses regenerative cooling of the main combustion chamber and radiation cooling of the exhaust nozzle, where the heat flux level permits. The additional pressure required to force the fuel coolant through the coolant passages can be supplied by a turbopump.

An expander cycle, i.e., the turbopump driving gas is returned to the main chamber for combustion and expansion at full engine area ratio, was selected over an open cycle, i.e., turbopump driving gas is discharged overboard at less than main chamber expansion ratio, due to the inherent capability of the former to provide a higher specific impulse performance.

2. Reaction Control System

The RCS provides impulse for small vehicle velocity changes, attitude maneuvers, and attitude or station keeping. The RCS rockets will be of the bi-propellant type utilizing GO_2/GH_2. The use of a common oxidizer and fuel for both main and reaction control propulsion simplifies the fuel handling along with utilizing boiloff from the main propellant tanks. An auxiliary means of providing gaseous propellants from liquid propellants should be provided by means of a heat source in smaller auxiliary propellant tanks.

The location and number of rocket nozzles required to yield sufficient redundancy was found to be a 12-nozzle configuration shown on page VI-5.

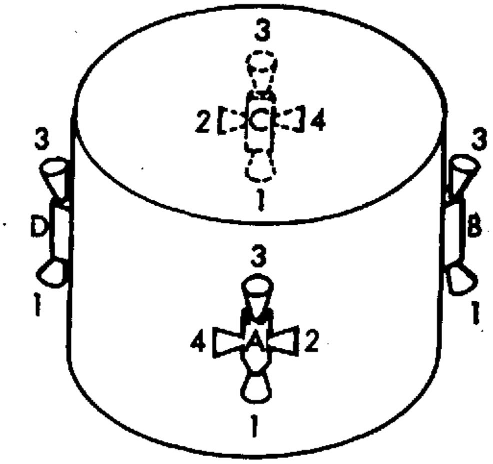

12 NOZZLES

In order to aid in the design of the gaseous bi-propellant RCS an analytical model was developed to predict the pressure and flow transients in the proposed GO_2/GH_2 reaction control rocket engine feed system. The one dimensional equations of momentum and continuity are reduced by the method of characteristics from partial derivatives to a set of total derivatives which describe the state properties along the feedline. System components, e.g., valves, manifolds, and injectors are represented by pseudo steady-state relations at discrete junctions in the system. Solutions were effected by a FORTRAN IV program on an IBM 360/65. The results allow evaluation of the relative effect of manifold volume, combustion lag time, feedline pressure fluctuations, propellant temperature, and feedline length on the chamber pressure transient for a 100 pound thrust-rocket engine. The analytical combustion model is verified by good correlation between predicted and observed chamber pressure transients.

The developed model enables a rocket designer to vary the design parameters analytically to obtain stable combustion for a particular mode of operation which is prescribed by mission objectives.

3. General

In the area of spacecraft propulsion devices, reaction control system (RCS) rocketry is unique. The RCS rocket maneuvers and steers a spacecraft in the absence of aerodynamic forces. These engines operate in the pulse mode for a major portion of the time; as a consequence, their design requirements differ substantially from those of larger devices. The following are the significant design requirements: high thrust to minimum impulse ratio, fast response time, and a long cycle life. The present RCS used in manned spaceflight is a liquid bipropellant system. The system basically consists of pressurized propellant tanks, propellant lines, and the rocket engine assembly, which is composed of propellant valves, injectors, and a thrust chamber.

The pulsed operation of the present RCS engine and its feed system are responsible for hydraulic transients capable of severely altering engine performance. Rapid operation of the propellant valves generates elastic waves in the propellant lines. The elastic waves generated in the oxidizer and fuel have different propagation velocities and as a result cause the oxidizer-fuel ratio in the engine to vary. The flow in the manifolds and internal passages of the injector is coupled to the thermochemical processes in the combustion chamber as well as to the oscillating feed system flow. The manner in which this coupling contributes to the observed combustion instability is unknown, but certainly significant.

4. Previous Work

The dynamic characteristics of large liquid-propellant rocket engine feed systems has been the subject of many analyses during the past two decades. The low-frequency instability analytical model currently used to predict stability limits has evolved from the contributions of many researchers [VI-1, -2]. Crocco et al [VI-3] showed that small combustion delays are instrumental in initiating high-frequency combustion instability. Such delays are probably in the gas phase, because gas mixing is the rate limiting step in the combustion process. As a result, several researchers [VI-4,-5] have proposed various gas mixing models, but only the model proposed by Szuch has been experimentally confirmed.

Previous methods for computing feedline dynamics are applicable only to liquid propellant rockets. Most of the rocket response studies in the literature incorporate the lumped-element approach [VI-6,-4]. With this method the major drawback is the distortion in the time-spatial relationship between components. The most recent and promising approach, Eschweiler and Wallace [VI-7], uses the method of characteristics to transform the one dimensional equations of continuity and momentum from partial derivatives to a set of total derivatives describing state properties along specified paths. System components, e.g., valves, tanks, injectors, are represented by pseudo-steady state relations at discrete junctions in the system.

The present study extends the characteristic method of analysis to develop an analytic model of a gaseous hydrogen-oxygen RCS engine. The model is capable of predicting the dynamic response of the system and the individual components when the fuel and oxidizer valves are activated by a command signal. The unique aspects of this model are its capability of predicting non-steady compressible flow through feedlines and engine components and incorporation of ignition lag, and variable combustion lag times.

5. Analysis

5.1 Feedline Model

The one dimensional unsteady Euler equation of motion and the equation of continuity are used to describe the flow of gas through a pipe.

$$\frac{\partial u}{\partial t} + u \frac{\partial u}{\partial x} + \frac{1}{\rho} \frac{\partial P}{\partial x} = 0 \qquad \text{(VI-1)}$$

$$\frac{\partial \rho}{\partial t} + \rho \frac{\partial u}{\partial x} + u \frac{\partial \rho}{\partial x} = 0 \qquad \text{(VI-2)}$$

It is assumed that the pipe flow is free of compression shocks, i.e., $\rho = \rho(P)$, and also external forces, friction, and heat conduction are neglected.

The theory of characteristics is used to obtain the compatibility relations, which describe the properties of the flow along a characteristic. The compatibility relations are

$$\frac{D^+}{Dt} \left(\frac{2}{\gamma-1} a + u \right) = 0 \qquad \text{(VI-3)}$$

$$\frac{D^-}{Dt} \left(\frac{2}{\gamma-1} a - u \right) = 0 \qquad \text{(VI-4)}$$

The characteristic slopes corresponding to Equations (VI-3) and (VI-4) are

$$\frac{dx}{dt} = u + a \quad \text{(in direction of flow)} \qquad \text{(VI-5)}$$

$$\frac{dx}{dt} = u - a \quad \text{(against direction of flow)} \qquad \text{(VI-6)}$$

The complete derivation of equations (VI-3), (VI-4), and (VI-6) is presented by Sidransky and Smith [VI-8]. Also, one notes that, for isentropic flow, the compatibility equations yield the classical Riemann invariants. Equations (VI-3) through (VI-6) can be non-dimensionalized by specifying a reference velocity, a_r, and a specific reference length, x_r. The reference time becomes $t_r = x_r/a_r$. Equations (VI-3) and (VI-4) are simplified by setting the Riemann invariants equal to $\wp$ and Q, respectively.

$$\wp = \frac{2}{\gamma-1} A + U \qquad \text{(VI-7)}$$

$$Q = \frac{2}{\gamma-1} A - U \qquad \text{(VI-8)}$$

and the characteristic slopes become

$$\frac{dx'}{dt'} = U + A \qquad \text{(VI-9)}$$

$$\frac{dx'}{dt'} = U - A \qquad \text{(VI-10)}$$

where: $x' = x/x_r$, $t' = t/t_r$, $A = a/a_r$, and $U = u/a_r$.

The numerical scheme described by Markowsky [VI-9] may be used to obtain the properties of the flow along the length of pipe. Boundary conditions are either specified by a valve, orifice, or the junction of the feedline and propellant supply tank. The latter junction is considered to be a nozzle intake surface and described by

$$A^2_T = A^2 + \frac{\gamma-1}{2} U^2 \qquad \text{(VI-11)}$$

5.2 Valve and Injector Model

A propellant valve will be considered as a variable resistance orifice and an injector as a multiple orifice which can be modeled as a single orifice with an equivalent flow area. The flow will be considered quasi-steady, frictionless, and adiabatic. The governing equations are the continuity

$$\dot{m} = \rho_u \, A_u \, u_u = \rho_t \, A_t \, u_t \tag{VI-12}$$

and the quasi-steady energy equation

$$JE_u + \frac{u_u^{\,2}}{2g} = JE_t + \frac{u_t^{\,2}}{2g} \tag{VI-13}$$

Combining Equations (VI-12) and (VI-13) with the thermodynamic relations for a perfect gas, one obtains the equation for the mass flow through an orifice.

$$\dot{m} = C_d \, A_o \left[2g \, \frac{n}{n-1} \, P_u \, \rho_u \left(\frac{P_d}{P_u} \right)^{2/n} \frac{1 - (P_d/P_u)^{\frac{n-1}{n}}}{1 - (A_d/A_u)^2 (P_d/P_u)^{2/n}} \right]^{1/2} \tag{VI-14}$$

In the preceding equation, the downstream pressure and temperature were substituted for the throat pressure and temperature and corrected by an empirical factor "C_d". Once m is calculated, the upstream and downstream velocities are readily obtained from Equation (VI-12). Hence,

$$u_d = \dot{m}/\rho_d \, A_d \quad , \quad u_u = \dot{m}/\rho_u \, A_u \tag{VI-15}$$

The valve and/or injector may now be treated as a resistance junction once the resistance, i.e., $1/A_o \, C_d$ is specified. The simulation of these resistance components is considered to occur at discrete locations along the length of the feed system, as shown in Figure VI-1.

In this study a valve is simulated as a time dependent variable resistance orifice. Once an instantaneous value of resistance has been determined, the valve conditions may be computed from Equation (VI-14) and the corresponding compatibility condition. It is the specification of the valve resistance which forms the simulation feature of this component. Details of simulating valves in this manner are set forth in Ref. [VI-7]. An injector is treated as a fixed resistance component with a variable back pressure. As such, one pressure is obtained from the manifold conditions and the second pressure is obtained from the combustor model. Features also included which extend the versatility and usefulness of the model are hot gas ingestion through the injectors and hot gas ingestion into the manifolds.

5.3 Manifold Model

The manifold model considers the gas to be homogeneous, quasi-steady and assumes the gas mass, m_m, in the manifold at any time is given by the perfect gas law,

$$m_m = \rho_m V_m = \frac{V_m M_m}{R_o T_m} P_m \tag{VI-16}$$

The rate of change of manifold pressure may be obtained by differentiating Equation (VI-16) with respect to time and setting the result equal to the mass flow in ($\dot{m}_o$) minus the mass flow out ($\dot{m}_i$)

$$\frac{dm_m}{dt} = \frac{M_m V_m}{R_o T_m} \frac{\partial P_m}{\partial t} - \frac{M_m V_m}{R_o T_m^2} P_m \frac{\partial T_m}{\partial t} + \frac{V_m P_m}{R_o T_m} \frac{\partial M_m}{\partial t} = \dot{m}_o - \dot{m}_i \tag{VI-17}$$

solving for $\partial P_m/\partial t$ gives

$$\frac{\partial P_m}{\partial t} = \frac{R_o T_m}{M_m V_m} (\dot{m}_o - \dot{m}_i) + \frac{P_m}{T_m} \frac{\partial T_m}{\partial t} - \frac{P_m}{M_m} \frac{\partial m_m}{\partial t} \qquad \text{(VI-18)}$$

In order to obtain the rate of change of manifold gas temperature and molecular weight, one must perform an energy and mass balance respectively, on the manifold. The manifold pressure at time "t" can be found by setting $\partial P_m/\partial t = [P_m(t) - P_m(t - \Delta t)]/\Delta t$ and solving for $P_m(t)$. The energy balance yields

$$T_m(t) = \frac{c_{vm}(t-\Delta t)}{c_{vm}(t)} \frac{m_m(t-\Delta t)}{M_m(t)} T_m(t-\Delta t) + \frac{c_{po}(t-\Delta t)}{c_{vm}(t)} \frac{m_o(\Delta t)}{m_m(t)} T_o(t-\Delta t)$$

$$- \frac{c_{pm}(t-\Delta t)}{c_{vm}(t)} \frac{m_1(\Delta t)}{m_m(t)} T_m(t-\Delta t) \qquad \text{(VI-19)}$$

where

$$m(\Delta t) = [\dot{m}(t) + \dot{m}(t-\Delta t)]\ \Delta t/2.$$

Therefore $\partial T_m/\partial t$ can be approximated by $[T_m(t) - T_m(t-\Delta t)]/\Delta t$ and $\partial M_m/\partial t$ can be found in a similar manner by using a mass balance to find $M_m(t)$.

For hot gas ingestion into the manifold the sign of m_1 in Equation (VI-18) becomes positive and in Equation (VI-19) the last term on the right hand side becomes

$$+ \frac{c_{pc}(t-\Delta t)}{c_{vm}(t)} \frac{m_i(\Delta t)}{m_m(t)} T_c(t).$$

5.4 Combustion Model

In formulating a combustion model, the flow of propellants through a chamber may be simplified by assuming that addition of thermal energy takes place at constant pressure. This is a good assumption, if the thrust chamber Mach number is less than 0.2. The process is adiabatic because no heat is transferred to the walls. However, the process is not isentropic, because energy has to be expended on accelerating the gases and this energy becomes unavailable. Further simplifying assumptions are:

(1) The pressure at the injector face corresponds to the pressure one computing interval earlier $P_c(t-\Delta t)$.

(2) The gas mass in the combustion chamber is homogeneous.

(3) The pseudo-steady state approximates the transient for each computing time interval Δt, ($\Delta t < 0.000003$ seconds).

(4) The propellant gas generation rate is determined from the injection rate with a variable time delay, τ, due to mixing and chemical reaction.

(5) The physical dimensions of the combustion chamber are constant with time, that is, chamber ablation, or nozzle throat erosion is negligible over the time period of interest.

The analytic combustion model, with the above assumptions, is based on a mass and energy balance of the entering propellants through the injector, the hot gas exiting the nozzle, and the residual gas left in the chamber. The mass balance on the combustor yields

$$m_c(t) = m_c(t-\Delta t) + m_{io}(\Delta t) + m_{if}(\Delta t) + m_{ioi}(\Delta t) + m_{ifi}(\Delta t) - m_{ne}(\Delta t) \quad \text{(VI-20)}$$

where

$$m_c(t-\Delta t) = m_{co}(t-\Delta t) + m_{cf}(t-\Delta t) + m_{ci}(t-\Delta t)$$

and again

$$m(\Delta t) = [\dot{m}(t) + \dot{m}(t-\Delta t)]\ \Delta t/2.$$

The mixture ratio of the incoming propellants is obtained by dividing the increments of oxidizer by the increments of fuel entering in time interval Δt.

$$MR = \frac{m_{io}(\Delta t)}{m_{if}(\Delta t)}$$

A more meaningful mixture ratio, i.e., one considering the time due to mixing in a homogeneous reactor, is the accumulated mass mixture ratio, which is

$$\begin{aligned} MR(t) = \Big(& [m_{co}(t-\Delta t) + m_{io}(\Delta t) + m_{ni}(\Delta t) - m_n(\Delta t)]\ MR(t-\Delta t) \\ & + m_{co}(t-\Delta t) + m_{io}(\Delta t)\Big) \Big/ \Big(m_{cf}(t-\Delta t) + m_{if}(\Delta t) \\ & + m_{ni}(\Delta t) - m_n(\Delta t) + [m_{cf}(t-\Delta t) + m_{if}(\Delta t)]\ MR(t-\Delta t)\Big) \end{aligned} \qquad \text{(VI-21)}$$

The accumulated mass mixture ratio is made up of the entering propellants and the residual mass in the combustor.

The combustor gas temperature is obtained by considering an energy balance on the combustion chamber and neglecting the lower order kinetic and potential energy terms. Hence,

$$\begin{aligned} T_c(t) = \Big(& [m_c(t-\Delta t)\ c_{vc}(t-\Delta t) - \frac{m_n(t-\Delta t)}{2}\ c_{pc}(t-\Delta t)]\ T_c(t-\Delta t) \\ & + [m_{io}(\Delta t) + m_{if}(\Delta t)]\ c_{pc}(\tau+t)\ T_{CT}(\tau+t) \\ & + [m_{io}(\Delta t) + m_{ioi}(\Delta t)]\ c_{pio}(\Delta t)\ T_{io}(\Delta t) \\ & + [m_{if}(\Delta t) + m_{ifi}(\Delta t)]\ c_{pif}(\Delta t)\ T_{if}(\Delta t)\Big) \Big/ [m_c(t)\ c_{vc}(t) + \frac{m_n(t)}{2}\ c_{pc}(t)] \end{aligned}$$

(VI-22)

The combustion gas temperature is determined by applying the characteristic exhaust velocity efficiency to the theoretical value, therefore

$$T_{CT} = T_{CTT} \eta^2_{c*} \qquad \text{(VI-23)}$$

where

$$(\tau+t) = t_{\text{combustion lab}} + t_{\text{injection}}$$

and

T_{CT} = the combustion temperature of mass $[m_{io}(\Delta t) + m_{if}(\Delta t)]$ at time $(\tau+t)$.

The gas properties, i.e., M, c_p, and γ, are obtained from combustion performance data, which are functions of the mixture ratio. This is done because equilibrium and frozen combustion performance of hydrogen-oxygen is available in the form of ratio of specific heat (γ), specific heat at constant pressure (c_p), combustion temperature (T_{CTT}), and molecular weight (M) as a function of mixture ratio and pressure. The equilibrium and frozen combustion performance of hydrogen-oxygen used was that presented by Gordon and McBride [VI-10], corrected for gaseous propellant combustion.

With $T_c(t)$, $M_c(t)$ and $m_c(t)$ known, the chamber pressure may be calculated from the ideal gas law, hence,

$$P_c(t) = m_c(t)\, R_o T_c(t)/[V_c M_c(t)] \qquad \text{(VI-24}$$

The mass flow through the nozzle is given by the standard nozzle relations:

for choked flow,

$$\dot{m}_n(t) = A_{nt}\, C_{dn}\, P_c(t) \left[\frac{g\, \gamma_c(t)\, M_c(t)}{R_o\, T_c\, (t)}\right]^{1/2} \left[\frac{2}{\gamma_c(t) + 1}\right] \left(\frac{\gamma_c(t) + 1}{2[\gamma_c(t) - 1]}\right)$$

(VI-25)

and for nonchoked flow,

$$\dot{m}_n(t) = A_{nt}\, C_{dn}\, P_c(t) \left[\frac{2\, g\, \gamma_c(t)\, M_c(t)}{[\gamma_c(t) + 1] R_o T_c(t)}\right]^{1/2} \left[\left(\frac{P_a}{P_c(t)}\right)^{\frac{2}{\gamma_c(t)}} - \left(\frac{P_a}{P_c(t)}\right)^{\frac{\gamma_c(t)+1}{\gamma_c(t)}}\right]^{1/2} \tag{VI-26}$$

With the above combustion model, calculations of the chamber pressure and temperature of the residual gases requires an iterative solution. The solution is accomplished by selecting the efflux mass, $\dot{m}_n(t)$, through the nozzle and if the computed value of $\dot{m}_n(t)$ from Equation (VI-25) or (VI-26) does not agree within a prescribed delta, a new choice is made and the process is repeated until convergence to a desired tolerance is achieved.

Combustion lags, i.e., due to gas mixing and chemical reactions, are incorporated into this model by specifying a finite period of time between the instant the propellant enters the chamber (time = $t_{\text{injection}}$), and the time when it is burned (time = $t_{\text{injection}} + t_{\text{combustion lag }(\tau)}$).

6. Results and Discussion

6.1 Feedline Dynamics

The feeding system and engine assembly arrangement which is investigated is the fast response type. That is to say, the oxidizer and fuel valves feed directly into the manifolds, thus eliminating any pipe fill and emptying time lag which are inherent when the propellant valves and manifolds are separated by a length of feedline.

Figure VI-2 illustrates the effect of feedline dynamics on manifold pressure and mixture ratio with combustion suppressed. The valve opening and closing time is 5 milliseconds (ms.). This valve was used throughout this study along with the valve resistance given by Eschweiler and Wallace [VI-7]. The initial conditions for this and succeeding runs are given in Table VI.3 along with the pertinent design parameters.

The variation in fuel and oxidizer manifold pressure is caused by the pressure waves, which are initiated when the valve is opened. The opening of the propellant valve initiates an expansion wave propagating upstream from the valve towards the gaseous supply tank. The junction between the supply tank and the feedline can be considered to be a nozzle intake surface, and therefore nearly a constant pressure surface, so that the incoming expansion wave is reflected as a compression wave. The reflected compression wave travels downstream and is partially swallowed and reflected upon reaching the valve. The valve boundary is not a constant pressure surface so the reflected wave maintains the same sign, i.e., compression waves are reflected as compression waves and expansion waves are reflected as expansion waves. So, the wave, upon reaching the valve, is reflected as a slightly weaker wave. This phenomena is most evident in the fuel side of the feed system due to the greater wave propagation velocity which results in a higher frequency of pressure oscillation. The result of the out of phase oscillation in the two feedlines is to produce a variable mixture ratio shown in Figure VI-2. From the preceding observations and discussion, one can conclude that the feedline dynamics are capable of producing alterations in the mixture ratio, i.e., accumulated mass mixture ratio, and consequently in engine performance.

Table VI.3

Summary of System Parameters

RUN	P_T (psia)	T_T (°R)	L_O (in.)	L_F (in.)	d_p (in.)	D_v (in.)	D_i (in.)	P_c (psia)	L* (in.)	V_c (in.^{3})	A_c (in.^{2})	D_{nt} (in.)	η_{c*}
250 - 257	125	200	60	60	.5	.292	.378	80	25	17.8	3.56	.952	.95
450 - 457	125	400	60	60	.5	.339	.433	80	25	17.8	3.56	.952	.95
471	125	"	60	6	"	"	"	"	"	"	"	"	"
472	125	"	30	30	"	"	"	"	"	"	"	"	"
473	125	"	30	60	"	"	"	"	"	"	"	"	"
500	150	500	60	60	.5	.336	.403	100	15	8.54	2.85	.852	—
510, 512	150	500	60	60	.5	.336	.403	100	15	8.54	2.85	.852	.95
502, 560, 562, 563	125	500	60	60	.5	.354	.447	80	25	17.8	3.56	.952	.95
501	750	530	—	—	—	—	.7	500	15	17.2	6.87	1.2	.81

6.2 Combustion Model Verification

The application of the entire analytic model to simulate the only available experimental test setup, Stechman et al [VI-11,-12,-13], was prohibitive due to the extreme complexity of the test setup. It was felt that the pressure drop readout from the flow orifices, which were located near the engine assembly, could be used to obtain the experimental oxygen and hydrogen mass flow rates. Once the experimental flow rates were calculated, they could be incorporated into the present model in order to evaluate its predictive ability. This course of action is considered valid because the experimental test results were obtained under essentially constant feedline conditions.

The experimental P_c distribution shown in Figure VI-3 is for a 1000 LB_f thrust (vacuum) gaseous H_2 - O_2 spark ignited rocket engine with a design chamber pressure of 500 psia.

The method of obtaining the mass flow rates from the pressure drop data incorporated the use of the steady state flow rate data supplied by Stechman [VI-13], in order to obtain the discharge coefficients for both the flow orifices. The disadvantage in using the steady state discharge coefficient is suspected to have caused the artificially higher mass flow rates during startup and shutdown. The startup pressure rise is very rapid due to the driving pressure of the supply tank and so the steady state value of the orifice coefficient is approached faster. But during shutdown, the emptying of the feedlines is a longer and weaker pressure transient, and so an artificially greater calculated flow rate results. The higher flow rates calculated for shutdown manifest as a longer decay pressure transient.

The ability of the theoretical model to predict the observed variation in chamber pressure during the startup transient and also the magnitude of the observed over-pressurization warranted the conclusion that the predictive ability of the combustion model is in good agreement with observed data.

6.3 Effect of Manifold Volume

The design chamber pressure for both runs shown in Figure VI-4 is 100 psia, while the oxidizer and fuel manifold volumes for Runs 510 and 512 are 0.128 and 1.024 in.^{3}, respectively.

The chamber pressure distribution incorporates a time delay due to ignition and combustion. The ignition lag time used for the majority of the runs is based on the time required for the cold flow chamber pressure to attain a value of 0.5 psia. The combustion lag time, (τ), is composed of a chemical reaction lag time and a mixing lag time. A constant value of 0.05 ms was used for the chemical reaction lag time while the mixing lag time could be either a constant or that prescribed by the mixing model of Szuch. The combustion lag times for both runs of Figure VI-4 incorporate the gas mixing lag time of Szuch.

The variation in chamber pressure is seen to follow the corresponding oscillations in mixture ratio. The initial fluctuations in mixture ratio are caused by the fuel feedline pressure fluctuations, while the larger oscillation in mixture ratio is caused by a compression wave approaching and being reflected from the oxidizer propellant valve. The manifold volume tends to have a strong influence on the startup transient. The effect of increasing the manifold volume by a factor of 8 is shown to increase the chamber pressure rise and decay times by 85 and 70 percent respectively.

In the literature, the usual methods of determining the manifold volume that is needed to feed the injectors entails multiplying the injector flow area by a constant. The value three was chosen by Stechman for the ratio of manifold volume to injector flow area because this value provides the desired chamber pressure rise and decay rates while providing a reasonable volume for the manifolds.

6.4 Effect of Combustion Lag Time and Propellant Temperature

Figure VI-5 is composed of four separate runs, which incorporate combustion lag times of 0.0 ms., mixing model of Szuch plus 0.05 ms., 0.5 ms., and 0.75 ms. The mixture ratio distribution for the run in Figure VI-5b is not shown since it is essentially identical to that of run 560. The procedure is also followed in Figures VI-6 and VI-7.

In Figure VI-5a, the smoothness of this curve confirms the stability of an instantaneous combustion case. The relative smoothness of the P_c distribution in Figure VI-5b also predicts stable combustion for the empirical mixing model of Szuch. The fluctuations in chamber pressure are shown to increase with increasing combustion lag time. This observation is in agreement with the experimental observations of Crocco [VI-14]. The variations in chamber pressure caused by increasing τ are evident in the distortion of the mixture ratio distribution. The variations in mixture ratio cause a corresponding variation in combustion gas temperature which in turn causes the chamber pressure to vary.

The low frequency P_c oscillations of 55 cycles per second (cps) in Figures VI-5a, -5b, -5c, and -5d are caused by the oxidizer feedline dynamics, which are known to be a function of feedline length and propellant temperature. The high frequency oscillations suspected to be caused by the magnitude of τ and reinforced by a coupling between τ and the feed system sensitivity to P_c. The above mentioned coupling is suspected to have produced the P_c oscillations of 1000 and 665 cps in Figures VI-5c and -5d, respectively.

The effect of reducing the propellant temperature by a factor of 0.8 and 0.4 is shown in Figures VI-6 and -7, respectively. By examining Figures VI-5, -6, and -7 in sequence, one notices that the instantaneous combustion case is inherently stable with increasing propellant density, while the opposite is observed for larger τ's. The P_c variation exhibits an increase in the magnitude and duration of the high frequency oscillations as τ and the propellant density are increased. The pressure sensitive feeding system, in responding to the chamber pressure fluctuation initiated by the combustion lag, allows a greater mass flow fluctuation through the orifice, due to the greater propellant density. This type of trend is also documented by Feiler [VI-15] and Feiler and Heidmann [VI-6].

The high frequency oscillation in P_c shown in Figures VI-5c, -6c, and -7c were approximately 1000, 800, and 665 cps with corresponding chamber pressure variations of 4.5, 14, and 10 percent respectively. The magnitude of the chamber pressure variations are based on the design chamber pressure of 80 psia. By increasing τ to 0.75 ms., the high frequency oscillations in P_c shown in Figures VI-5d, -6d, and -7d were approximately 665, 665, and 570 cps, with corresponding chamber pressure variations of 9, 9, and 12.5 percent, respectively. The low frequency oscillations shown in Figures VI-5, -6, and -7 were 55, 49, and 37.5 cps with a corresponding chamber pressure variation of 21, 19, and 15 percent.

The chamber oscillations shown in Figures VI-5, -6, and -7 may be compared with the combustion instabilities observed in some rocket motor tests. The experimentally observed combustion instabilities are known to exist in two separate modes. One is a high frequency mode, with frequencies ranging from 100 to as high as 5000 cps. The other mode is the low frequency type, where the frequencies range from 10 to 100 cps.

If one considers the cylindrical combustion chamber as a simple closed organ pipe, the fundamental frequencies for the longitudinal and transverse direction would be 1860 and 7800 cps. Therefore, from the range of high frequency P_c oscillation reported in the literature, one may conclude that organ pipe type oscillations could be initiated and reinforced by the predicted P_c oscillations of 1000, 800, and 665 cps.

Figure VI-8 illustrates the effect of combustion lag and propellant temperature on the chamber pressure when the feedline dynamics are suppressed, i.e., the upstream valve pressure is maintained at the steady state design value. The results show that the chamber pressure distribution becomes smoother, due to the steady mass flow from the propellant valves, which tend to maintain a nearly constant mixture ratio of gas flow into the combustion pressure-sensitive manifolds. Also, the high frequency variations in chamber pressure were reduced in magnitude, thus indicating that a coupling exists between the feedline dynamics and the combustion lag time.

The magnitude of the chamber pressure variation for τ = 0.5 ms. is reduced by a factor of 11.2 between runs 452 and 456, and 4.0 between runs 252 and 256. The magnitude of the chamber pressure variation for τ = 0.75 ms. is reduced by a factor of 1.17 between runs 453 and 457, and 1.92 between runs 253 and 257. Therefore, one can conclude that even with a stable feedline system, i.e., operating at constant pressure, P_c, fluctuations still exist if τ is greater than 0.4 ms. Also, Figure VI-8 confirms the in-phase coupling existing between the feeding system and the P_c fluctuations, which tends to reinforce and increase the observed P_c oscillations.

The steady-state overpressurization of the runs shown in Figure VI-8 is due to the sizing of the expansion nozzle for ideal flow conditions, i.e., C_d = 1.0, whereas in the actual runs a C_d of 0.98 was used.

6.5 Effect of Shorter Feedline Lengths

Additional runs were made in order to determine the effect of feedline length on chamber pressure oscillations.

The oxidizer and fuel valve pressures shown in Figure VI-9a infer that the previously mentioned coupling between the feedline dynamics and combustion lag is mainly a coupling of the fuel feedline dynamics and the combustion lag time. Feiler [VI-15] reached this same conclusion. In that the hydrogen flow is sufficiently sensitive, a coupling can exist between the hydrogen flow oscillations and chamber pressure oscillations, which can drive a combustion instability. Figure VI-9b verifies the above statement by showing that if the hydrogen feedline length is sufficiently short and the feedline oscillations are damped out before combustion, the previously noticed pressure fluctuations no longer exist. The following two figures, i.e., Figures VI-9c and -9d, represent the effect of superimposing rapid fuel and oxidizer feedline pressure oscillations early in the startup transient. The indication is that the coupling of the fuel flow and combustion lag time initiates the high frequency oscillations while the oxidizer side of the feeding system is responsible for the low frequency oscillations.

The area of combustion instability has been the object of many publications, but at best, the analytical work is still of a qualitative nature due to the complexity of the flow and reactions in a combustion chamber. This study has not proposed a new or magic solution to the problem of combustion instability, but has given a quantitative perspective of the consequences of varying the design parameters, which are qualitatively known to affect combustion stability. The present model should enable a designer to obtain the relative importance of the various parameters and eliminate or control combustion instabilities to improve engine performance.

7. Conclusions

1) A gaseous bi-propellant RCS rocket engine is shown to exhibit performance variations due to the pressure waves generated by the rapid opening of the propellant valves. The pressure waves generated were shown to be partially swallowed upon reflection from the valves and therefore damp out with time.

2) Increasing the manifold volumes by a factor of 8 is shown to increase the chamber pressure rise and decay times by 85% and 70% respectively.

3) The effects of feedline pressure fluctuations, combustion lag time, and propellant temperature on the chamber pressure are summarized below.

a) The combustion process is inherently stable for $\tau = 0.0$, i.e., the chamber pressure does not exhibit rapid oscillations.

b) The incorporation of an empirical mixing lag time model was shown to yield smooth combustion for a propellant temperature of 500°R and somewhat rougher combustion with increasing propellant density.

c) Increasing τ and propellant density is shown to cause high frequency oscillations in P_c which increase in magnitude and duration as τ and propellant density are increased. The calculated chamber pressure oscillation of 1000, 800, and 665 cycles per second for $\tau = 0.5$ ms., is suspected to be the mechanism which initiates the experimentally observed high frequency P_c oscillation.

d) When the feedline pressure fluctuations are suppressed, the high frequency variations in chamber pressure for $\tau = 0.5$ and 0.75 ms. were reduced in magnitude, thus indicating that a coupling exists between the feedline pressure fluctuations and τ.

e) The low frequency P_c oscillations are shown to be primarily the result of the feedline pressure fluctuations, while the high frequency oscillations, i.e., > 100 cps, are controlled by the coupling between τ and the fuel feedline system.

REFERENCES

VI-1 Summerfield, Martin, "A Theory of Unstable Combustion in Liquid Propellant Rocket System", J. Am. Rocket Soc., Vol. 21, No. 5, Sept. 1951, pp. 108-114.

VI-2 Crocco, Luigi and Cheng, Sin-I, "Theory of Combustion Instabilites in Liquid Propellant Rocket Motors. AGARDograph No. 8, Butterworth Sci. Pub. (London), 1956.

VI-3 Crocco, L.; Grey, J. and Harrje, D. T., "On the Importance of the Sensitive Time Lag in Longitudinal High-Frequency Rocket Combustion Instability", Jet Propulsion, Vol. 28, No. 12, p. 841, 1958.

VI-4 Szuch, J. R., "Digital Computer Program for Analysis of Chugging Instabilities", NASA TND-7026, 1970.

VI-5 Hersch, Martin, "A Mixing Model for Rocket Engine Combustion", NASA TND-2881, 1965.

VI-6 Feiler, Charles E.; Heidmann, Marcus F., "Dynamic Response of Gaseous-Hydrogen Flow System and its Application to High-Frequency Combustion Instability", NASA TND-4040, 1967.

VI-7 Eschweiler, J. C.; Wallace, H. W., "Liquid Rocket Engine Feed System Dynamics by the Method of Characteristics", ASME Annual Aviation and Space Conference, Beverly Hills, California, June 16-19, pp. 271-280, 1968.

VI-8 Sidransky, F. S. and Smith, M. M., "Nonsteady Liquid and Gas Flow with Heat Addition and Shock Perturbation", NASA TND-3684, Oct. 1968.

VI-9 Markowsky, J. J., "An Analytical Model for Predicting the Pressure and Flow Transients in a Gaseous H_2 - O_2 100 LB_f Thrust Reaction Control Rocket Engine", Ph.D. Thesis, Cornell University, Ithaca, N. Y., 1971.

VI-10 Gordon, S.; McBride, B. J., "Theoretical Performance of Liquid Hydrogen with Liquid Oxygen as a Rocket Propellant", NASA Memorandum 5-21-59E, 1959.

VI-11 Stechman, R. C., et al,"GH_2/GO_2 1,000 lb_f Thrust Rocket Engine Test Program, P/N X25650, MIR #365, The Marquardt Corp., Van Nuys, Calif., April 1970.

VI-12 Stechman, R. C., Personal communication, The Marquardt Corp., Van Nuys, Calif., August 11, 1970.

VI-13 Stechman, R. C., Personal communication, The Marquardt Corp., Van Nuys, Calif., March 16, 1971.

VI-14 Crocco, L., "Aspects of Combustion Stability in Liquid Propellant Rocket Motors, Part I", ARS Journal, November 1951, pp. 163-178.

VI-15 Feiler, C. E., "Effect of Combustion Parameters on the Stability of Gaseous Hydrogen-Liquid Oxygen Engine", NASA TMX-52360, 1967.

NOMENCLATURE

A	Cross-sectional area when subscripted with v, o, or i, non-dimensional acoustic velocity when not subscripted or when subscripted with r or T only.
a	Acoustic velocity.
c_p	Constant pressure specific heat.
c_v	Constant volume specific heat.
d	Diameter of feedline.
D	Diameter.
E	Enthalpy of gas.
F	Thrust.
g	Dimensional constant.
J	Dimensional constant.
L*	Characteristic chamber length.
L	Feedline length.
M	Molecular weight.

MR	Mixture ratio.
m	Mass.
$\dot{m}$	Mass flow rate.
n	Polytropic exponent.
P	Pressure.
	Riemann invariant, (wave moving with the flow).
Q	Riemann invariant, (wave moving against the flow).
R_o	Gas constant.
T	Temperature.
t	Time
t_{start}	Time when valve begins to open.
t_{stop}	Time when valve begins to close.
Δt	Computing time interval.
U	Nondimensionalized velocity.
u	Velocity.
V	Volume.
x	Axial distance.
γ	Ratio of specific heat.
ρ	Density.
τ	Combustion time delay.

Subscripts

c	Refers to combustion chamber.
cf	Refers to fuel in combustion chamber.
ci	Refers to initial mass in combustion chamber.
co	Refers to oxidizer in combustion chamber.

CT	Refers to chemical reaction temperature
CTT	Refers to theoretical combustion temperature.
c*	Refers to characteristic exhaust velocity efficiency.
d	Refers to downstream.
F	Refers to fuel.
i	Refers to injector.
if	Refers to fuel at injector.
ifi	Refers to initial mass at fuel injector.
io	Refers to oxidizer at injector.
ioi	Refers to initial mass at oxidizer injector.
m	Refers to manifold.
n	Refers to nozzle.
ne	Refers to nozzle exit.
nt	Refers to nozzle throat.
o	Refers to orifice or valve.
O	Refers to oxidizer.
P	Refers to propellant (oxidizer and fuel).
r	Refers to reference condition.
T	Refers to tank.
t	Refers to throat.
u	Refers to upstream.
V	Refers to valve.
VF	Refers to fuel at valve.
VO	Refers to oxidizer at valve.

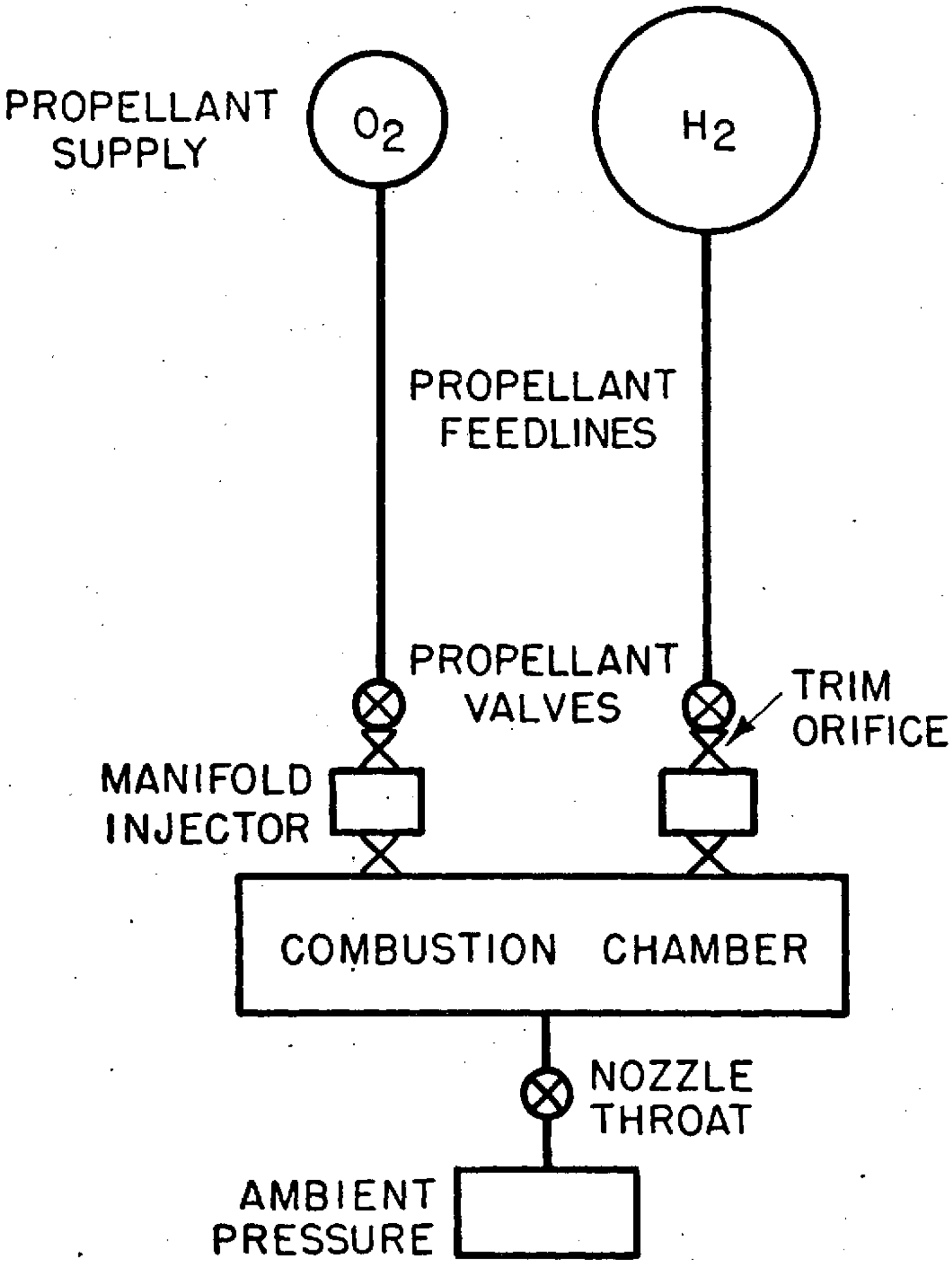
PROPELLANT
SUPPLY
O_2
H_2
PROPELLANT
FEEDLINES
PROPELLANT
VALVES
TRIM
ORIFICE
MANIFOLD
INJECTOR
COMBUSTION CHAMBER
NOZZLE
THROAT
AMBIENT
PRESSURE

NOTE

⧖ = DENOTES ORIFICING OR EQUIVALENT INTERNAL PRESSURE DROP.

Figure VI-1

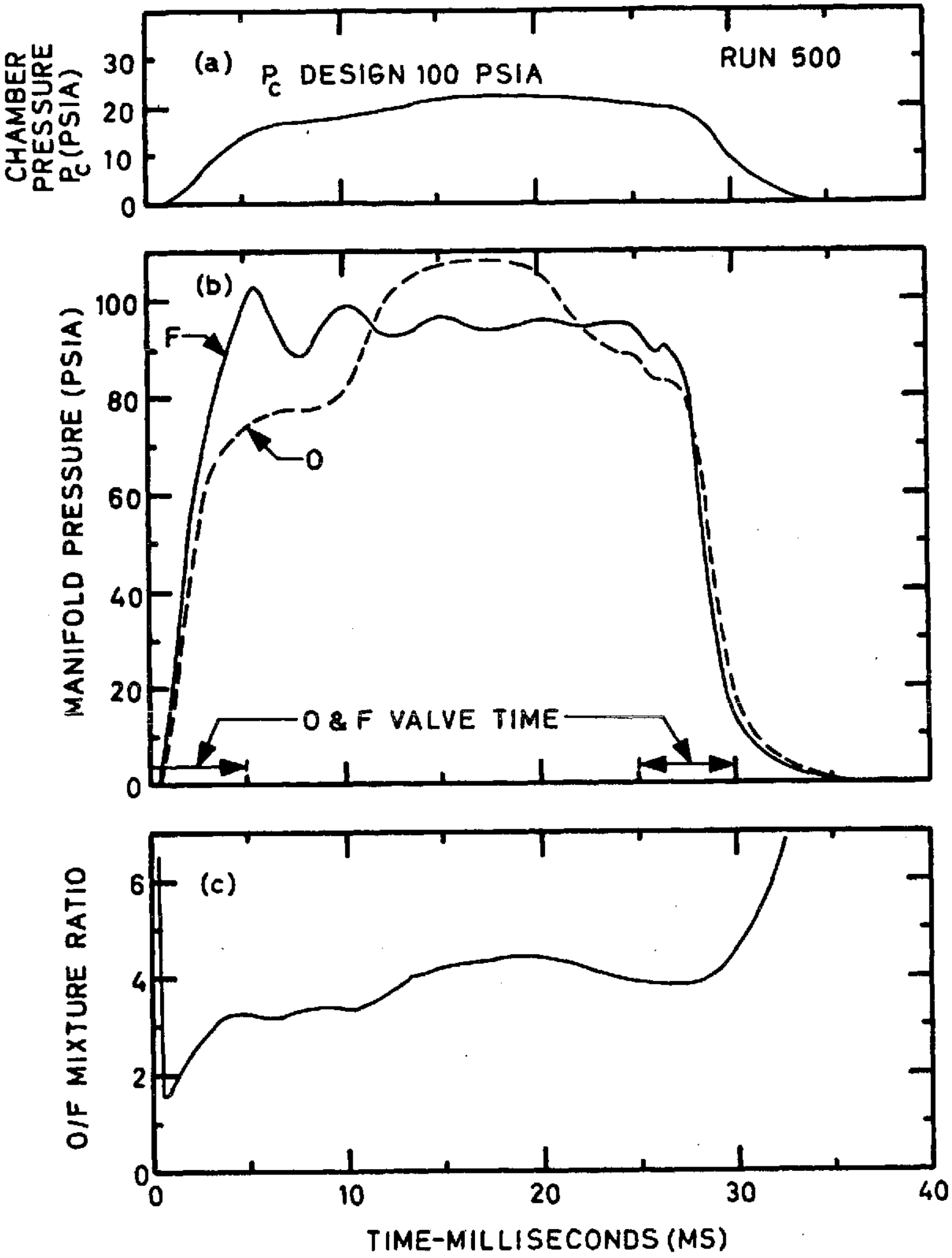

Figure VI-2. Cold flow run.

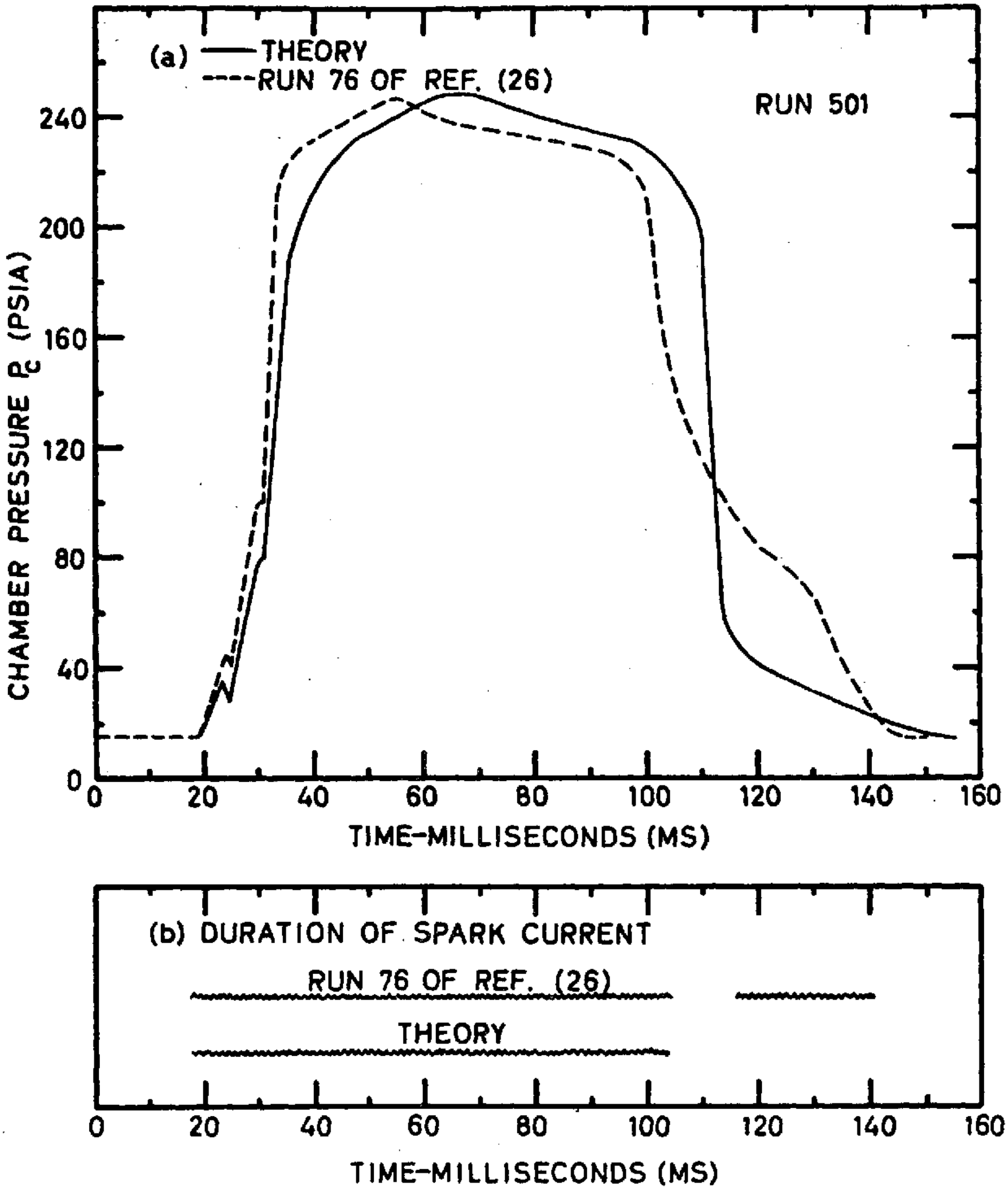

Figure VI-3. Analytical combustion model verification.

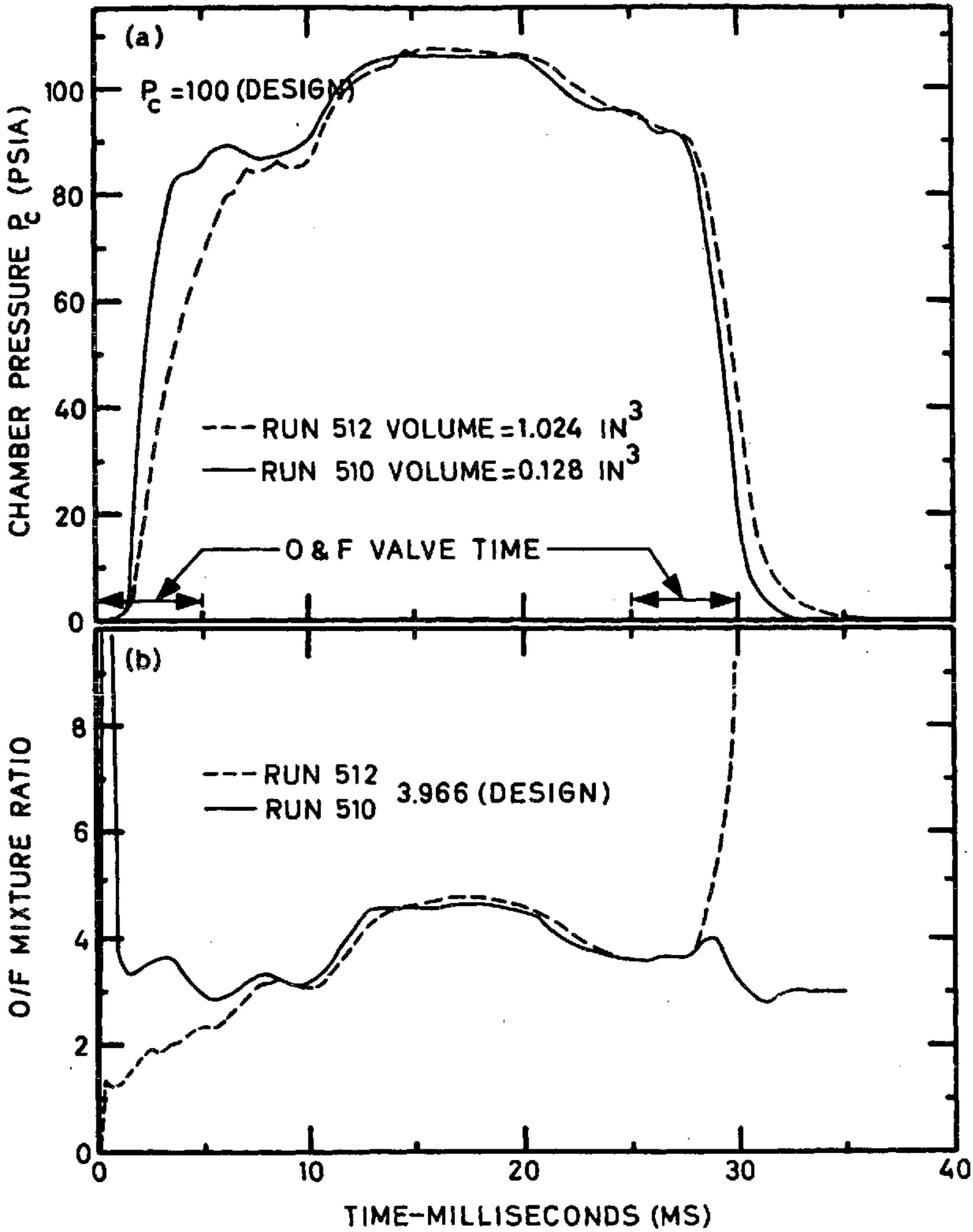

Figure VI-4. Effect of manifold volume on the chamber pressure distribution.

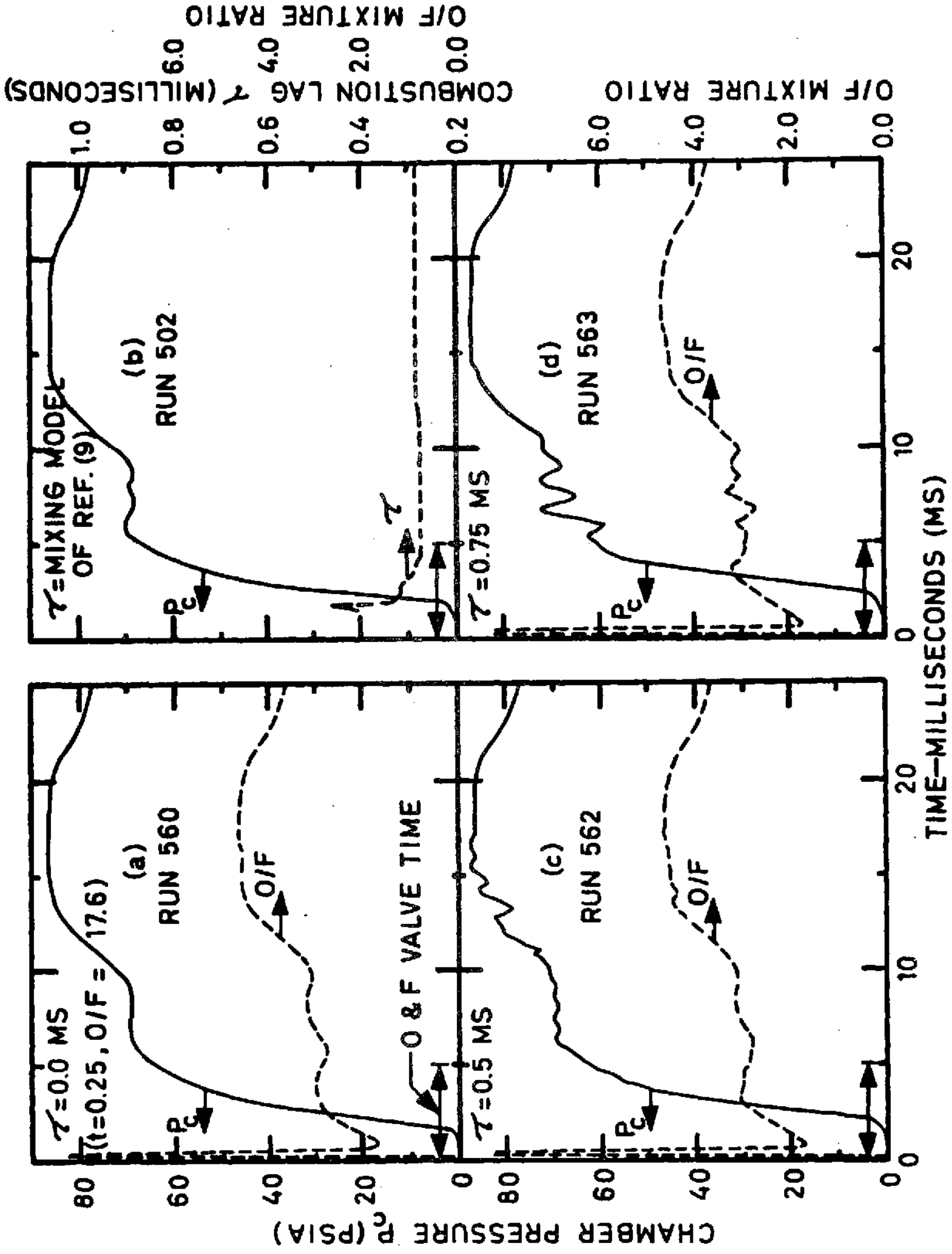

Figure VI-5. Effect of combustion lag time on the chamber pressure distribution for propellant temperature of 500°R.

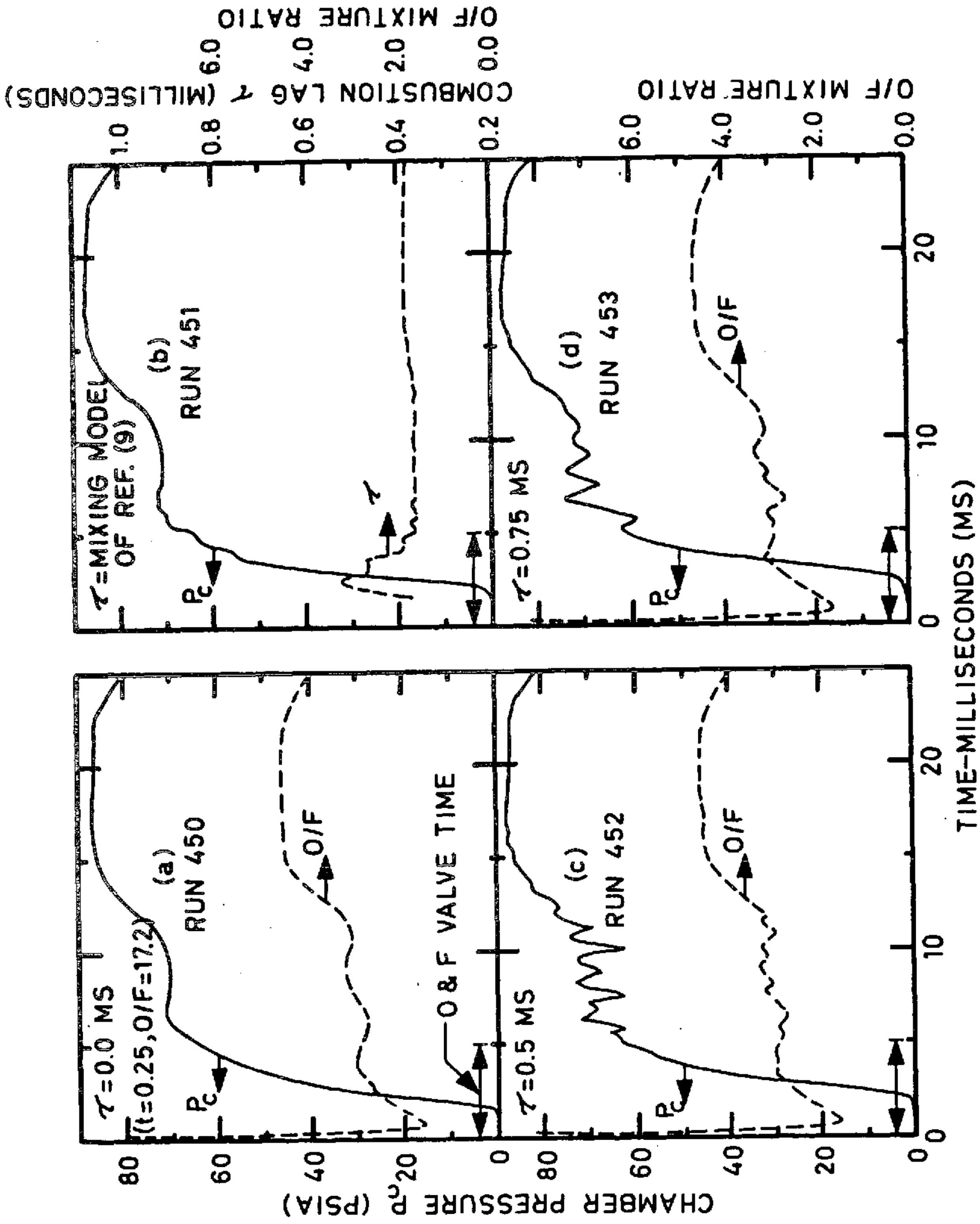

Figure VI-6. Effect of combustion lag time on the chamber pressure distribution for propellant temperature of 400°R.

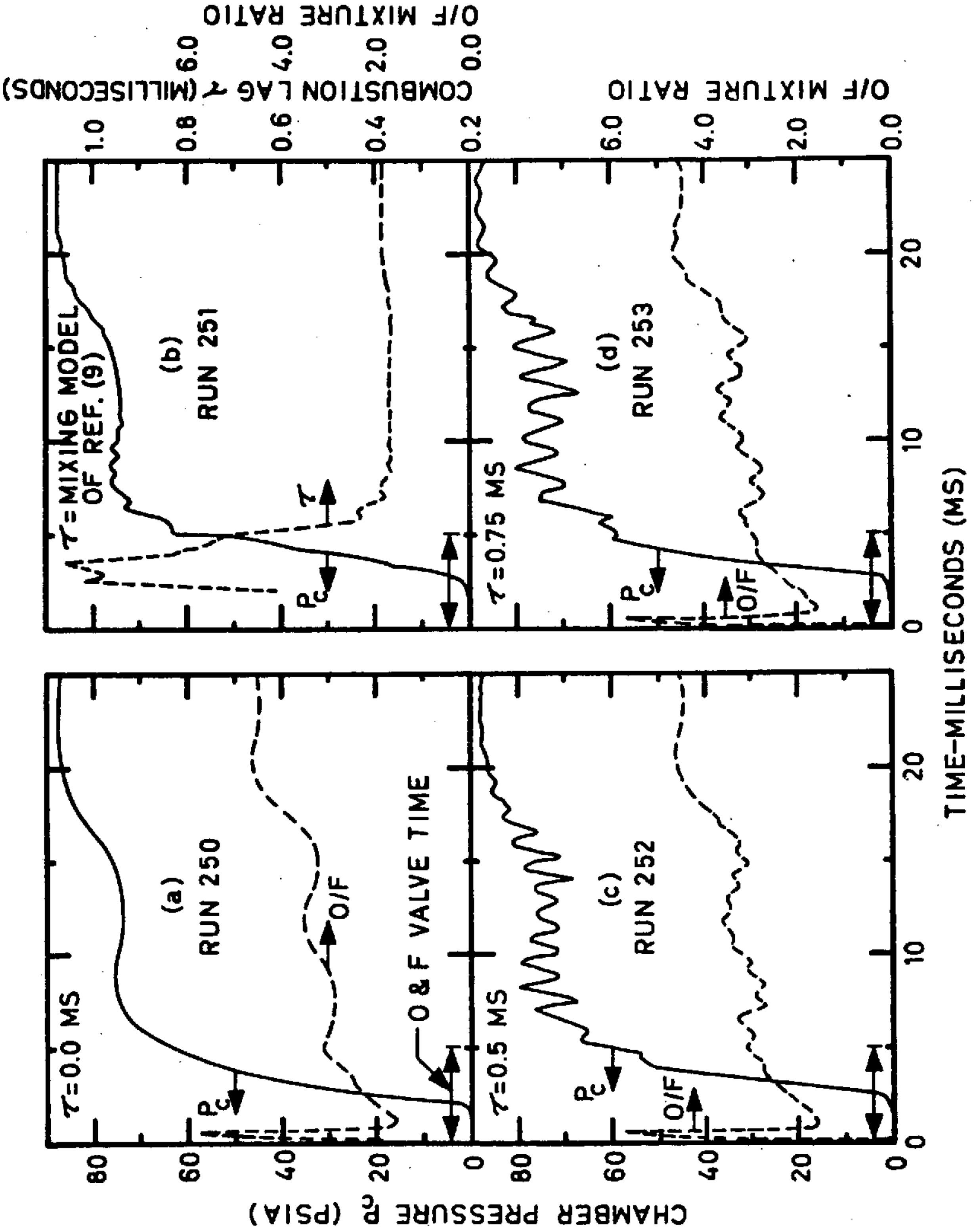

Figure VI-7. Effect of combustion lag time on the chamber pressure distribution for propellant temperature of 200°R.

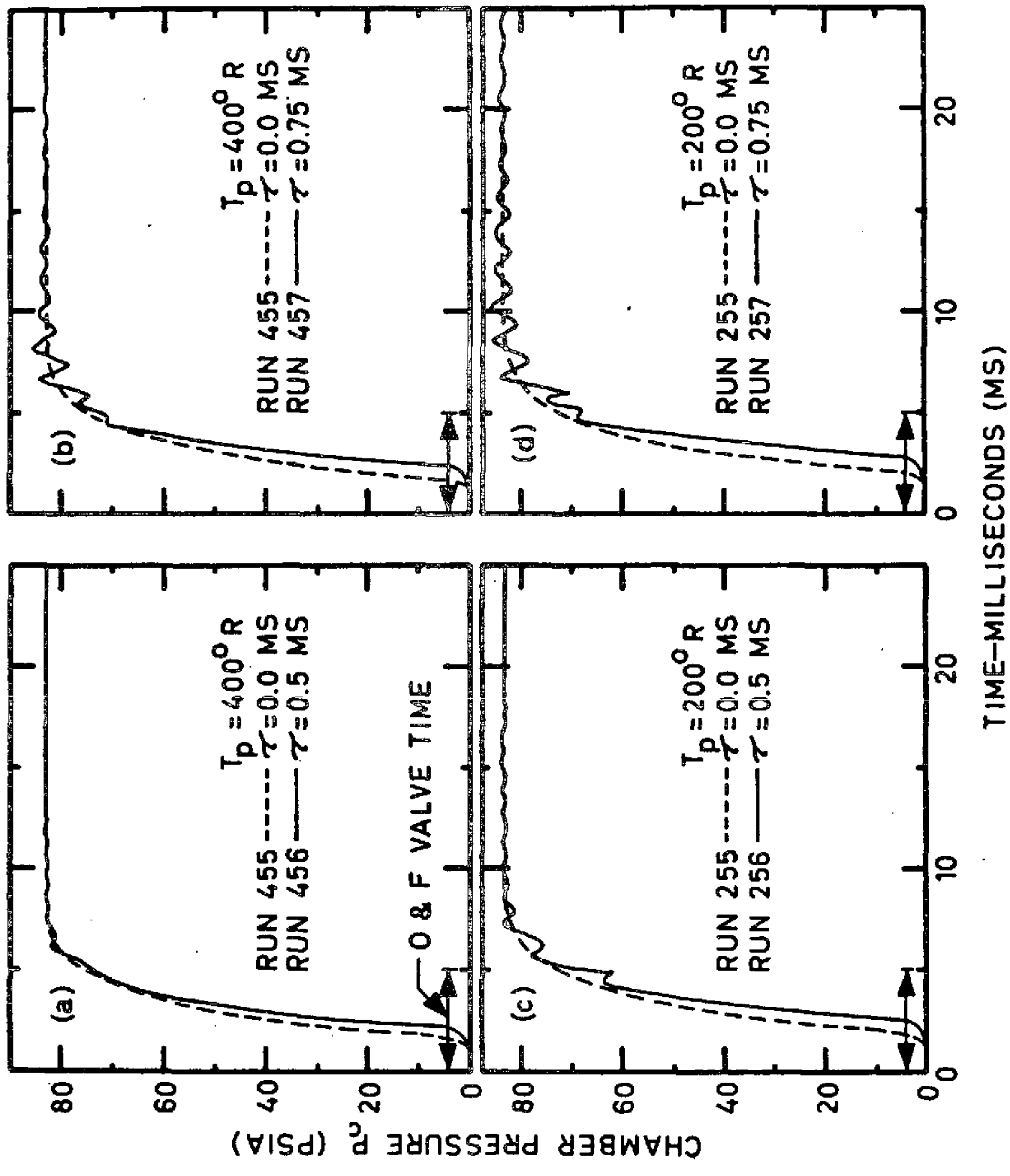

Figure VI-8. Effect of suppressing feedline pressure fluctuations on chamber pressure distribution.

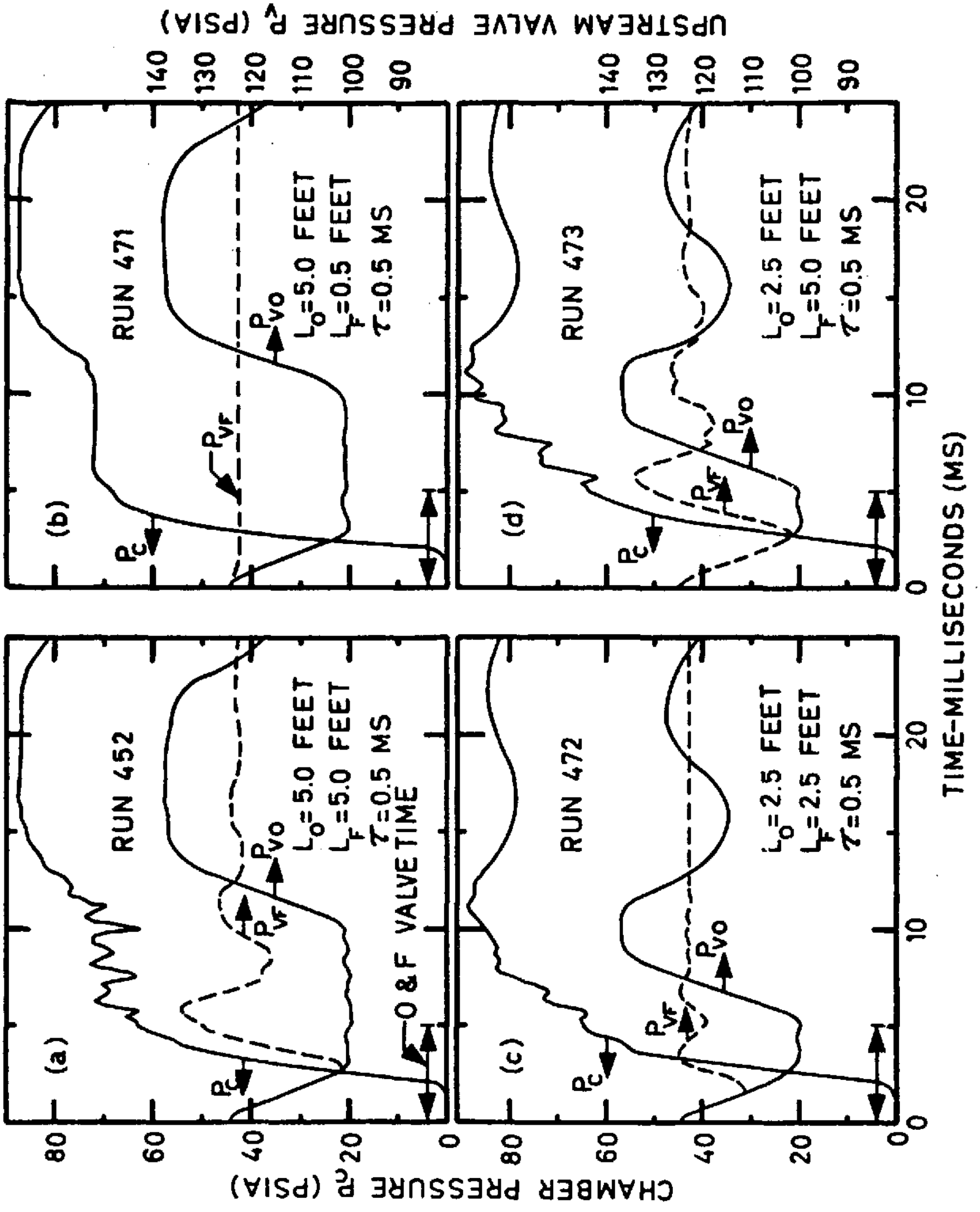

Figure VI-9. Effect of feedline length on the chamber pressure distribution for a fixed combustion lag time of 0.5 ms.

Chapter VII: Electrical Power System

1. Introduction

The LSV power subsystem generates, stores, and controls electrical power for distribution to the spacecraft subsystems. The energy requirements are based on a round-trip mission time of four hours — two and a half hours for descent from Lunar orbit to Lunar surface and one and a half hours for ascent from Lunar orbit to docking with orbiting Lunar base. The design of the LSV is based on deployment in the 1978-1985 time period and includes a permanent base in Lunar orbit which will provide refueling and refitting facilities for the shuttlecraft. While docked with the Lunar orbit base, or by the Lunar base, the LSV power will be drawn from the respective base. The concept of reusability and refittibility is a major consideration in selecting an electrical power system.

Except in the propulsion field, probably no other systems are being developed over such a broad spectrum for spacecraft applications as are electrical power generation systems. This is especially true for manned spacecraft applications where power requirements are significantly higher than for most unmanned payloads.

Three sources of energy are available for conversion to electrical power on spacecraft: chemical, solar, and nuclear. Systems which utilize each type of energy source have been developed and flown in this country's space program. Chemical energy may be stored in self-contained packages, with batteries, as an example, or it may be supplied in the form of a fluid or fluids from external subsystems which are consumed in the energy-conversion system, e.g., fuel cells. Photovoltaic or solar cells have been used successfully on numerous scientific unmanned missions. The third, and equally successful, conversion technique used in some unmanned spacecraft has been the radioisotope-fueled thermoelectric generator. It should be noted, however, that most of these applications have required less than 100 watts of power. The Mercury spacecraft provided one exception to this rule — it used on the order of 500 watts maximum power for what ultimately turned out to be a 34-hour mission.

Thus, with the previously mentioned candidate power systems only batteries and the fuel cells will be considered due to the recharge frequency and energy requirements of the LSV. The LSV's power system will supply energy at a nominal 29 volts DC. Alternating current power can be supplied either from a central power conditioner or from individual subsystem power conditioning devices.

2. Power System Requirements

Table VII.1 provides a summary of the ascent and descent power and energy requirements for one round-trip mission of the LSV. The duty times used as the basis for the estimation of the energy requirements are also shown in the table. Also, the load requirements are based on 1970 technology and therefore will be conservative with the expected advances in the guidance, navigation, and environment control areas.

The total electrical energy requirements for a round trip from Lunar surface to Lunar orbit and back again are 6742 w-hrs. Adding ten percent for wiring and conversion losses results in an energy requirement of 7416 w-hrs. During the mission the power requirements are maintained at a nearly constant level of 2,000 watts with peaking occurring at a level of approximately 2500 watts.

Table VII.1

Approximate Electrical Load Requirement

	Av. Load Watts	Duty Time (hrs.) Ascent/Descent	Energy (w-hrs.)* Ascent/Descent
Guidance & Navigation			
Computer & Celestial Sensors	100	1.5/2.5	150/250
Inertial Measurement Unit (IMU)	100	1.5/2.5	150/250
Radar Pulse, Radar Ant Heater	190	0.5/0.5	95/95
IMU Pulse Torque Assembly	90	1.5/2.5	135/225
Coupling Data Units	50	1.5/2.5	75/125
Approach TV	22	0/1.0	0/22
Main Engine			
Circulating Pumps, H_2-O_2 Tanks, Valves	250	0.1/0.1	25/25
RCS Engines (16 units)			
Valves	240	0.5/0.5	120/120
Environment Control System			
200 watts/man	1200	1.5/2.5	1800/3000
Electrical Control Assembly	20	1.5/2.5	30/50
Total Ascent/Descent			2580/4162
Round Trip Total	2262		6742
Round Trip Total + 10%	2488		7416

*watt-hours

2.1 Payload Support

Payload support has been incorporated in the power system load requirements. The environmental control system requirements are 200 watts/man, with a maximum of a six man payload allotted. If a fewer number of men are included in the payload, residual power of 200 x (6 - number of passengers) watts can be used for payload support.

3. Candidate Power Systems

Two alternate power systems have been considered and evaluated. The following paragraphs provide a description of each of the systems.

a) Batteries

Secondary batteries are simply those in which the components are compatible with each other; that have reasonably good stand life in the conditions under which they may be stored (with or without a trickle charge), that undergo few, if any, chemical side reactions and thus show high current efficiency, and can, therefore, be electrically recharged.

There are three types of secondary batteries, i.e., designated to be charged and discharged many times:

		cycles	watt-hours/Lb_m
1)	Nickel-cadmium	10,000	15
2)	Silver-cadmium	10,000 (approx.)	25
3)	Silver-zinc	500 (approx.)	60

The above cycle life times are based on depth of discharge of the order of 20 to 25%, which are currently used in space. Future improvements will yield similar cycle life for a depth of discharge of 30% [VII-6].*

The advantage of the nickel-cadmium couple over other secondary batteries include small voltage excursions, high rate charge acceptance, long shelf life, and low temperature operation. The silver-cadmium secondary battery approaches the long life of the nickel-cadmium and the high energy density of the silver-zinc batteries. The silver-cadmium cells have approximately twice the energy density of the nickel-cadmium and a cycle life 1 to 2 orders of magnitude greater than the silver-zinc cell which may be outweighed, for many applications, by the low cell voltage regulation [VII-2]. Because they may be charged more rapidly than silver-zinc cells, silver-cadmium cells are useful when rapid repetition of cycles is required.

---

*See References.

The silver-zinc secondary battery is the highest energy density battery in common use. However, it does not yet have the good cycle life of the nickel-cadmium battery. Silver-zinc cycle life is still measured in hundreds of cycles as compared with thousands of cycles for the other two.

For the battery candidate power source, silver-zinc batteries were selected based on simplicity, reliability, proven design, high energy output per unit weight, high peak-current capability, and reusability. The disadvantages of silver-zinc cells are their relatively short useful lifetimes (approximately 500 cycles at 30% depth of discharge) and their limited temperature range of -55°F to +100°F.

The total electrical energy requirement for a battery power system design for 30% depth of discharge for one round trip mission is 24,700 watt-hours. The total battery weight required would be 412 pounds. A three battery arrangement would provide a safety margin even if two batteries fail. Each battery would weigh 137 lb_m and have 20 cells. This specification is almost identical to the descent battery used in the LEM [VII-3].

b) Fuel Cell

A fuel cell is an electrochemical device in which energy is derived from a continually-supplied chemical reaction and is converted directly into electrical energy.

Candidate fuel cells are as follows:

1) Pratt & Whitney Aircraft, Type PC8B-3, 2KW, 105 watts parasitic load weight: 104 pounds per module, liquid cooled [VII-4].
2) Allis-Chalmers, 2KW, capillary matrix type, gas/liquid cooled, weight: 169 pounds per module, 100 watts parasitic load [VII-5].

Three fuel cells are required to offer the same redundancy as for the all battery system, i.e., two may fail without endangering mission success.

4. Power System Comparison

The addition of further discussion on fuel cells or possible fuel cell and battery combination is not persued due to the particular type of power requirement needed for the LSV. The LSV will be used for supplying the lunar base at regular or irregular intervals and also for exploration of the moon. Therefore, the LSV will be dormant most of the time, and used for regular scheduled and emergency missions. Fuel cells are designed primarily for continual operations, with a power down mode. Between five or six hours and, say, three months of service, fuel cells usually show higher energy densities than batteries. But, because of more difficult storage of reactants and of need for removal of products, the total system is more complicated. So, for a mission time of less than five hours and on-off operation, fuel cells are not as feasible as static batteries [VII-6].

The fuel cells system weight is approximately 595 lbs whereas the equivalent battery system weight is 511 lbs. The volume of the three batteries would approximate 1/6 that of the fuel cell combination. The fact that the LSV vehicle can be refitted and also have batteries recharged indicates that batteries are more feasible from the viewpoint of weight and volume. Therefore, three batteries composed of silver-zinc plates with 20 cells a piece and a potassium hydroxide electrolyte are proposed. Silver-zinc batteries are usually tailormade and therefore no single standard line of cell has evolved. Because of the variation in cell structure details and the consequent performance variations, virtually no parametric performance data exists outside of the manufacturer's hands.

5. Design Data Requirements

The requirements of battery-operated-characteristics data depends upon the electric-power-system design in which the batteries are used. A relatively simple and conservative design system generally requires a minimum of detailed operating-characteristic data. As the design becomes more sophisticated and the requirements for high-efficiency storage and utilization of source energy becomes more critical, the requisite amount and accuracy of battery characteristic data, i.e., voltage versus time or current versus time curves, increase. The data required for the final design is:

1) Discharge voltage as a function of time under the actual load conditions expected.

2) Charge voltage and current as a function of time under the actual charging conditions expected. If the charging conditions are unknown, the battery data should contain enough information to derive the charging current and voltage required.

3) Quantity of electrical energy available from the battery at certain critical points in the mission, and the assurance that at all other periods the energy availability exceeds the requirements.

4) Rate of heat evolution as a function of time under the actual charge and discharge conditions expected, and a complete temperature profile of the battery as a function of time.

5) Impedance and phase-shift characteristics of the battery as a function of frequency.

6) Efficiency of the battery's energy storage and its associated electronics.

7) Probability of battery failure as a function of time and conditions of use.

8) Battery voltage transients for critical load changes.

Most, if not all, of the above data requirements depend upon system-design concepts as well as environmental variables such as temperature, charge and discharge currents, and system-load characteristics and specifications (which vary with the changing spacecraft design and mission).

REFERENCES

VII-1 Performance Forecast of Selected Static Energy Conversion Devices, 29th Meeting of Agard Propulsion and Energetics Panel, Liegel, Belgium, June 12-16, 1967.

VII-2 Bauer, Paul, "Batteries for Space Power Systems", NASA Sp-172, 1968.

VII-3 Apollo Operations Handbook, Lunar Module LM 7 and subsequent Volume I Subsystems Data, LMA 790-3-LM 7, Grumman Aerospace Corp., New York, February 1970.

VII-4 Pratt and Whitney Aircraft, "Fuel Cells for LM- Derivative Spacecraft", Ref. No. 69-1287, prepared for Grumman Aircraft Engineering Corp., March 19, 1969.

VII-5 Improved Lunar Cargo and Personnel Delivery System, Volume 111A: Conceptual Design and Subsystem Analysis, Lockheed Missiles and Space Co., Sunnyvale, California, Contract NAS 8-21006, June 1968.

VII-6 Manned Spacecraft, Engineering Design and Operation, Edited by Purser, P. E.; Faget, M. A.; Smith, N. F., Fairchild Publications, New York, 1964.

Chapter VIII: Landing Gear Design

1. Introduction

The major emphasis of lunar landing gear design activity has been directed toward designing effective means of vehicle arrestment and stabilization for two vehicles, the Surveyor and the LEM. Consequently, the development of systematic landing gear design procedures which would be applicable to a wide range of landing vehicles has not been necessary. However, as further exploration and eventual colonization of the moon take place, the need for a wide range of reusable landing vehicles has been predicted. The objective of this chapter is to develop a systematic landing gear design method which could be applied, in general, to reusable lunar landing vehicles.

Lunar landing gear systems design consists of developing design criteria and concepts of vehicle arrestment and stabilization so as to achieve some mission objective. U.S. designers' conceptions of spacecraft capable of controlled, soft landings on the moon have been characterized by vehicles with legs. The legs, which have been trusses with built-in energy absorbers, are designed to prevent damage to craft and crew during the landing impact, and to bring the vehicle to rest in an upright attitude. For a given design concept, sub-optimal landing gear systems design involves choosing values for the design parameters such that the solution will be "best" based on some performance criteria. The design iteration cycle consists of selecting initial design parameter values, determining if this solution satisfies the design criteria, and choosing new parameter values to "improve" the solution consistent with the design criteria.

The design method developed in this study applies a digital simulation of the landing vehicle to generate a solution surface, and a constrained optimization algorithm to locate the local optima on this surface. An initial design solution is supplied to the simulation-optimization routine and serves as a starting point for the optimization procedure which eventually leads to an approximate mathematical locally optimal design solution. Different starting points lead to alternative locally optimal designs, from which a "best" design is chosen based on vehicle performance characteristics.

The mathematical model of the system consists of an objective function, system constraints which result from the design criteria, and a digital simulation which determines vehicle performance characteristics for specific design parameter values. The optimality of the mathematical local optima, with respect to the real local optima, depends on the accuracy and completeness of the model and the relative optimality of any arbitrary design assumptions. Thus, an optimal solution of a model involving only the major design parameters of a system is mathematically suboptimal unless all secondary design parameters have been fixed, by chance, at optimal levels.

2. Problem Definition

The landing vehicle-landing site system is described by three basic types of parameters: those involving the vehicle, those parameters describing the landing gear, and those parameters describing the landing conditions. See Table VIII.1. The landing gear design variables are those system parameters over which the designer has control. The

Table VIII.1

VEHICLE PARAMETERS

- Mass
- Moments of Inertia
- Geometry
- Mass Distribution

LANDING GEAR DESIGN PARAMETERS

- Number of Gears
- Geometry (size, orientation, etc.)
- Location of Hardpoints
- Location of Footpads
- Stroking Characteristics of Energy Absorbers
- Mass of Energy Absorbers
- Size of Footpad
- Mass of Footpad

LANDING CONDITION PARAMETERS

- Surface Slopes
- Soil Characteristics
- Surface Roughness (protrusions, indentations, etc.)
- Vertical Velocity
- Horizontal Velocity
- Pitch, Yaw, Roll
- Pitch Rate, Yaw Rate, Roll Rate

other parameters are either fixed (mass, moments of inertia, etc.) or are random variables (initial touchdown conditions). A landing gear systems design involves selecting values for the thirty or more design variables so that the solution satisfies the design criteria for the fixed system parameters and for the designated ranges of touchdown parameters. If only three values for each design variable are considered, a total number of $3^{30} = 2.05 \times 10^{15}$ design combinations must be evaluated. Since one simulation run requires approximately five seconds of computer time, the total time required to evaluate all design combinations is approximately 3.2×10^{7} years.

2.1 Landing Gear Design Criteria

Landing gear design criteria define the limits of the landing conditions for which the vehicle will land with a particular outcome. For example, one design criterion might specify the limits of the initial landing conditions for which no crew injury or craft damage should occur. An alternate criterion might set limits on the initial landing conditions for which slight crew injury and craft damage would occur. These limits on the initial landing conditions can be thought of as related to confidence limits of the random variables involved, even though the distributions of these variable have not been discussed in the literature.

2.2 The Constraint Set

The system constraints are limits on the vehicle performance characteristics which result directly from the design criteria. For example, the design criteria involving no crew injury may be translated to limits on maximum vehicle deceleration. Similarly, a vehicle stability constraint may correspond to the design criteria pertaining to vehicle damage or final attitude. Thus, the landing gear design criteria become constraints on the vehicle design variables and performance characteristics which are not to be violated for a given range of initial landing conditions.

2.3 Design Model Objective Function

In general, a set of design criteria may be satisfied by more than one design solution. It is therefore desirable to develop a criterion so that the "best" solution can be determined. This criterion may be expressed mathematically in the form of an objective function which is to be minimized or maximized during the optimization process. For example, one logical design objective is that of minimizing total vehicle cost. Another objective might be minimizing total landing gear weight. Still another design objective might be maximizing the range of initial landing conditions for which the vehicle can land successfully.

3. Landing Gear Design: An Optimal Solution

The landing of a lunar vehicle is a probabilistic event[*] in that the landing conditions vary from site to site and the vehicle touchdown parameters are random variables dependent on the pilot and the guidance equipment. An optimal solution for this probabilistic problem is a solution which is feasible[**] for all anticipated combinations of landing conditions and which is "best" in some sense.

---

[*] In general, there are two basic system models: the deterministic model and the probabilistic model. The former differs from the latter in that the latter is characterized by the existence of one or more random system variables.

[**] A feasible solution is one that violates none of the constraints.

Optimal landing gear design solutions are approximated in the literature by determining locally optimal design solutions for several "worst case" combinations of landing conditions. The reliability[*] of each design is then evaluated by checking its feasibility for many other combinations of initial conditions[**]. The optimal solution is the "best" solution of this group based on considerations such as the value of the objective function and the reliability of the design.

A major area of landing gear design difficulty involves determining the "worst case" initial landing conditions for which an optimal solution is to be determined. Since the "worst case" conditions are not independent of the specific gear design, their calculation becomes a trial and error process. While the optimization process is complicated when more than one "worst case" landing gear combination exists, an additional problem occurs when the locally optimal solutions for any one set of initial conditions are infeasible for other "worst case" combinations. When such difficulties arise, the concept of design reliability becomes necessary. The reliability approach is limited, however, because it is impractical to test the feasibility of a solution for all anticipated initial condition combinations. Thus, the reliability of a design is usually only estimated.

---

[*] The reliability of a design is the number of combinations of initial landing conditions for which the design is feasible divided by the total number of possible initial condition combinations.

[**] Ideally, a solution that is feasible for a "worst case" set of landing conditions will be feasible for all anticipated landing conditions.

4. Study Objectives and Design Assumptions

A complete landing gear design study involves some broad trade-off analyses. For example, there is the conceptual trade-off between an energy absorbing landing gear system which is attached to the vehicle and an energy absorbing landing platform located at each landing site. Other trade-off studies might involve the cost of improving the guidance equipment to a point where an unsophisticated, non-energy absorbing landing gear system would be sufficient. Such studies are, however, lengthy and beyond the scope of this analysis. The landing gear concept used in this study is an extrapolation from the present LEM design in that the shock absorbers are reusable. The vehicle control capabilities have also been updated.

The primary objective of this study is to develop a computerized approach for approximating locally optimal landing gear design solutions for mathematical models of lunar landing vehicles. Mathematical programming techniques will be used to approximate locally optimal solutions for specific initial landing conditions for constrained models of two, three, and four design parameters. The effect on these solutions to changes in initial landing conditions will then be evaluated. Vehicle stability and crew safety will be the design criteria from which the constraint set is developed. A three-dimensional digital simulation of the landing vehicle will be used to determine design performance results.

The vehicle mass, dimensions, and moments of inertia used in this analysis are consistent with preliminary estimates of those of the proposed lunar shuttle vehicle. See Table VIII.2. The geometry of the proposed vehicle is shown in Figure VIII-1.

Table VIII.2: Vehicle Design Variables

Vehicle Mass	400 slugs
Moments of Inertia	8000 slug-ft^2
X-direction Velocity	4 ft/sec
Y-direction Velocity	0 ft/sec
Z-direction Velocity	-2 ft/sec
Pitch	+5°
Roll	0°
Yaw	0°
Pitch Rate	+0.1 rad/sec
Roll Rate	0 rad/sec
Yaw Rate	0 rad/sec
R/H	0.75
Gravity Vector	0,0, -32/6 (zero slope)
Tangential Soil Coefficient	0.00001
Vertical Soil Coefficient	0.00001
Strut Extension Force	1000 pounds
Maximum Stroke	±1.25 ft.
Elastic Range of Strut	0.003 ft.

Due to the large number of design parameters, it is impractical to treat each as a design variable. Therefore, the design parameters of compressive strut force and landing gear radius are chosen as design variables while the other design parameters are fixed at levels consistent with previous study results. The compressive strut force is the force at which continuous contraction of the landing gear strut occurs. The gear radius, R, is shown in Figure VIII-1. Studies by Black (12), NASA-ASEE (2), and Lockheed (3) indicate these parameters to be of major importance in landing gear design.

4.1 Landing Gear Design Assumptions

The landing gear system chosen for the shuttle craft consists of a three gear, inverted tripod design. See Figure VIII-2. Landing gear studies by Black (8) and Bendix (1) indicate that the optimum number of gears depends primarily on gear weight and that both the three and four gear systems have resulted in successful designs. The three gear design was chosen in this study for the following reasons:

1. The present study attempts to optimize the forward two gear designs and assumes a front-foot-touchdown landing*. Thus, the design of the rear gear(s) is of secondary importance.
2. The digital simulation of a three gear design costs approximately one-fourth less than one of a four gear design.

Two basic gear leg configurations are presented in the literature: the cantilever configuration and the inverted tripod configuration. See Figure VIII-3. Mantus (13) reports that the cantilever design is superior to the inverted tripod configuration. A Bendix report (1) suggests that the inverted tripod design might be optimal for certain unspecified conditions. In the present study, the inverted tripod gear design was arbitrarily chosen over the cantilever design primarily to reduce the complexity of the simulation. Each inverted tripod is made up of three energy absorbing struts which act as columns with pinned ends. The struts are designed to extend or contract a maximum of 1.25 feet from the original length. The constant force-deflection characteristics of the energy absorbers are similar to those of the crushable honeycomb cartridges used in the LEM design. Since the shuttle craft requires a reusable landing gear system, an energy absorber similar to the NASA, MSFC Friction Shock Absorber is indicated (17). See Figure VIII-4. This reusable energy absorber is designed to produce a constant force-deflection characteristic.

---

*Landing gear design consists of designing for front-foot-touchdown and rear-foot-touchdown landing conditions. This work only considers the first of these two cases.

The location of the footpads and the strut attachment points on the vehicle (the hardpoints) were chosen so as to result in the optimal tripod configuration as reported by Bendix (1):

1. The secondary struts should be symmetric about the primary strut and of the same length.
2. The angle of the primary strut should be 30 degrees from the vertical.

The mass of the struts, energy absorbers, and footpads are negligible compared to the mass of the vehicle and are neglected in the digital simulation of the craft. The size of the footpad and the soil characteristics are such that a pinned foot condition holds*.

---

*When a footpad is in contact with the surface, it is assumed to be pinned until there is a tendency for it to lift off.

Since the vehicle will land at established sites, it is assumed that the landing area will be free of large indentations or protrusions. The landing surface slopes are assumed to be less than ± 10 degrees. For these landing conditions, Black (8) suggests that the ratio of the projected gear radius, Rx, to the height of the vehicle center of gravity be approximately 1.3. Initially, the Rx/H ratio for the present design is set at 0.75 because of the ideal initial landing conditions specified in Table VIII.2.

Vehicle control capabilities are limited by the pilot and the accuracy of the guidance equipment. Listed in Table VIII.3 are the projected design ranges of the initial landing conditions as reported by Bendix (6).

Table VIII.3: Initial Condition Ranges

Vertical Velocity	0-10 ft/sec
Horizontal Velocity	0-5 ft/sec
Pitch, Yaw, Roll	± 5 degrees
Pitch rate, Yaw rate, Roll rate	± .1 rad/sec
Ground Slope	± 10 degrees

As in the Apollo project, vehicle decelerations of 30 ft/sec^2 horizontal and 180 ft/sec^2 vertical are assumed to result in no crew injury.

4.2 Basic Design Approach

Before the optimization of the system design parameters can proceed, a specific set of initial conditions must be selected. Table VIII.2 shows the initial conditions for which the optimal landing gear solutions will be determined. A touchdown velocity vector of 4 ft/sec horizontal and -2 ft/sec vertical was chosen because such a shallow approach landing is thought to be critical with respect to vehicle toppling. The symmetry of zero degrees yaw, roll, and ground side slope allows for the monitoring of only one of the two forward gears. Since these initial conditions are probably not the "worst case" landing conditions, the concept of safety margins* is incorporated into the design. The safety margins mean that the vehicle will be able to land successfully for more severe initial conditions than those listed in Table VIII.3. These safety margins are also significant because of the impracticality of testing the feasibility of a design solution for all possible combinations of initial conditions.

4.3 Stability Margin

The general practice in previous studies has been to define stability in the absolute sense; that is, the landing was considered stable if the vehicle did not overturn. Some quantitative measure of the relative stabilities of stable landings is desirable for a mathematical analysis of the system.

If all energy which tends to topple the vehicle in Figure VIII-5 is dissipated, then $MgL(1-\cos\beta)$ is a measure of the amount of energy that would have to be added to the system to cause toppling. Thus, for any successful landing, the minimum of $MgL(1-\cos\beta)$ is defined to be the stability margin of that landing.

$$\text{Stability Margin} = \text{Min } MgL(1-\cos\beta)$$

The quantities L and β, which are necessary to determine stability margin, result from the digital simulation of the landing vehicle.

---

* A safety margin may be generally defined as the excess of capability over demand.

The number of integration cycles necessary to guarantee that the minimum of MgL(1-COS) has been reached must be estimated. Figure VIII-6 is a graph of MgL(1-COS) vs. Time for 200 integration cycles. In this graph, the primary strut force is the same for all curves, while the secondary strut force is different for each curve. At the end of 200 integration cycles the velocities of the vehicle were less than 0.1 ft/sec[*]. The stability margin for each combination of primary and secondary strut forces is determined from the minimum point of each curve.

4.4 Constraint Set

One logical vehicle design criterion involves specifying the range of initial landing conditions for which no crew injury should occur.See Table VIII.3. The constraints are limits on vehicle performance such that no crew injury results for initial landing conditions within the specified ranges.

In this study, three general kinds of constraints prevent crew injury. The first kind restricts the maximum strut stroke to less than or equal to 1.0 foot, resulting in a 0.25 foot stroke safety margin which is intended to prevent strut bottoming for severe landing conditions. The second type of constraint limits the maximum decelerations of the vehicle. The final constraint restricts the stability margin[**] of the vehicle and is intended to prevent toppling for severe landing conditions. Mathematically, the constraints are,

---

[*] The maximum deceleration occurred within the first few integration cycles while the maximum strokes became asymptotic as the number of cycles reached 200.

[**] A 2000 foot-pound minimum stability margin constraint value was arbitrarily chosen.

$$\begin{aligned}
&\text{STROKE}(i) && \leq 1.0\ \text{ft} && i = 1, 2, 3 \\
&\text{AOX} && \leq 30\ \text{ft/sec}^2 && \\
&\text{AOZ} && \leq 180\ \text{ft/sec}^2 && \\
&\text{STABILITY MARGIN} && \geq 2000\ \text{ft-lbs.} &&
\end{aligned}$$

In this study, a feasible design solution is one which satisfies the above constraint set.

5. Analysis Techniques

5.1 Three Dimensional Digital Simulation

The time history of motion of a vehicle can be obtained by numerical integration of the equations of motion governing that vehicle. This process is referred to as digital simulation. A simulation is designated as being three-dimensional when the equations of motion are such that three-dimensional motion is possible. The simulation used in this study is a modified version of the three-dimensional digital simulation developed by Walton and Durling (10).

5.2 Mathematical Optimization

Mathematical modeling, as a basis for multi-variate systems analysis and optimization, has been shown effective in areas ranging from traffic flow to military tactics. It is these same operations research techniques that are applied to the problem of landing gear design in this study. The general mathematical formulation of the present landing gear optimization problem is:

$$\text{Minimize} \quad f(U) \qquad [1a]$$

$$\text{Subject to:} \quad H(X,U) = 0 \qquad [1b]$$

$$P(X,U) \leq 0 \qquad [1c]$$

where

$$U = \begin{bmatrix} u_1 \\ u_2 \\ u_3 \\ \cdot \\ \cdot \\ \cdot \\ u_n \end{bmatrix} \text{ - Design Variables} \qquad X = \begin{bmatrix} x_1 \\ x_2 \\ x_3 \\ \cdot \\ \cdot \\ \cdot \\ x_m \end{bmatrix} \text{ - State Variables}$$

and

$$H^T = (h_1, h_2, \ldots\ldots, h_m)$$

$$P^T = (p_1, p_2, \ldots\ldots, P_k)$$

The design variables, U, for this problem are the compressive strut force levels and the landing gear radius. The state variables, X, are the vehicle performance characteristics resulting from a specific design vector and initial touchdown conditions. The state equations, $H(X,U) = 0$, for this study are not explicit equality constraints as shown in [1b], but are in the form of a digital simulation. Thus, instead of solving [1b] for X (given U), the state variables are determined from digital simulation. Significant is the fact that the derivatives of functions of state variables with respect to the design variables must be approximated from the digital simulation results. The optimization process involves determining changes in the design variables, dU, which will reduce the objective function, f, and satisfy the constraints.

Formulation, Eq. 1, is a special case of a general problem for which an optimization algorithm has been developed by Bartel, Haug, and Rim (14). The constrained minimization algorithm was developed for the following mathematical programming problem:

$$\begin{aligned} &\text{Minimize} && f(X,U) \\ &\text{Subject to:} && H(X,U) = 0 \\ & && P(S,U) \leq 0 \end{aligned} \qquad [2]$$

The computer program listing for this algorithm appears in Appendix B in Ref. 18.

5.3 Four-Parameter Optimization

The mathematical model for the four-parameter analysis is,

Minimize Gear Weight

		Constraint Number
Subject To:	STROKE(i) $\leq$ 1.0 ft.	1, 2, 3
	AOZ $\leq$ 180 ft/sec^2	4
	AOX $\leq$ 30 ft/sec^2	5
	STABILITY MARGIN $\geq$ 2000 ft-pounds	6
	U(i) $\geq$ 500 pounds	7, 8, 9
	U(4) = R $\geq$ 10.0 ft.	10

where,

$$\text{Gear Weight}^{*} = \left[0.1\left[[X1H(i,j) - R\cos(60°)]^2 + [Y1H(i.j) - R\sin(60°)]^2 + (\text{constant})^2\right]^{1/2}\right]^{1.6} \cdot F(i)^{1/3} \qquad \begin{aligned} i &= 1, 2, 3 \\ j &= 1 \end{aligned}$$

where X1F(i), Y1F(i), and Z1F(i) are the coordinates of the 1th footpad.

---

[*] In this study, the design load is taken as .8 times the Euler critical buckling load for columns with pinned ends. The strut wall thickness is taken to be a constant 0.15 inches.

5.4 Four-Parameter Results

The local optimum* for this model corresponding to high primary strut forces and low secondary strut forces is,

U(1) = U(3) = 500
U(2) = 8964
U(4) = 11.2
Weight = 28.3

Design 1

Similarly, the results for initial low stroke force levels in struts one and two and a high stroke force level in strut three is shown as Design 2:

U(1) = 734
U(2) = 559
U(3) = 2155
U(4) = 13.9
Weight = 28.1

Design 2

The last local optimum investigated corresponds to high secondary strut forces and low primary strut forces. The resulting solution is,

U(1) = 1102
U(2) = 500
U(3) = 2119
U(4) = 13.9
Weight = 29.2

Design 3

---

* In the four-parameter model, the optimization routine was halted when oscillation about some solution became evident. The minimum weight feasible solution obtained up to this point was designated as the local optimum.

Significant is the fact that further minimization of the objective function was prevented in each case due to the binding of the stability margin constraint, the minimum strut force and maximum stroking constraints.

5.5 Design Sensitivity Analysis

Results from the four-parameter analyses indicate the existence of at least three locally optimal minimum weight landing gear designs with stability margins of 2000 ft-pounds. These local optima exist for the specific initial landing conditions, and the feasibility of these solutions for other touchdown conditions must be determined. The "best" design solution could then be chosen from among the three candidate designs based on the relative weight and reliability of each. Since a design reliability estimate may involve 100,000 simulation runs, no serious attempt will be made in this direction. Instead, the performance characteristics of the three designs will be determined for five combinations of initial conditions. Table VIII.4 shows these feasibility results. Note that while none of the designs topple for the initial conditions tested, all exceeded the actual stroke limit of 1.25 feet. This result indicates that the 0.25 feet stroke buffer was not sufficient to prevent bottoming for more severe landing conditions. Therefore, the mathematical stroking constraint must be reduced and new locally optimal solutions found. The time required to find these new solutions will be minimal because good estimates of the optimal solutions can be obtained from the computer printout of the optimization iteration runs already completed. The idea is to choose an initial solution which has a maximum stroke equal to that of the new stroking limit, and a stability margin of 2000 ft-pounds. Such a solution should be a good estimate of the mathematical local optimum.

Table VIII.4: Design Sensitivity Results

	VOX	VOZ	Ground Slope[*]	Yaw	Solution 1	
					Maximum Stroke[**]	Stability Margin
	4	-2	5°	0°	1.01	2003
	4	-2	10°	0°	1.05	2000
(a)	4	-4	10°	0°	1.30	2054
	4	-4	10	+10°	1.13	0
	4	-4	10°	-10°	1.13	0

	VOX	VOZ	Ground Slope[*]	Yaw	Solution 2	
					Maximum Stroke[**]	Stability Margin
	4	-2	5°	0°	1.06	1707
	4	-2	10°	0°	1.12	1232
(b)	4	-4	10°	0°	1.82	2116
	4	-4	10°	10°	1.48	0
	4	-4	10°	-10°	2.11	0

	VOX	VOZ	Ground Slope[*]	Yaw	Solution 3	
					Maximum Stroke[**]	Stability Margin
	4	-2	5°	0°	1.04	1705
	4	-2	10°	0°	1.09	1227
(c)	4	-4	10°	0°	1.79	2094
	4	-4	10°	10°	1.45	0
	4	-4	10°	-10°	2.14	0

---

[*] A positive ground slope indicates a downhill landing. A vehicle forward pitch of 5° with respect to the landing surface was maintained throughout the analysis.

[**] Maximum stroke occurred for strut three in all cases.

6. Results and Conclusions

The application of the techniques of digital simulation and mathematical optimization to the problem of optimal landing gear design has been demonstrated. Locally optimal landing gear design solutions have been approximated for a mathematical model of four design variables. The utility of a locally optimal design is shown to depend not only on its objective function value, but also on its estimated reliability. The reliability concept is limited, however, because of the time required to test the feasibility of a given locally optimal design for all anticipated landing condition combinations.

The philosophy of optimizing for the nominal initial conditions of zero degrees yaw, roll, and ground side slope, and including safety margins in the constraint levels is shown to have several advantages. The symmetry which results from these initial conditions requires the monitoring of only one of the two forward tripods. Thus, instead of six stroking constraints, only three are now necessary. The symmetry of the approach also makes the definition of stability margin possible. This quantitative definition of stability is a measure of the relative stabilities of stable landings and is used to compare alternative design solutions.

The study results show that there exist at least three locally optimal, weight competitive landing gear design solutions to the four-parameter mathematical vehicle model. This observation is significant in that the optimal designs in the literature characteristically display high primary and low secondary strut force levels. While this traditional local optimum has resulted in a highly successful design for the LEM, further investigation may demonstrate the superiority of a non-traditional design under certain circumstances. However, the the range of initial conditions tested, Design 1 (the most nearly traditional design) did indicate a greater reliability potential than either of the other two designs.

Even though the starting points (initial designs) for the optimization runs were arbitrarily chosen, an average of five minutes of computer time was required to approximate each local optimum using an IBM 360-65 computer. The locally optimal solutions to this four-design parameter model averaged 28.5 pounds per tripod*.

Although a maximum of four design parameters has been considered in this study, many more design variables could be optimized using the present algorithm. For example, the force-displacement characteristics of the energy absorbers could be included in the design variable set. Similarly, the parameters involving the design of the rear gear(s) could also be considered in the analysis. Conversely, treating the number of gears as a design variable would be impractical in that the resulting model would be an integer programming problem. Therefore, a more reasonable approach might be to develop both a three gear and a four gear design and choose the better of the two.

---

*A similar shuttle vehicle proposed by Bendix (1) had a tripod weight of 32.5 pounds for a four gear design. This tripod weight is deceptively low, however, because it does not include the weight of the energy absorbers, footpads, ball joints, protective shields, connecting bolts, and outrigging, all of which are included in landing gear weight. The total gear weight for the Bendix vehicle was 660 pounds.

The apparent advantage of the computerized design improvement approach over the analagous graphical method, (1)(2)(3), is primarily one of time. Although both methods require approximately the same number of landing simulation runs, the graphical method involves plotting and interpreting design performance results at each iteration. The resulting graphs must be analyzed to determine if any constraints are violated, and to estimate the changes in the design variables which will improve the objective function value consistent with the constraint set. Using the computerized approach, the above analyses are completed in a few seconds.

NOMENCLATURE

M	mass (slugs)
I	moment of inertia (slug-ft^2)
VOX	velocity of center of gravity in X-direction (ft/sec)
VOZ	velocity of center of gravity in Z-direction (ft/sec)
AOX	acceleration of center of gravity in X-direction (ft/sec^2)
AOZ	acceleration of center of gravity in Z-direction (ft/sec^2)
ϕ	pitch (degrees)
θ	roll (degrees)
ψ	yaw (degrees)
$\frac{d\phi}{dt}$	pitch rate (rad/sec)
$\frac{d\theta}{dt}$	roll rate (rad/sec)
$\frac{d\psi}{dt}$	yaw rate (rad/sec)
R	gear radius (ft)
R_x	projection of R on the X-axis
H	height of vehicle center of gravity (ft)
T	time (sec)
W_s	strut weight (pounds)
F	strut force (pounds)
W_t	tripod weight (pounds)
L_s	strut length (ft)
U(i), i = 1, 2, 3	strut force design variables (pounds)
U(4) = R	gear radius (ft)
V_{fx}, V_{fy}, V_{fz}	footpad velocity (ft/sec)
F_{fx}, F_{fy}, F_{fz}	footpad forces (pounds)
c_x, c_y, c_z	soil coefficients (ft/pound-sec)
U1F(i), Y1F(i), Z1F(i)	body-centered footpad coordinates (ft)

REFERENCES

1. Bendix - "Manned Flying System Landing Gear Study", Final Report, Bendix Products Aerospace Division, June 1966, Chapter 2.

2. Faculty Systems Engineering Institute: "Lunar Logistics Vehicle", NASA-ASEE, September 1969.

3. Lockheed - "Improved Lunar Cargo and Personnel Delivery Systems", Final Report, Lockheed Missiles and Space Company, June 1968.

4. Blanchard, Ulysse J., "Full-Scale Dynamic Landing-Impact Investigation of a Prototype Lunar Module Landing Gear", NASA TN D-5029, Langley Research Center, March 1969.

5. Blanchard, Ulysse J., "Evaluation of a Full-Scale Lunar-Gravity Simulator by Comparison of the Landing-Impact Tests of a Full-Scale and 1/6-Scale Model", NASA TN D-4474, Langley Research Center, June 1968.

6. Bendix - "An Approximate Solution of Lunar Vehicle Landing Stability", Midterm Report, Lunar Landing Dynamics Systems Investigation, Bendix Products Aerospace Division, June 1964.

7. Walton, W. C. Jr., R. W. Herr and H. W. Leonard, "Studies of Touchdown Stability for Lunar Landing Vehicles", Journal of Spacecraft, Vol. 1, No. 5, September 1964.

8. Black, R. J, "Quadrupal Landing Gear Systems for Spacecraft", Journal of Spacecraft, Vol. 1, No. 2, March 1964.

9. Admire, John and Alden Mackey, "Dynamic Analysis of a Multi-Legged Lunar Landing Vehicle to Determine Structural Loads During Touchdown", NASA TN D-2582, Huntsville, January 1965.

10. Walton, W. C. Jr., and Barbara J. Durling, "A Procedure for Computing the Motion of a Lunar-Landing Vehicle During the Landing Impact", NASA TN D-4216, Langley Research Center, 1967.

11. Fox, Richard, "Optimization Methods for Engineering Design", Reading, Massachusetts, Addison-Wesley Publishing Company, 1971.

12. Black, R. J., "General Features of Landing Gear Systems for Widely Different Design Specifications", Midterm Report, Lunar Landing Dynamics Systems Investigation, Bendix Products Aerospace Division, June 1964.

13. Mantus, M., "Landing Dynamics of the Lunar Module", Grumman Aircraft Engineering Corporation, June 15, 1967.

14. Bartel, D. L., E. J. Haug and K. Rim, "The Optimum Design of Spatial Frames Using the Method of Constrained Steepest Descent with State Equations", Journal of Engineering for Industry, Trans. ASME, Series B, Vol. 93, 1971.

15. Goldstein, Herbert, Classical Mechanics, Reading, Massachusetts, Addison-Wesley Publishing Company, c. 1950.

16. Deitrick, R. F., C. D. Conaway, L. W. Gammell and R. H. Jones, "Structures and Mechanical Environment", Surveyor 1 Flight Performance Final Report, SSD 68223, Vol. 3, Section 5.11.2, Hughes Aircraft Company, El Segundo, California, 1966.

17. Bendix - "Manned Flying System Landing Gear Study", Final Report, Bendix Products Aerospace Division, June 1966, Chapter 9.

18. Rojeski, Peter J., "A Systems Analysis Approach to Landing Gear Design", Ph.D. Thesis, Cornell University, Ithaca, N.Y., 1972.

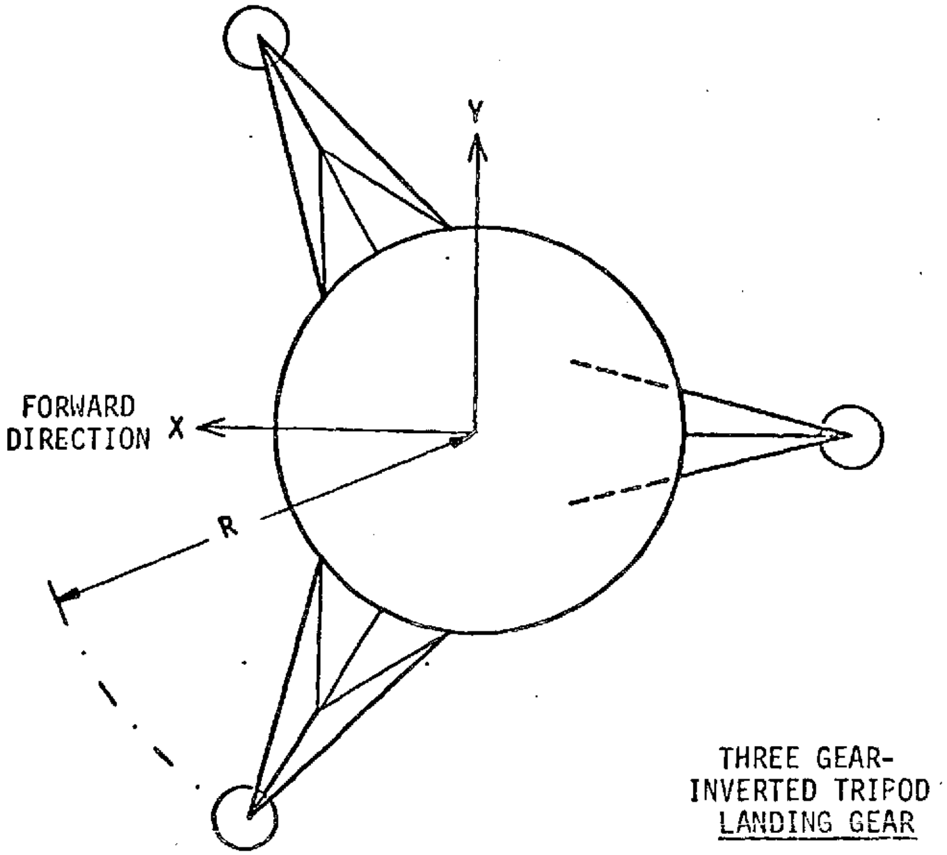
Y
FORWARD DIRECTION
X
R
THREE GEAR-
INVERTED TRIPOD
LANDING GEAR

Figure VIII-1

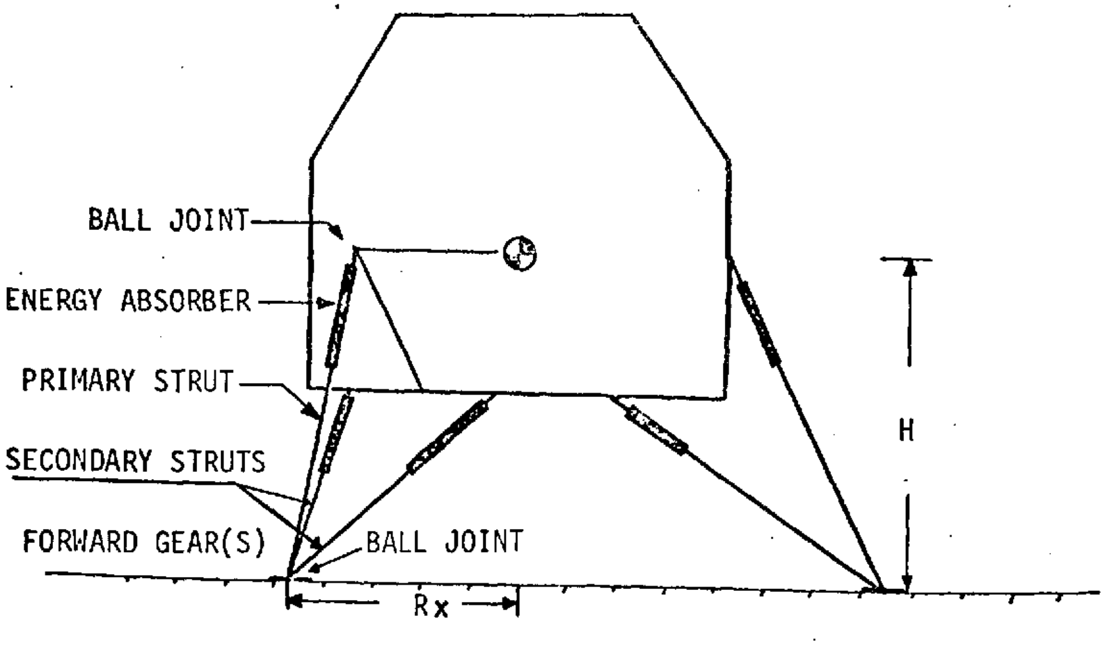
BALL JOINT
ENERGY ABSORBER
PRIMARY STRUT
SECONDARY STRUTS
FORWARD GEAR(S)
BALL JOINT
H
Rx

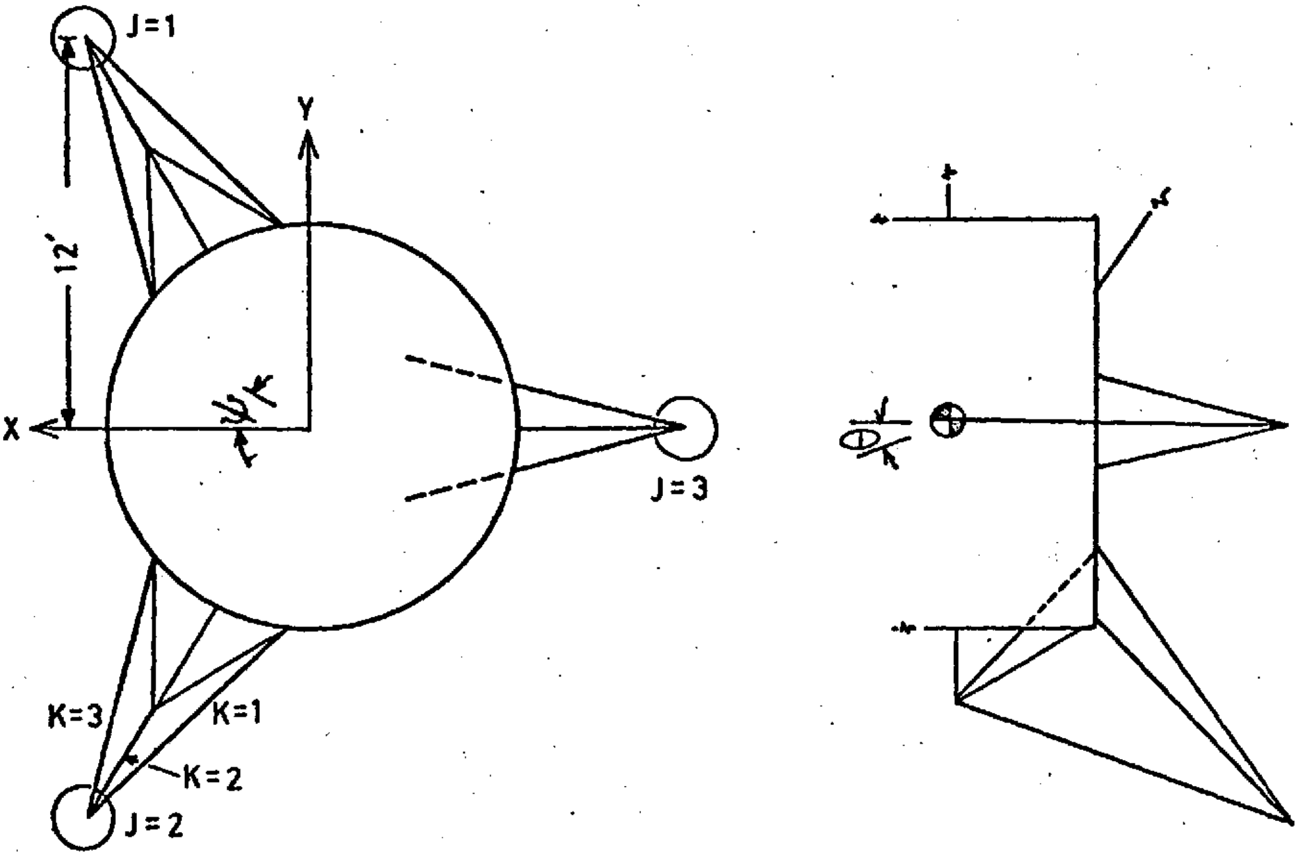
J=1
Y
12'
X
ψ
J=3
θ
K=3
K=1
K=2
J=2

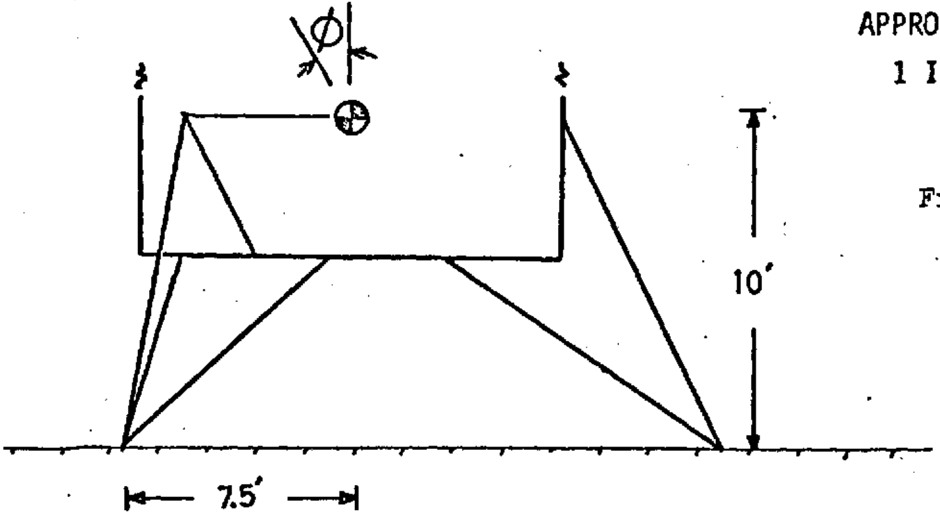

LUNAR LANDING VEHICLE:
LANDING GEAR DESIGN

APPROXIMATE SCALE
1 IN. = 6 FT.

Figure VIII-2

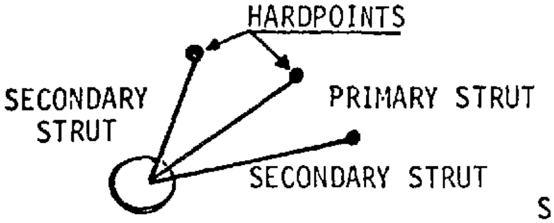
HARDPOINTS
SECONDARY STRUT
PRIMARY STRUT
SECONDARY STRUT

INVERTED TRIPOD DESIGN

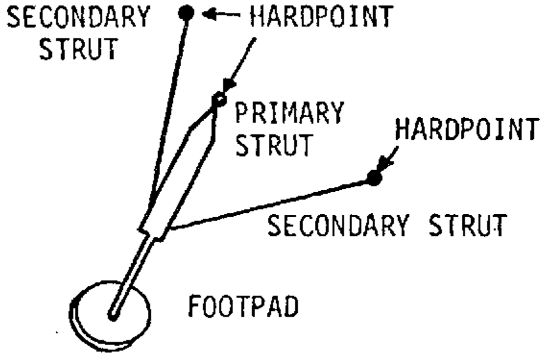
SECONDARY STRUT
HARDPOINT
PRIMARY STRUT
HARDPOINT
SECONDARY STRUT
FOOTPAD

CANTILEVER DESIGN

Figure VIII-3

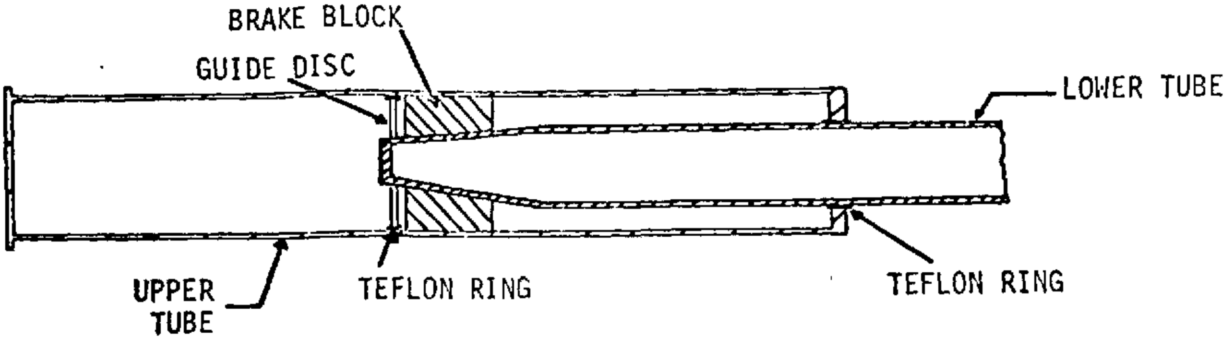
BRAKE BLOCK
GUIDE DISC
LOWER TUBE
UPPER TUBE
TEFLON RING
TEFLON RING

NASA FRICTION SHOCK ABSORBER CONCEPT

Figure VIII-4

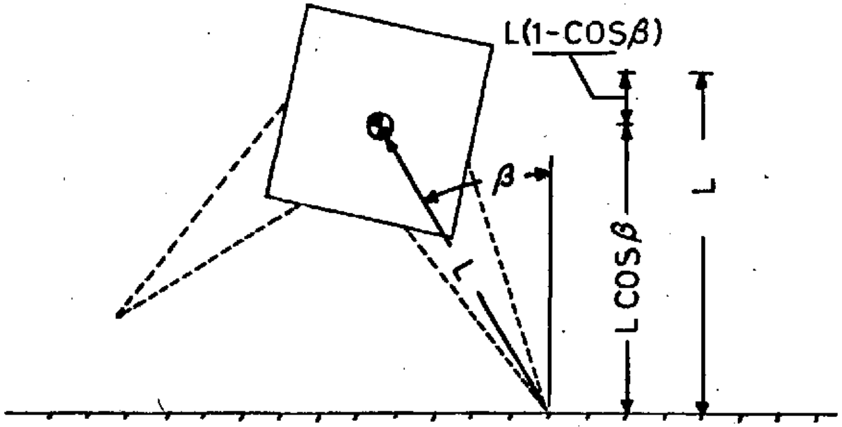
L(1-COSβ)
β
L
L COS β
L

STABILITY MARGIN PARAMETERS:

Figure VIII-5

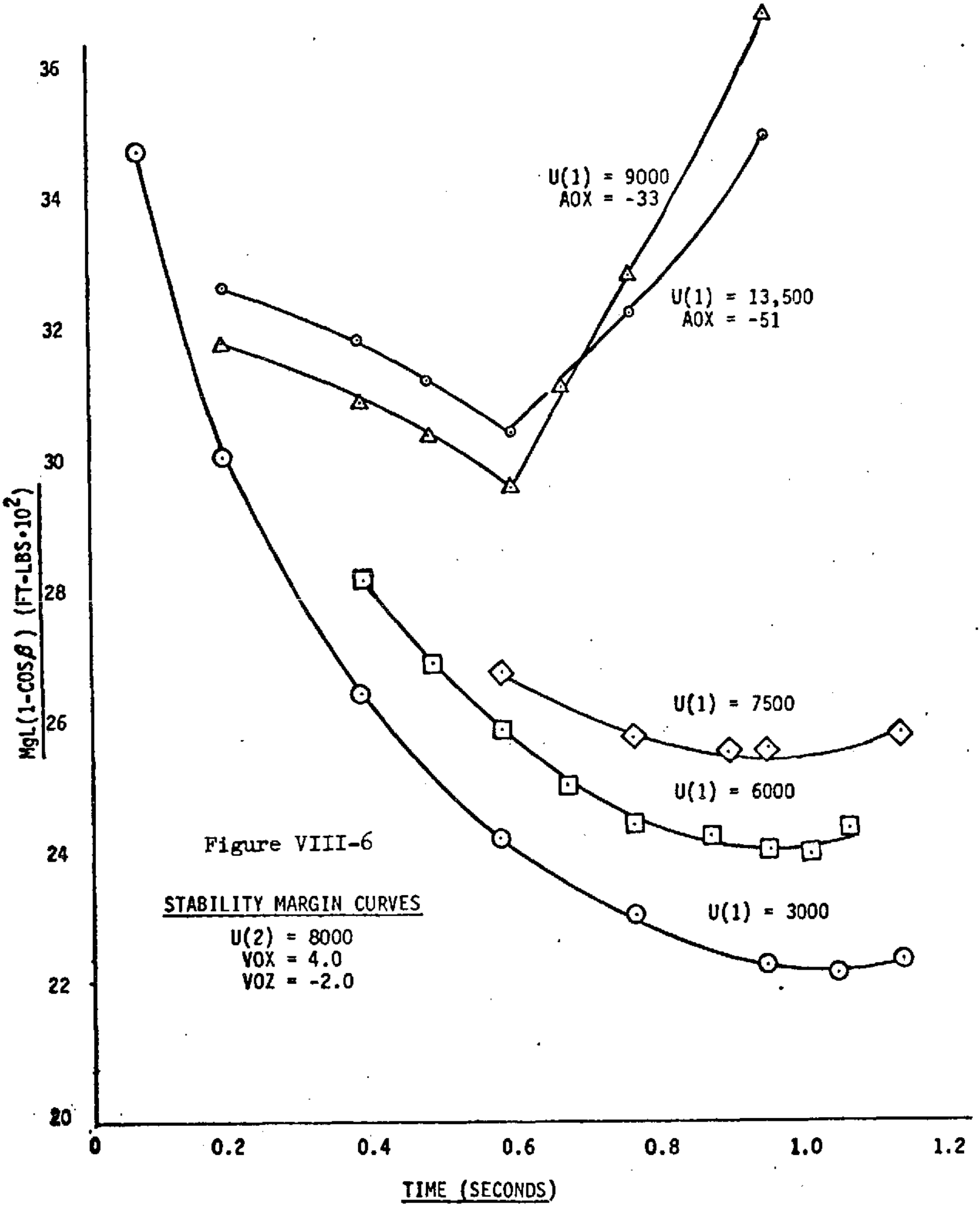

Figure VIII-6

STABILITY MARGIN CURVES

U(2) = 8000
VOX = 4.0
VOZ = -2.0